CFD ANALYSIS OF UAVs USING VORSTAB, FLUENT, AND ADVANCED
AIRCRAFT ANALYSIS SOFTWARE

BY

Benjamin Sweeten

Submitted to the graduate degree program in Aerospace Engineering
and the Graduate Faculty of the University of Kansas
in partial fulfillment of the requirements for the degree of
Master's of Science

_____
Dr. Shahriar Keshmiri, Chairperson

Committee members*   _____ *
Dr. Ray Taghavi

_____ *
Dr. Saeed Farokhi

_____ *
Dr. Richard Hale

Date Defended: <u>April 27, 2010</u>

The Thesis Committee for Benjamin Sweeten certifies
that this is the approved Version of the following thesis:

CFD ANALYSIS OF UAVs USING VORSTAB, FLUENT, AND ADVANCED
AIRCRAFT ANALYSIS SOFTWARE

Committee:

_____

Dr. Shahriar Keshmiri, Chairperson

_____

Dr. Ray Taghavi

_____

Dr. Saeed Farokhi

_____

Dr. Richard Hale

Date approved:_____

Acknowledgements

I would like to thank NASA and the National Science Foundation for the contributions to the University of Kansas Aerospace Engineering Department. Without their support and funding, this research would have not taken place. Also, thank you to Dr. Shahriar Keshmiri for his leadership and guidance during my graduate and undergraduate career. Dr. Keshmiri helped in every aspect of my research, from selecting classes, funding, and research topics. Thank you to Dr. Richard Hale for his guidance on the Meridian UAV. He has high expectations of his students, and is willing to put out the same amount of effort if not more. Thank you to my professors that I have had throughout my education. They have given the knowledge needed for my career path. Thank you to Dr. Lan, for allowing me to use his program and giving me guidance during the learning process of this program. Thank you to Andy Pritchard, the Aerospace Engineering Department's airplane and power plant mechanic. Andy worked with me on many projects and research. He offered his guidance and experience to everyone, and he was a major influence on my graduate career. Thank you to all my fellow colleagues and students for their help. In particular Dave Royer, Jonathan Tom, and Bill Donovan for answering and helping with all questions that were asked of them. Without their hard work the Meridian would have never flew. I would like to thank my family for offering their support and anything I needed during my college career. Lastly, I would like to thank my fiancée Jessica Donigan for her love and support. She dealt with me in a very difficult time and has always been there for me. Thank you to everyone that I may

have neglected to mention. There have been many people that gave me guidance and

support during my graduate and undergraduate career.

Abstract

The University of Kansas has long been involved in the research and development of uninhabited aerial vehicles, UAVs. Currently a 1,100 lb UAV has been designed, built, and flown from the University. A major problem with the current design of these UAVs is that very little effort was put into the aerodynamics. The stability and control derivatives are critical for the flight of the vehicle, and many methods can be used to estimate them prior to flight testing. The topic of this research is using high fidelity computer software, VORSTAB and FLUENT, to determine the flying qualities of three different UAVs. These UAVs are the 1/3 scale YAK-54, the MantaHawk, and the Meridian. The results found from the high fidelity computation fluid dynamics programs were then compared to the values found from the Advance Aircraft Analysis, AAA, software. AAA is not considered to be as accurate as CFD, but is a very useful tool for design. Flight test data was also used to help determine how well each program estimated the stability and control derivative or flying qualities.

The YAK-54 results from both programs were very close to each other and also to the flight test results. The results from the other two UAVs varied largely, due to the complexity of the aircraft design. VORSTAB had a very difficult time handling the complex body of the Meridian. Its results showed the aircraft was unstable in several different modes, when this is known to not be the case after several flight tests.

From these results it was determined that VORSTAB, while a high fidelity program, has difficulty handling aircraft with complex geometry. If the aircraft is a traditional style aircraft with non-complex geometry VORSTAB will return highly accurate results that are better than AAA. The benefit of AAA is that a model can be created rather quickly and the results will typically be within an acceptable error range. A VORSTAB model can be very time consuming to make, and this can outweigh the improved results. It is rather simple to determine if the VORSTAB results are valid or not, and the input file can be easily improved to increase the accuracy of the results. It is always a smart idea to use both software programs to check the results with one another.

FLUENT was used to determine the possible downwash issue over the Meridian fuselage. This software is a widely accepted program that is known to produce very accurate results. The major problem is that it is very time consuming to make a model and requires someone with a large amount of knowledge about the software to do so. FLUENT results showed a possibility for a large boundary layer near the tail and flow separation at high angles of attack. These results are all discussed throughout the report in detail.

Table of Contents

Table of Contents Continued

List of Figures

List of Figures Continued

List of Figures Continued

List of Tables

List of Symbols

Symbol	Description	Units

Normal

a	Speed of Sound	ft/sec
A or AR	Aspect Ratio	-----
b	Wing Span	ft
$\tilde{c}$	Mean Geometric Chord	ft
c_r	Root Chord	ft
c_t	Tip Chord	ft
C_D	Drag Coefficient	-----
$C_{D\alpha}$	Variation of Airplane Drag with Angle of Attack	1/rad
$C_{D\delta e}$	Variation of Airplane Drag with Elevator Deflection	1/rad
C_{Du}	Variation of Airplane Drag with Speed	1/rad
C_{Dq}	Variation of Airplane Drag with Pitch Rate	1/rad
C_l	Rolling Moment Coefficient	-----
$C_{l\beta}$	Variation of Airplane Rolling Moment with Angle of Sideslip	1/rad
$C_{l\delta a}$	Variation of Airplane Rolling Moment with Aileron Deflection	1/rad
$C_{l\delta r}$	Variation of Airplane Rolling Moment with Rudder Deflection	1/rad
C_{lp}	Variation of Airplane Rolling Moment with Rate of Change of Roll Rate	1/rad
C_{lr}	Variation of Airplane Rolling Moment with Rate of Change of Yaw Rate	1/rad
C_L	Lift Coefficient	-----
C_{L_ih}	Variation of Airplane Lift with Differential Stabilizer Angle	1/rad
$C_{L\alpha}$	Variation of Airplane Lift with Angle of Attack	1/rad
$C_{L\delta e}$	Variation of Airplane Lift with Elevator Deflection	1/rad
C_{Lq}	Variation of Airplane Lift with Pitch Rate	1/rad
C_{Lu}	Variation of Airplane Lift with Dimensionless Speed	1/rad
C_m	Pitching Moment Coefficient	-----
C_{m_ac}	Pitching Moment Coefficient about Aerodynamic Center	-----
$C_{m\alpha}$	Variation of Airplane Pitching Moment with Angle of Attack	1/rad
$C_{m\delta e}$	Variation of Airplane Pitching Moment with Elevator Deflection	1/rad
C_{mq}	Variation of Airplane Pitching Moment with Pitch Rate	1/rad
C_{mT}	Variation of Airplane Pitching Moment due to Thrust	-----
$C_{mT\alpha}$	Variation of Airplane Pitching Moment due to Thrust with Angle of Attack	1/rad
C_n	Yawing Moment Coefficient	-----
$C_{n\beta}$	Variation of Airplane Yawing Moment with Angle of Sideslip	1/rad
$C_{n\delta a}$	Variation of Airplane Yawing Moment with Aileron Deflection	1/rad
$C_{n\delta r}$	Variation of Airplane Yawing Moment with Rudder Deflection	1/rad
C_{np}	Variation of Airplane Yawing Moment with Rate of Change of Roll Rate	1/rad
C_{nr}	Variation of Airplane Yawing Moment with Rate of Change of Yaw Rate	1/rad
$C_{nT\beta}$	Variation of Airplane Yawing Moment due to Thrust with Sideslip	1/rad
C_{Tx}	Variation of Airplane Thrust in X Direction	-----
C_{Txu}	Variation of Airplane Thrust in X-axis with respect to speed	-----
C_y	Sideforce Coefficient	-----

Normal Continued

$C_{y\beta}$.....................Variation of Airplane Sideforce with Angle of Sideslip.......................1/rad

$C_{y\delta a}$.................Variation of Airplane Sideforce with Aileron Deflection.....................1/rad

$C_{y\delta r}$.................Variation of Airplane Sideforce with Rudder Deflection.....................1/rad

C_{yp}..........Variation of Airplane Sideforce with Rate of Change of Roll Rate.............1/rad

C_{yr}..........Variation of Airplane Sideforce with Rate of Change of Yaw Rate.............1/rad

$d\varepsilon/d\alpha$..Downwash Gradient..-----

$d\sigma/d\beta$..............................Sidewash Gradient...-----

D..Drag...lbs

e...Oswald's Efficiency Factor...-----

F_y...Sideforce..lbs

h..Height...ft

i_h..Horizontal Tail Incidence Angle..deg

I_{xx}, I_{yy}, I_{zz}.....................Airplane Moments of Inertia about XYZ............................slugs-ft^2

I_{xz}...............................Airplane Products of Inertia about XYZ.............................slugs-ft2

L...Lift...lbs

L, boundary layer.................Flow Distance Along Body...ft

N..Yawing Moment..ft-lbs

N.D. ....Non-dimensional...-----

M...Pitching Moment...ft-lbs

M_∞...Free Stream Mach Number...-----

p..Roll Rate..rad/sec

P_s...Static Pressure..lbs/ft^2

P_T.......................................Total Pressure..lbs/ft^2

q.......................................Pitch Rate...rad/sec

$q = 0.5\rho V^2$...........................Aircraft Dynamic Pressure...................................lbs/ft^2

r..Yaw Rate..rad/sec

u..x-component of Velocity...ft/sec

U..Axial Free Stream Velocity...ft/sec

v..y-component of Velocity...ft/sec

V..Velocity..ft/sec

$\tilde{V}$......................................Volume Coefficient of Tail..-----

w..z-component of Velocity...ft/sec

S...Area...ft^2

Re................................Reynolds Number...-----

x...Axial Station Along Fuselage..ft

x_{ac}.................Distance from Aerodynamic Center and Reference Point.........................ft

x_{cg}...................Distance from Center of Gravity and Reference Point............................ft

x_{vs}.................Axial Distance Between Vertical Tail a.c and Airplane c.g. ....ft

2d..............................Two Dimensional..-----

2ddp..............................Two Dimensional Double Precision.....................................-----

3d..............................Three Dimensional..-----

3ddp..............................Three Dimensional Double Precision.....................................-----

Greek

α ....Angle of Attack.. deg

α_dot ....Rate of Change of Angle of Attack .... deg/sec^2

β...Sideslip...deg

$\tilde{\delta}$................................Average Boundary Layer Thickness.................................... -----

δ^*... Displacement Thickness... -----

$\delta_{e,a,el,r}$ ....Control Surface Deflection...................................... deg

Δ ....Change in .... -----

η .... Dynamic Pressure Ratio .... -----

Γ ....Circulation ....m^2/sec

λ.. Taper Ratio .... -----

ν... Kinematic Viscosity ....m^2/sec

π...3.14... -----

ρ... Density ....lbs/ft^3

τ ....Angle of Attack Effectiveness Factor...................................... -----

θ...Momentum Thickness... -----

ω ....Angular Velocity .... rad/sec

ψ .... Stream Function .... -----

Acronyms

AAA.................................. Advanced Aircraft Analysis

CAD ....Computer Aided Design

CFD............................... Computational Fluid Dynamics

CReSIS....................Center for Remote Sensing of Ice Sheets

KUAE .... University of Kansas Aerospace Engineering

NSF................................. National Science Foundation

PC..Personal Computer

TAS..True Airspeed

UAV................................. Uninhabited Aerial Vehicle

Subscripts

a.. Aileron

B...................................... Body Stability Axis System

e...Elevator

el..Elevon

f .... Fuselage

h.. Horizontal Tail

o..................................... Coefficient at Zero Deflection

r ....Rudder

v.. Vertical Tail

w.. Wing

wf ....Wing Fuselages

1... Steady State Condition

1   <u>Introduction</u>

The shape and design of an aircraft can dramatically influence how the aircraft handles and is controlled. The stability and control derivatives are essential for flight simulation and handling qualities. There are several equations that can be used to estimate some of the derivatives, but not all of them. These equations are just estimations and can be magnitudes off. Therefore, better methods have to be used before investing millions of dollars on an aircraft.

Wind tunnel tests, are a method that results in derivatives that are highly accurate. The problems with wind tunnel tests are that it is very expensive and can be very time consuming. Also, the wind tunnel models are scaled down to fit in the tunnel, and this can have a dramatic change on the results, since the results do not always scale up as easily. Air will flow over a smaller body differently than a larger body, due to the changes in Reynolds number and other flow characteristics. Using an experienced wind tunnel expert and a highly accurate tunnel can minimize these problems, but will be very expensive. Over the past couple of decades computer simulation has become much more prevalent. Computational Fluid Dynamic software is much more accurate than it once was and is becoming more user friendly, but it still requires an expert to create a 3-D full aircraft CFD model. The mesh generation for a model can be difficult and requires a great deal of experience. This software is expensive to purchase, but can be used over and over again. Also, many different test cases can be run to determine flying qualities in various situations. There are also several different programs that are readily available that can produce

high fidelity results, and some of these programs can be purchased at a reasonable price.

Three different computer programs were used to determine the stability and control derivatives on three different UAVs. Two of the aircrafts were being designed and built to fly while the other one was already a production aircraft. The 1/3 scaled YAK-54 model was a production aircraft purchased by the University of Kansas, and the Meridian and MantaHawk were designed at the University of Kansas. The Meridian is a 1,100 lb aircraft that was designed to fly in the Polar Regions. Advanced Aircraft Analysis (AAA) and VORSTAB were used on all three aircraft and FLUENT was also used on the Meridian. FLUENT is a very high fidelity CFD program, but requires a large amount of experience and time. High level CFD programs can be very expensive and time consuming when performing aerodynamic analysis. This is why engineers prefer to use engineering level programs, such as AAA, to generate the derivatives quickly. The main goal of this research was to use high fidelity CFD programs to test the validity of these engineering level programs. The stability and control derivatives found from each software program were compared to each other and conclusions about the software were drawn.

2 <u>Literature Review</u>

It is a wise idea to examine current and past research going on in the field of study. This gives the researcher a chance to see what is currently going on, or has previously been examined in the past. It can also give the researcher ideas on topics and experiments to conduct. The research that was conducted in this paper is aerodynamic analysis, using high fidelity CFD programs, to determine the stability and control derivatives of UAVs with low Reynolds numbers. Therefore, the literature review topics consisted of stability and control analysis software, low Reynolds number aerodynamics, and the CFD software that was used in this research. A brief summary of each article will be given and then the conclusion drawn from these papers.

2.1 <u>Wavelike Characteristics of Low Reynolds Number Aerodynamics</u>

Lifting surfaces will demonstrate several uncharacteristic flow patterns when flown at a low Reynolds number. These patterns include a drag increase greater than the rate of increasing lift, acoustic disturbances, and variances in drag across the span of the lifting surface. This has a great effect on the design of micro or small UAVs since they have rather small Reynolds numbers. Spanwise flow can usually be ignored at higher velocities, but due to the low Reynolds number the flow can travel in the spanwise direction. Using velocity potential theory, boundary layer theory, and sinusoidal wave theory, the drag variation can be modeled as a sinusoidal wave along the span. These results were then comparedt to the research conducted by Guglielmo

and Selig, where the drag magnitude was observed to be happening in a wave form along the span. The goal of this research was not to exactly match the Guglielmo and Selig data, but to demonstrate that the drag magnitude and flow can be modeled using sinusoidal wave theory. This goal was successfully accomplished even though it did not match the trend observed by Guglielmo and Selig. All of this can be found in detail in Ref [1].

This research shows how the low Reynolds number can affect the flow around the aircraft's lifting surfaces. At low speeds the drag magnitude can vary along the span of the lifting surface, and in turn this can dramatically affect the other stability and control of the aircraft. If the flow is traveling at different speeds and in different directions (spanwise) the aircraft will not react how it typically would at higher speeds. The control surfaces would not have the same impact when the flow is varying.

2.2 <u>A Generic Stability and Control Methodology For Novel Aircraft Conceptual Design</u>

Stability and control is the most serious requirement for flight safety, and yet there is not a standard or reliable method for determining stability and control in the design phase. There are several methods used and many are considered acceptable within the industry. A major weakness, of most methods, is the design and sizing of the control effectors. Currently very simple methods are used for the sizing, and are done so in the cruise, landing, and take-off conditions of the flight envelope. This

research shows that sizing should be done so in the grey areas of the flight envelope, where non-linear aerodynamics prevail.

A method for generating stability and control was designed over a four year period and is called AeroMesh. This method is capable of handling both conventional and unconventional and symmetric or asymmetric flight vehicles. Design constraints and various flight conditions are first implemented into the program. An input file is then created for a CFD program called VORSTAB. This CFD software will estimate the stability and control derivatives as well as determine the size, position, and hinge lines of the control effectors. A 6 degree-of-freedom model is then used to determine stability and control in the trimmed and untrimmed condition. This 6-DOF model uses control power to determines the stability and control derivatives in the trimmed and untrimmed conditions. All information was taken from Ref [2].

This research shows just how important a high fidelity CFD program can be do the design of the control effectors and their sizing. The design criteria are at the extremes of the flight envelope, so the control effectors are designed at the point of non-linear aerodynamics. Using VORSTAB can help eliminate the use of simple methods that are low fidelity.

2.3 <u>Theoretical Aerodynamics in Today's Real World, Opportunities and Challenges</u>

CFD has revolutionized the aerodynamic industry, but it still faces many challenges in predicting and controlling various flows. These flows include UAV

low Reynolds number, high angle of attack, boundary layer transition, three-dimensional separation, and others. Since this is the case it is wise to combine theoretical, computational, and experimental approaches when analyzing the flow. These problems that a typical CFD program, has with the flow, is discussed and ways to analytically solve these problems are given. Multiple approaches are applied to the flow to find solutions. Using all three of the solution methods allows the users to see the short comings of each method. It is a very important and critical skill set to know and understand how to set up a problem up from the beginning, and then make approximations using mathematical and physics-based models. This principle should then be applied to a modern computational method. All information was taken from Ref [3].

It can be seen that not only a CFD program should be used during the design process, but also other methods. The research in this report covers both analytical methods, AAA, and high fidelity methods, VORSTAB and FLUENT. Understanding how to set up problems is very important due to the high complexity of modern CFD programs. A small error in the input can dramatically influence the results. It is also very important for the user to be able to interpret the results, and this skill set comes from understanding the theoretical methods.

2.4 The Lockheed SR-71 Blackbird – A Senior Capstone Re-Engineering Experience

At the University of Texas at Arlington, the senior aerospace class re-engineered the Lockheed SR-71 Blackbird in a two part design course. Currently in

the aerospace industry, it is very rare for a company to start a design from scratch, but rather add to or modify previous research.

There were no changes made to the SR-71 model, but rather the aircraft was reanalyzed. A CAD model of the aircraft was created, and from there the stability and control derivatives were determined in a two different ways. VORSTAB was the primary method for obtaining the derivatives, but also the Dr. Roskam method was used. The Roskam method is outlined in an eight book series about aircraft design. This second method is the same as using the AAA software. Both methods derivatives were then compared to the actual SR-71 data. The VORSTAB results were off by an order of magnitude, but followed the correct trends with the exception of the yawing moment coefficient due to sideslip and yawing moment coefficient due to roll rate. All other aspects of the design process were completed ranging from aircraft systems to flight performance. All information was taken from Ref [4].

The re-engineering of the SR-71 by the senior design class at the University of Texas at Arlington is very similar to the topic of this thesis. Several methods of analysis were used to determine the stability and control derivatives, and the results were then compared to one another.

3   Stability and Control Derivatives

The stability and control derivatives come from the aerodynamic forces and moments acting on upon the aircraft components. These components are defined as the wings, tails, fuselage, and any other surface on the aircraft. The flow around an entire aircraft is too complex to allow formulas to determine the derivatives. Wind tunnel tests or high fidelity computational fluid dynamics should be used to estimate the control derivatives with a high level of accuracy. To define and understand the stability and control derivatives one must have a basic understanding of aerodynamic principles; it will be assumed that the reader has this basic knowledge. The aircraft forces and moments are broken into two distinct directional motions, longitudinal motion and lateral-directional motion. Coupling between longitudinal and lateral-directional dynamics is assumed to be zero for stability and control derivative estimation.

3.1   Longitudinal Motion

Longitudinal motion is due to the forces and moments of the aircraft in the x-z plane in terms of the stability axes system, Figure 1 from Ref [5]. These forces and moments include drag force, lift force, and pitching moment. The aircraft orientation also affects these three, as well as the deflection of control surfaces. These forces and moment will be discussed in subsections of this chapter.
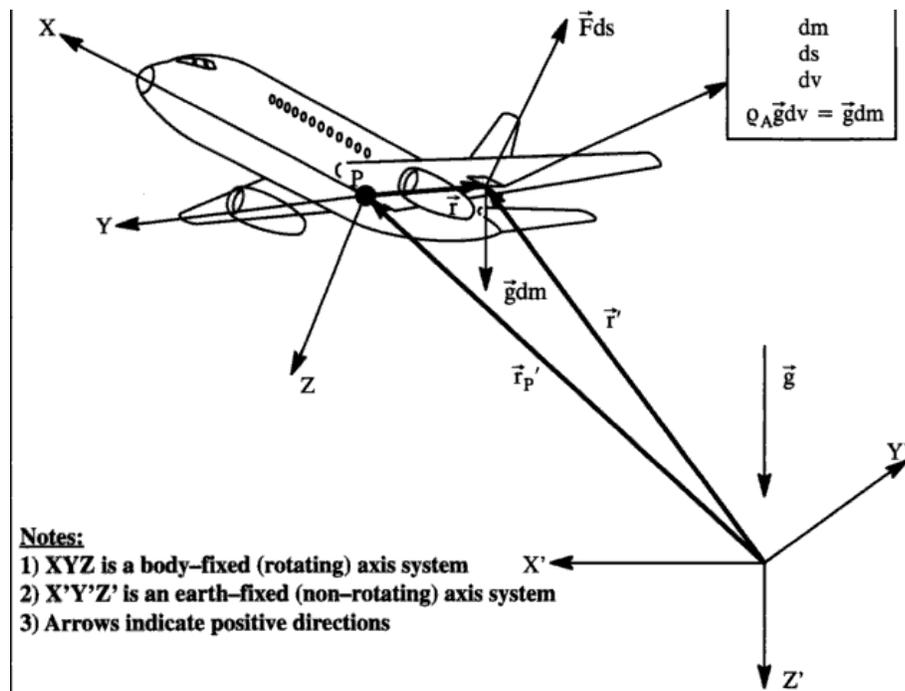
Figure 1: Earth-Fixed and Body-Fixed Axes System (From Ref [5])

3.1.1 Drag Coefficient, C_D

Drag is the force that acts in the opposite direction of motion. There are two types of drag that contribute to the entire aircraft drag. Parasite drag is drag due to the shape of the aircraft when there is zero lift produced, and induced drag is the drag produced due to the production of lift. The following are influences on the drag: airplane wetted area, skin friction, angle of attack, control surface deflection, speed, and dynamic pressure. Eq [1] and Eq [2] are two equations for determining drag, Ref [5] and Ref [6] respectively.

- $C_D = D/(q \cdot S)$ Eq [1]

- $C_D = C_{D_n} + C_L^2/(\pi \cdot A \cdot e)$ Eq [2]

9

3.1.2   Change in Airplane Drag due to Change in Angle of Attack, $C_{D\alpha}$

This coefficient represents variation of the drag coefficient with angle of attack. Typically, drag increases as the angle of attack increases, or in other terms, the drag changes as the angle of attack moves away from the steady state condition. It also increases as the Mach number increases. This derivative, $C_{D\alpha}$, can be estimated by differentiating Eq [2] which then produces Eq [3], Ref [6].

$$C_{D_\alpha} = (2 \cdot C_{L_1} \cdot C_{L_\alpha})/(\pi \cdot A \cdot e) \qquad\qquad \text{Eq [3]}$$

3.1.3   Change in Airplane Drag due to Change in Elevator Deflection, $C_{D\delta e}$

Deflection of the elevator produces an incremental change in aircraft drag, described by the derivative $C_{D\delta e}$. This derivative is determined at an angle of attack of zero. It is acceptable to neglect the change in drag due to these control surface deflections in low speeds, but high fidelity computer simulations will still calculate this derivative. However, when trim drag is important, this increase in drag cannot be neglected. The elevator deflection might be used to trim the aircraft, and therefore it is important for the overall drag.

3.1.4   Lift Coefficient, C_L

The lift is defined as the force acting on a surface that is perpendicular to oncoming flow in the upward direction. This means that it is also perpendicular to the drag force vector. Lift is what keeps the aircraft in the air. The aircraft wings, fuselage, and tails all can produce lift. The fuselage does not produce much lift, and is usually found as a wing-fuselage combination. The horizontal tail is affected by

the fuselage boundary layer, propeller slip stream, or jet exhaust. Therefore, when determining the horizontal tail lift, the downwash effect has to be accounted for. The following equations can be used to determine the overall lift of the aircraft, calculated for zero angle of attack, Ref [5].

- $$L = C_L \cdot q \cdot S \qquad\qquad \text{Eq [4]}$$

- $$C_L = C_{Lwf} + C_{Lh} \cdot (q_h/q) \cdot (S_h/S) \qquad\qquad \text{Eq [5]}$$

The wing-fuselage combination and horizontal tail lift coefficients can be broken into components. Methods for estimating these lift coefficient values can be found in Ref [7].

3.1.5 <u>Change in Airplane Lift due to Change in Angle of Attack, $C_{L\alpha}$</u>

Similar to the drag, the lift is affected by the angle of attack of the aircraft. As the angle of attack increases, the aircraft lift will increase until the stall point. This allows the aircraft to climb. Once a certain angle of attack is reached, the lift will begin to decrease because the aircraft has reached a stall point. The angle of attack of the stall point is dependent upon the geometry of the aircraft, the flow, and the altitude. This is why an aircraft has a maximum angle of attack. As the subsonic speed increases, the $C_{L\alpha}$ increases, but around transonic region it begins to decrease. The angle of attack also has an effect on every lifting surface. At certain angles of attack, the downwash or flow off the wings could blanket out the tail and render them ineffective. Eq [6] can be used to determine the lift coefficient due to angle of attack, Ref [5]. Eq [6] is found by partial differentiation of the first-order Taylor series of the lift Eq [7], Ref [5].

- $$C_{L_\alpha} = C_{L_{\alpha wf}} + C_{L_{\alpha h}} \cdot (q_h/q) \cdot (S_h/S) \cdot (1 - d\epsilon/d\alpha)$$ Eq [6]

- $$C_L = C_{L0} + C_{L_\alpha} \cdot \alpha + C_{L_{i_h}} \cdot i_h + C_{L_{\delta_e}} \cdot \delta_e$$ Eq [7]

3.1.6   Change in Airplane Lift due to Change in Elevator Deflection, $C_{L\delta e}$

The deflection of the elevator will change the camber of the horizontal tail airfoils and therefore change the lift of those airfoils. Highly cambered airfoils usually have higher lift.   Therefore, depending on the camber direction of the horizontal tail and the direction of deflection, the lift of the horizontal tail will increase or decrease. The effect of the elevator deflection on the total aircraft lift coefficient can be found in Eq [8], Ref [5].   This is also found by partial differentiation of the first-order Taylor series of lift Eq [7], Ref [5].

- $$C_{L_{\delta e}} = C_{L_{\alpha h}} \cdot (q_h/q) \cdot (S_h/S) \cdot \tau_e$$ Eq [8]

3.1.7   Pitching Moment Coefficient, C_m

This is defined as the aerodynamic force that creates a moment that causes the aircraft to pitch, or rotate upwards and downwards. Lifting forces create this resultant force that causes the aircraft to pitch. The point that the aircraft rotates about is typically defined as the center of gravity. Center of pressure is defined as the point at which the pitching moment coefficient is equal to zero. Aerodynamic center is the point about which the pitching moment coefficient does not vary with angle of attack. As the angle of attack changes the center of pressure location will change. These two points create the pitching moment coefficient; the center of pressure location changes cause the change in the pitching moment. Most aircraft are inherently stable as long

as the center of gravity is ahead of the aerodynamic center. Elevator deflection and angle of attack can dramatically change the pitching moment. The following equations define the pitching moment coefficient and estimation of this value, Ref [5].

- $$M = C_m \cdot q \cdot S \cdot \bar{c}$$

  Eq [9]

- $$C_m = C_{mac_{wf}} + C_{L_{wf}} \cdot \frac{x_{cg} - x_{ac_{wf}}}{c} +$$

$$C_{L_h} \cdot \left(\frac{q_h}{q}\right) \cdot \left(\frac{S_h}{S}\right) \cdot \frac{x_{ac_h} - x_{cg}}{\bar{c}}$$

Eq [10]

3.1.8   Change in Airplane Pitching Moment due to Change in Angle of Attack, $C_{m\alpha}$

As stated previously, the center of pressure can move forward and aft as the angle of attack changes. This results in a changing moment arm and an increasing or decreasing pitching moment. The angle of attack also changes the lift on the aircraft, and therefore changes the aerodynamic force that creates the pitching moment. This derivative, $C_{m\alpha}$, is called the static longitudinal stability derivative which should be negative for an inherently longitudinally stable aircraft. For example, if the aircraft that is statically stable is pitched upward it naturally returns to steady state and pitches down or vice-versa if pitched downward. If it was not stable, the aircraft would want to continue pitching upward and could flip over. The horizontal tail has a large affect on this since it is used to pitch the aircraft. Horizontal tail incidence angle can dramatically affect this derivative due to the lift it creates on the tail. Eq [11] can be used to estimate this derivative, Ref [5].

- $$C_{m\alpha} = C_{m\alpha wf}\left(\frac{x_{cg} - x_{ac_{wf}}}{c}\right) -$$

$$C_{L\alpha h}\left(\frac{q_h}{q}\right)\left(\frac{S_h}{S}\right)\left(\frac{x_{ach} - x_{cg}}{\bar{c}}\right)(1 - d\varepsilon/d\alpha)$$

<div align="right">Eq [11]</div>

3.1.9   <u>Change in Pitching Moment due to Change in Elevator Deflection, C_{mδe}</u>

This derivative is referred to as the longitudinal control power derivative and is typically negative. The effectiveness of the elevator is basically due to the volume coefficient of the horizontal tail, Eq [12], and the angle of attack effectiveness of the elevator, τ, Ref [5]. The larger the size of the elevator is, the more effect it has on the pitching moment. For example, a fully moving horizontal tail has just as much effect as the incidence of the horizontal tail. Eq [13] is used to estimate the derivative, Ref [5].

- $$\bar{V}_h = \frac{\left(\frac{S_h}{S}\right)(x_{ach} - x_{cg})}{\bar{c}}$$

<div align="right">Eq [12]</div>

- $$C_{m\delta e} = -C_{L\alpha h}\left(\frac{q_h}{q}\right)\bar{V}_h$$

<div align="right">Eq [13]</div>

3.2   <u>Lateral-Directional Motion</u>

The rolling motion is referred to as the lateral motion, and the yawing motion is referred to as the directional motion. These two motions are results of control surface deflections and sideforces, where sideslip plays a large role in lateral-directional motion. This is the angle of directional rotation from the aircraft centerline to the direction of the wind. The sideslip angle can be thought of as the directional angle of attack. The forces and moments that are defined in the lateral-

directional motion are sideforce, yawing moment, and rolling moment. Similar to longitudinal control, there are several variables that affect these forces and moments.

3.2.1 Rolling Moment, C_l

The rolling moment is the aircraft's rotation about the x-axis in the stability coordinate system. Several different things can cause and influence the rolling moment, and those are sideslip, angle of attack, the moment reference center (usually center of gravity), deflection of control surfaces, and airspeed. The control surfaces that affect the rolling moment are the aileron (lateral control surface) and rudder (directional control surface). Elevator deflection influence can usually be ignored since the deflections are symmetrical and theoretically cancel each other out. Eq [14] is the dimensional form of the rolling moment and Eq [15] shows the first order Taylor series form of the rolling moment, Ref [5].

- $$L = C_l \cdot q \cdot S \cdot b$$

  Eq [14]

- $$C_l = C_{l_0} + C_{l_\beta} \cdot \beta + C_{l_{\delta_a}} \cdot \delta_a + C_{l_{\delta_r}} \cdot \delta_r$$

  Eq [15]

3.2.2 Change in Airplane Rolling Moment due to Change in Sideslip, C_{l_β}

This derivative is often referred to as the airplane dihedral effect. The reason for this is because the airplane dihedral angle can have a huge influence on the rolling moment especially when at a sideslip. If the aircraft is at a sideslip and has a dihedral angle on the wings, one of the wings will be hit with more air than the other. This will cause a higher lift on that wing and in turn cause the airplane to roll. Rolling moment derivative due to sideslip can be estimated by summing the dihedral effect of

the individual components of the aircraft, Eq [16], Ref [5]. There are many factors that play into the individual components' dihedral effect. For example, the wings' location on the fuselage can affect the direction that the aircraft will want to roll. The vertical tail will also see a higher sideforce when the aircraft is at a sideslip. For a detailed explanation and ways to estimate the individual components of the dihedral effect refer to Ref [5].

$$C_{l_\beta} = C_{l_{\beta_{wf}}} + C_{l_{\beta_h}} + C_{l_{\beta_v}}$$ Eq [16]

3.2.3   Change in Airplane Rolling Moment due to Change in Aileron Deflection, $C_{l_{\delta a}}$

A positive aileron deflection is defined as the right aileron up and the left aileron down. This produces a rolling moment by decreasing the lift on the right wing due to the negative camber of the aileron, and increasing the lift on the left wing due to the positive camber of the aileron. These aileron deflections will also produce a yawing moment, and this is why most ailerons are deflected differentially. This differential deflection will help minimize the yawing moment that is produced. Flow separation can also occur with large aileron deflections, and this can reduce the effectiveness of the ailerons.

3.2.4   Change in Airplane Rolling Moment due to Change in Rudder Deflection, $C_{l_{\delta r}}$

The purpose of the rudder is to produce a yawing moment, but due to the typical location of the vertical tail and rudder a rolling moment is produced. With the rudder deflected, the free stream air will encounter the rudder and produce a sideforce. The resultant sideforce is typically located above the center of gravity and

will produce this rolling moment. This derivative is usually positive, but at high angles of attack it can switch signs because of the vertical tail moment arm location changes. Eq [17] shows how to estimate this derivative, Ref [5].

- $$C_{l_{\delta_r}} = C_{l_{\alpha_v}} \cdot \alpha_{\delta_r} \cdot \eta_v \cdot \frac{S_v \cdot x_{v_s}}{S \cdot b}$$
  Eq [17]

3.2.5 Sideforce Coefficient, C_y

This is the aerodynamic force that causes the aircraft to yaw and can cause a rolling moment if above or below the center of gravity. With zero angle of attack, sideslip, and control surface deflection, the sideforce should equal zero for a symmetrical aircraft. The sideforce is a result of sideslip, angle of attack, control surface deflection, and symmetry of aircraft. For an unsymmetrical aircraft, a sideforce could be produced from the side that has a larger amount of surface area being hit by the free stream air. Eq [18] calculates the dimensional sideforce and Eq [19] shows the first order Taylor series, Ref [5].

- $$F_y = C_y \cdot q \cdot S$$
  Eq [18]

- $$C_y = C_{y_0} + C_{y_\beta} \cdot \beta + C_{y_{\delta_a}} \cdot \delta_a + C_{y_{\delta_r}} \cdot \delta_r$$
  Eq [19]

3.2.6 Change in Airplane Sideforce due to Change in Sideslip, $C_{y\beta}$

Similar to the effect sideslip has on rolling moment, this derivative can be broken down into individual components. The wings' contribution depends on the dihedral angle. A larger dihedral will produce a large sideforce, because there is more surface area for the sideslip free stream to contact; however, the wings' contribution is generally negligible. Fuselage contribution depends on its shape and

size. Large fuselages have more contact surface area to produce larger sideforces. The vertical tail can produce a large sideforce due to the large moment arm from the center of gravity and the size of the tail. This derivative can be estimated using methods found in Ref [7].

3.2.7   Change in Airplane Sideforce due to Change in Aileron Deflection, $C_{y\delta a}$

This contribution to the sideforce is very small and more often than not negligible. If these rolling moment controls are close to a vertical surface the sideforce cannot be neglected. This happens by the increase in lift on one side and a decrease on the opposite side. These changes in lift are actually changes in pressure which, if close to a vertical surface, can produce a sideforce. Wind tunnel tests have to be completed to measure this in a reliable fashion.

3.2.8   Change in Airplane Sideforce due to Change in Rudder Deflection, $C_{y\delta r}$

The rudder has a large influence on the sideforce. The purpose of a rudder deflection is to create a sideforce that will produce a yawing moment. Depending on the location it will also produce a small rolling moment. This sideforce depends on the size of the vertical tail in relation to the wings. The lift curve slope of the vertical tail also plays into the influence of sideforce. The sideforce contribution of the rudder can be determined using Eq [20], Ref [5].

$$F_{y_r} = C_{y_{\delta_r}} \cdot \delta_r \cdot q \cdot S$$

Eq [20]

3.2.9 Yawing Moment, C_n

The aircraft yawing moment is the rotation about the z-axis in the stability coordinate system. For a symmetrical aircraft the yawing moment is equal to zero for zero angle of attack, sideslip, and control surface deflections. The same things that influence the rolling moment influence the yawing moment. Those influences are angle of attack, sideslip, speed, control surface deflections, and location of the moment reference center. Eq [21] is the dimensional form of the yawing moment and Eq [22] is the first order Taylor series, Ref [5].

- $$N = C_n \cdot q \cdot S \cdot b$$

  Eq [21]

- $$C_n = C_{n0} + C_{n\beta} \cdot \beta + C_{n\delta_a} \cdot \delta_a + C_{n\delta_r} \cdot \delta_r$$

  Eq [22]

3.2.10 Change in Yawing Moment due to Change in Sideslip, $C_{n\beta}$

This derivative is referred to as the static directional stability and plays a large role in Dutch roll and spiral dynamics. The derivative can be estimated by summing the components of the aircraft, Eq [23], Ref [5]. The wings' influence can be neglected since the flow is usually in line with the airfoil. The fuselage, on the other hand, can play a large role, but it depends on the shape and the amount of projected side area forward or aft of the center of gravity. Another impact on the fuselage contribution is the Munk effect, which shifts the aerodynamic center forward. The vertical tail also has a significant contribution. The size and location of the vertical tail determines the amount of contribution it has. Eq [24] shows the contribution of the vertical tail, Ref [5].

- $$C_{n\beta} = C_{n\beta_f} + C_{n\beta_w} + C_{n\beta_v}$$

  Eq [23]

- $$C_{n\beta_v} = C_{L\alpha_v}(1 - d\sigma/d\beta)\eta_v \frac{S_v x_{v_s}}{Sb}$$

  Eq [24]

3.2.11 Change in Yawing Moment due to Change in Aileron Deflection, $C_{n\delta a}$

With aileron deflections, the lift increases on the aileron with positive camber, downward deflection, and the lift decreases on the aileron with negative camber, upward deflection. An increase in lift will cause an increase in induced drag, and a decrease in lift will cause a decrease in induced drag. Higher drag on one wing will cause the aircraft to yaw. This type of yawing moment, called an adverse yawing moment, is undesirable because it tends to yaw the aircraft out of an intended turn. Therefore, either pilot input or differential ailerons are used to prevent the aircraft from yawing.

3.2.12 Change in Yawing Moment due to Change in Rudder Deflection, $C_{n\delta r}$

This derivative depends largely on the size of the vertical tail in relation to the wings. The lift curve slope of the vertical tail also plays a large role. The location of the vertical tail will determine the moment arm. Also, the size of the rudder will influence the yawing moment. Eq [25] is used to estimate the derivative, Ref [5].

- $$C_{n\delta_r} = -C_{L\alpha_v}\alpha_{\delta_r}\eta_v \frac{S_v x_{v_s}}{Sb}$$

  Eq [25]

3.3 Perturbed State

A perturbed state flight condition is defined as one for which all motion variables are defined relative to a known steady state flight condition, Ref [5]. It can

be thought of as the aircraft's motion varying from the steady state condition. These variations are increases or decreases in velocity in any direction, or acceleration in any direction or motion.

The longitudinal motion is influenced by a change in velocity in the u and w direction if the velocity is broken down into three components, u, v, and w. Pitch rate, q, also affects the longitudinal derivatives. It is assumed that the pitch rate has a negligible influence on the lateral-directional motion.

Some of the lateral-directional perturbation influences are the v component of a velocity change, yaw rate, and roll rate. Small roll rate perturbations cause non-symmetrical changes in local angles of attack over the lifting surface. It can easily be visualized how these changes in angle of attack will influence the lateral-directional derivatives. Small yaw rate perturbations cause changes in the local velocity on the lifting surfaces. They also cause changes in the angle of attack of the vertical tail. There are also perturbation influences from changes in the flight angles. For example, these flight angles can be the sideslip angle or angle of attack.

4 <u>AAA</u>

Advanced Aircraft Analysis, AAA, is a software program developed by DARcorporation that is an aircraft stability, control, and design tool. It is widely accepted as the industry standard and is used in 45 countries. The program follows the Dr. Roskam method of preliminary aircraft design. Although the program will model any size aircraft, the lower limit of the Reynolds number for calculations is 3e6. This means modeling of smaller aircraft may be inaccurate to some degree.

The software works for preliminary design all the way up to Class II cost analysis. Geometric and flight characteristics of the aircraft being modeled are input, and with a simple click of 'calculate', outputs are produced. This program helps eliminate errors in calculations and spreadsheets. If the designer does not understand how something is being determined, there is a help button that shows all of the equations used for each variable. This helps eliminate the black box feeling that comes from most modeling software programs. If this help is not enough, the books the program is based on are *Airplane Design I-VIII, Airplane Flight Dynamics and Automatic Flight Controls, Parts I and II*, by Dr. Jan Roskam, and *Airplane Aerodynamics and Performance*, by Dr. C.T. Lan and Dr. Jan Roskam, Ref [8].

AAA is used before the aircraft is ever built, but can also be used to model production vehicles. Using AAA, the stability and control derivatives can be found and compared with actual flight test data. Doing this helps validate the software, allowing the designer to be more comfortable with the results AAA produces when designing an aircraft from scratch.

5   VORSTAB

VORSTAB is a software program that was developed by Dr. Edward Lan for NASA. It has been used on several NASA research projects. The acronym name stands for Vortex Stability. Using vortex flow effect, the lateral-directional and longitudinal stability derivatives are determined for an aircraft. The program follows the Prandtl-Glauert equation, Eq [26], in subsonic flow, Ref [9]. The Prandtl-Glauert equation is the linearized full-potential equation, Eq [27], using small velocity perturbations assumptions, Ref [9].

-
$$\varphi_{xx}\left(1 - M_\infty{}^2\right) + \varphi_{yy} = 0 \qquad\qquad \text{Eq [26]}$$

-
$$\varphi_{xx}\left(1 - \frac{\varphi_x{}^2}{a^2}\right) + \varphi_{yy}\left(1 - \frac{\varphi_y{}^2}{a^2}\right) - \frac{2}{a^2}\varphi_x\varphi_y\varphi_{xy} \qquad\qquad \text{Eq [27]}$$

These are a few assumptions that VORSTAB uses for calculations.

- Assumes thin wing and therefore thickness effect is not accounted for in calculations.

- The boundary layer separation is not accounted for, and therefore the flow stays attached to the body.

- The wake aft of the wing is flat and does not increase in the z-direction.

The designer of the input model also makes assumptions based on the aircraft that is being modeled and the flight characteristics. A detailed description of the program can be found in Ref [10].

5.1   Creating a Model

VORSTAB runs an input file that the designer creates. There are 83 groups that are used to describe the aircraft and the test cases that are to be run. These groups break down a step by step procedure for creating the model and allow the designer to trouble shoot more easily. Not every group is used to describe the aircraft that is being modeled, and many groups are repeated several times. Detailed descriptions of the groups are found in Ref [11].

To create a model of the aircraft the designer needs to have detailed schematics of the geometry. Typically, this geometry comes from a CAD model. Using the CAD model the designer can find all of the geometry needed for VORSTAB. The software does not require that a fuselage be present in the model. The first step in creating the model is to specify the number of lifting surfaces that are to be modeled. These lifting surfaces include wings, horizontal tail, vertical tail, v-tail, and canards. The level flight geometry of each lifting surface is input into VORSTAB. If this is not done, the program assumes that the geometry is at zero angle of attack, when it might actually be more or less. For example, when the Meridian sits on the ground, the wings and tail are at a higher angle of attack when compared to level flight. The input lifting surface geometry required includes airfoil characteristics (thickness and camber), location in terms of distance from reference point (example: nose of aircraft), dihedral, twist, location of control surfaces, and much more. Also needed is the lift coefficient, drag coefficient, and pitching moment coefficient with respect to angle of attack. This step is repeated for each lifting

surface. Next, the fuselage data is input into VORSTAB. The geometry needed for this includes cross-section shape, camber, axial locations from a reference point, and much more. The more cross-sections used in this model, the more accurate the results will be. It must be made sure that the lifting surfaces are not inside of the fuselage. The fuselage model is also created in level flight for the same reason as the lifting surfaces. Scaling the input file is very important. The entire aircraft is scaled to a size where the largest cross-sectional radius of the fuselage is no larger than a measurement of 1 in any unit system.

Next, the type of case that is to be run is described. This includes the flight condition, control surface deflection angles, angle of attack, and more. With the input file complete, VORSTAB can run. If there is an error in the input file, the output file will stop at the group with the problem. This is a great advantage to find simple problems in the input file that the designer overlooked. VORSTAB also creates a file that can be opened with TECplot to see a graphical representation of the model. This graphical representation allows the designer to visually determine if something looks wrong with the model created.

6   <u>FLUENT</u>

FLUENT is a commercially sold computational fluid dynamics program that is widely accepted for its high fidelity. The program has many different capabilities and functions. Both 2-demensional and 3-demensional cases can be tested with laminar, invisid, or turbulent flow. Depending on the model and flow type, the designer chooses which flow field type is best. For large models, over 200,000 cells and a coupled solver, a standard PC with single memory cannot process the model. Super computers with multiple processors must be used to solve these larger models. The following are the steps followed to run a FLUENT model.

Step 1: Create a GAMBIT model with a mesh for the flow field. GAMBIT is a software program that allows the designer to easily create a geometric model of the object being tested. The geometry of the object and the flow field around the model are created. The size of the mesh will dramatically affect the accuracy of the results and the processing time.

Step 2: Export the mesh so that it can be imported into FLUENT.

Step 3: With FLUENT opened, select either 2-D or 3-D, depending on the mesh created in GAMBIT. There is also 2ddp and 3ddp. The "dp" stands for double precision, and is more accurate than just the standard 2d or 3d. Case run time is larger for this method, but the accuracy of the results is important to the validity of the model.

Step 4: Import the mesh and run a check to see if there are errors in the mesh. The size of the mesh can also be seen to verify that there are not too many cells to run the test on a standard PC.

Step 5: Choose the type of solver: segregated or coupled. Coupled solver requires much more computer memory. The 'solver' is the method that the program uses to solve the equations.

- Segregated solver- solves the equations one by one. Momentum, continuity, energy (if compressible flow), turbulent factor, and then check for convergence.

- Coupled solver- solves the same equations as the segregated solver, but does this simultaneously instead of one by one.

Step 6: Choose the type of flow: laminar, invisid, or turbulent. If choosing turbulent flow select the turbulent model to use. It is difficult to determine the most accurate turbulent model without testing several different ones. The accuracy depends on the mesh shape and flow pattern. Research has shown that the most accurate method for aerodynamics is Spalart-Allmaras.

Step 7: Set the fluid properties and boundary conditions. The fluid properties include but are not limited to density, viscosity, velocity, wall friction, and much more.

Step 8: Select the solution controls and discretization methods. This depends on the shape of the body and type of flow. A description of each solution and

discretization method should be read before the designer chooses which one is best for their model. The FLUENT online help menu should be used for these questions.

- SIMPLE and SIMPLEC are good choices for non-complicated flow problems (such as laminar flow).

- PISO is used for transient flows.

Step 9: Set the residuals and turn on what parameters are to be monitored. For example, the lift and drag of the body can be monitored.

Step 10: Iterate until the solution converges. The convergence criteria is determined by setting the residuals.

These steps can slightly vary from mesh to mesh, but in general these ten steps allow the user to run a FLUENT model.

7 <u>YAK-54</u>

The YAK-54 is a remote control aircraft that the Aerospace Engineering Department at the University of Kansas owns. This aircraft is a 1/3 scale version of the Russian Yakovlev Yak-54 acrobatic airplane. An autopilot system was installed into this aircraft to help test the robustness and capabilities of the system before the same system was installed on the larger and more expensive Meridian. Figure 2 shows a model of the YAK-54 used by the University of Kansas, Ref [12].

Figure 2: YAK-54

From the aircraft itself, detailed measurements were taken to create an exact CAD model of the aircraft that was used during flight tests. Taking measurements directly from the aircraft allowed abnormalities due to manufacturing to modeled and

accounted for. Table 1 shows some of the measurements taken from the YAK-54. To
create the CAD model, Unigraphics 6.0 was used. Figure 3 shows the final CAD
model of the YAK-54. The flight conditions used in AAA can be found in Table 2,
Ref [13].

Table 1: YAK-54 Lifting Surface Dimensions

Wing		
$S =$	10.9	ft^2
$b =$	7.9	ft
$\bar{c} =$	1.45	ft
$\lambda =$	0.46	
$AR =$	5.77	
$c_r =$	1.9	ft
$c_t =$	0.874	ft
Horizontal Tail		
$S =$	2.3	ft^2
$b =$	3	ft
$\bar{c} =$	0.767	ft
$\lambda =$	0.81	
$AR =$	3.91	
$c_r =$	0.844	ft
$c_t =$	0.684	ft
Vertical Tail		
$S =$	1.6	ft^2
$b =$	1.42	ft
$\bar{c} =$	1.21	ft
$\lambda =$	0.35	
$AR =$	1.25	
$c_r =$	1.67	ft
$c_t =$	0.584	ft
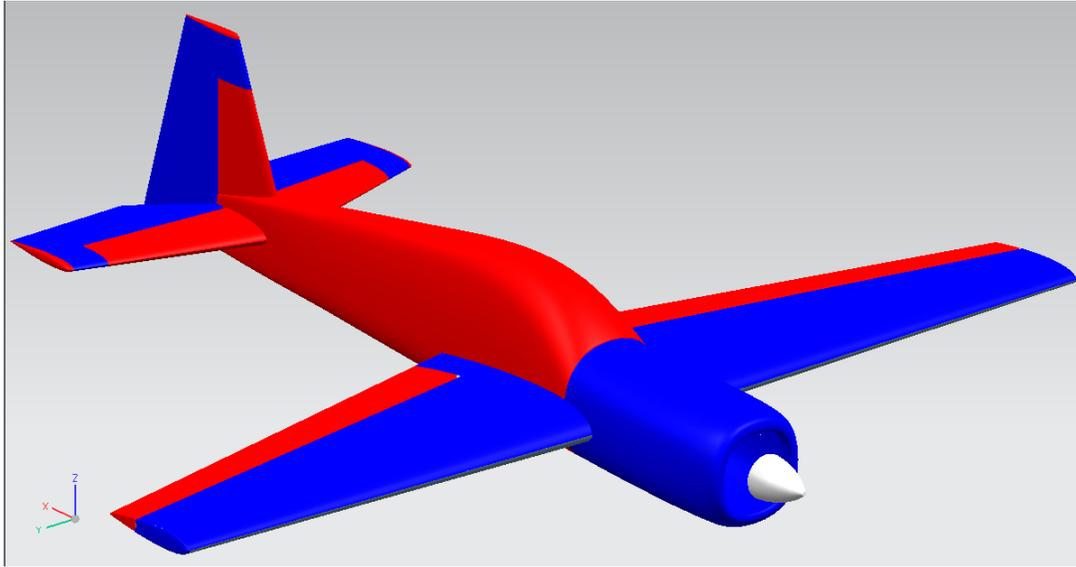
Figure 3: Unigraphics CAD Model of YAK-54

Table 2: YAK-54 Flight Conditions

Flight Conditions	
Altitude (AGL), h (ft)	400
Mach Number	0.106
TAS, U_1 (ft/sec)	118
Dynamic Pressure, q (lbs/ft^2)	16.4
C.G. location, fraction $\bar{c}$ (in)	25.5

The importance of creating a VORSTAB model of the YAK-54 was to gain experience with the program and see how accurate the program was since this vehicle had been flight tested. The need for a VORSTAB model also came from AAA overestimating the drag on vehicles with low Reynolds numbers. After flight tests, Edmond Leong tuned the AAA results to develop more accurate stability and control derivatives. This will all be discussed later.

7.1 AAA Modeling of the YAK-54

AAA was used to determine the YAK-54's dimensionless longitudinal and lateral-directional stability and control derivatives. Table 3 shows the trimmed condition values of the aircraft, Table 4 shows the longitudinal derivatives, and Table 5 shows the lateral-directional derivatives, all results were taken from Ref [13]. Table 6 shows the stability requirements for the YAK-54 produced by AAA, Ref [13].

Table 3: YAK-54 AAA Moment of Inertia and Trimmed Values

Mass Data	
Weight (lbs)	28
Ixx_B (slug-ft^2)	1.09
Iyy_B (slug-ft^2)	2.11
Izz_B (slug-ft^2)	3.04
Ixz_B (slug-ft^2)	0.05
Steady State-Trimmed	
C_{L1}	0.147
C_{D1}	0.053
C_{Tx1}	0.052
C_{m1}	-0.002
C_{mT1}	0.0009
Angle of attack, α_1 (deg)	1.79
Elevator Deflection Angle, δ_{e1} (deg)	-0.69

Table 4: YAK-54 AAA Longitudinal Derivatives

Longitudinal Coefficients and Stability Derivatives-Stability Axes		
Derivatives	(1/deg)	(1/rad)
C_{Du}	0.0011	0.0630
$C_{D\alpha}$	0.0015	0.0859
C_{txu}	-0.1546	-8.858
C_{Lu}	0.0017	0.0974
$C_{L\alpha}$	0.0792	4.538
$C_{L\alpha dot}$	0.0337	1.9309
C_{Lq}	0.0899	5.1509
C_{mu}	0.0004	0.0229
$C_{m\alpha}$	-0.0065	-0.3724
$C_{m\alpha dot}$	-0.078	-4.469
C_{mq}	-0.1484	-8.503
C_{mTu}	0.0000	0.0000
$C_{mT\alpha}$	0.0005	0.0286
Longitudinal Control and Hinge Moment Derivatives-Stability Axes		
Derivatives	(1/deg)	(1/rad)
$C_{D\delta e}$	0.0000	0.0000
$C_{L\delta e}$	0.0066	0.3782
$C_{m\delta e}$	-0.0153	-0.8766

Table 5: YAK-54 AAA Lateral-Directional Derivatives

Lateral-Directional Coefficients and Stability Derivatives-Stability Axes		
Derivatives	(1/deg)	(1/rad)
$C_{l\beta}$	-0.0004	-0.0229
C_{lp}	-0.0067	-0.3839
C_{lr}	0.0009	0.0520
$C_{y\beta}$	-0.0060	-0.3438
C_{yp}	0.0001	0.0060
C_{yr}	0.0041	0.2349
$C_{n\beta}$	0.0017	0.0974
$C_{nT\beta}$	-0.0001	-0.0057
C_{np}	-0.0003	-0.0172
C_{nr}	-0.0020	-0.1150
Lateral-Directional Control and Hinge Moment Derivatives-Stability Axes		
Derivatives	(1/deg)	(1/rad)
$C_{l\delta a}$	0.0061	0.3495
$C_{l\delta r}$	0.0003	0.0172
$C_{y\delta a}$	0.0000	0.0000
$C_{y\delta r}$	0.0034	0.1900
$C_{n\delta a}$	-0.0020	-0.1146
$C_{n\delta r}$	-0.0017	-0.0974

Table 6: YAK-54 AAA Stability Requirements

Type of Stability	Corresponding Derivatives	Criterion	Derivative (deg^{-1})	Stable/Unstable
Forward Speed	$C_{Txu} - C_{Du}$	< 0	-0.1557	Stable
Sideslip	$C_{y\beta}$	< 0	-0.3462	Stable
Vertical Speed	$C_{L\alpha}$	> 0	4.7625	Stable
Angle of Attack	$C_{m\alpha}$	< 0	-0.3813	Stable
Angle of Sideslip	$C_{n\beta}$	> 0	0.0954	Stable
Roll Rate	C_{lp}	< 0	-0.3817	Stable
Pitch Rate	C_{mq}	< 0	-10.040	Stable
Yaw Rate	C_{nr}	< 0	-0.1161	Stable
Lateral	$C_{l\beta}$	< 0	-0.0257	Stable

7.2   VORSTAB Modeling of the YAK-54

A YAK-54 input file was created for VORSTAB. This input file can be found in Appendix A. The input file modeled the entire aircraft include all three lifting surfaces and the fuselage. Table 7 shows the lift, drag, pitching moment coefficients, and how those three coefficients are affected by pitch rate. Due to the assumption that the flow stays attached to the body, there is not a stall point for this model. Figure 4 through Figure 7 shows Table 7 in graphical form.

Table 7: YAK-54 VORSTAB Longitudinal Coefficient and Pitch Rate (1/rad)

α (deg)	C_L	C_D	C_M	C_{Lq}	C_{Dq}	C_{Mq}
-5	-0.376	0.025	-0.205	8.95	0.000	-10.6
0	0.013	0.020	-0.219	8.84	0.000	-10.1
5	0.438	0.021	-0.317	8.36	0.000	-8.99
10	0.820	0.034	-0.409	8.63	0.000	-10.2
15	1.14	0.075	-0.476	8.22	0.000	-9.95
20	1.40	0.142	-0.548	7.63	0.000	-9.43
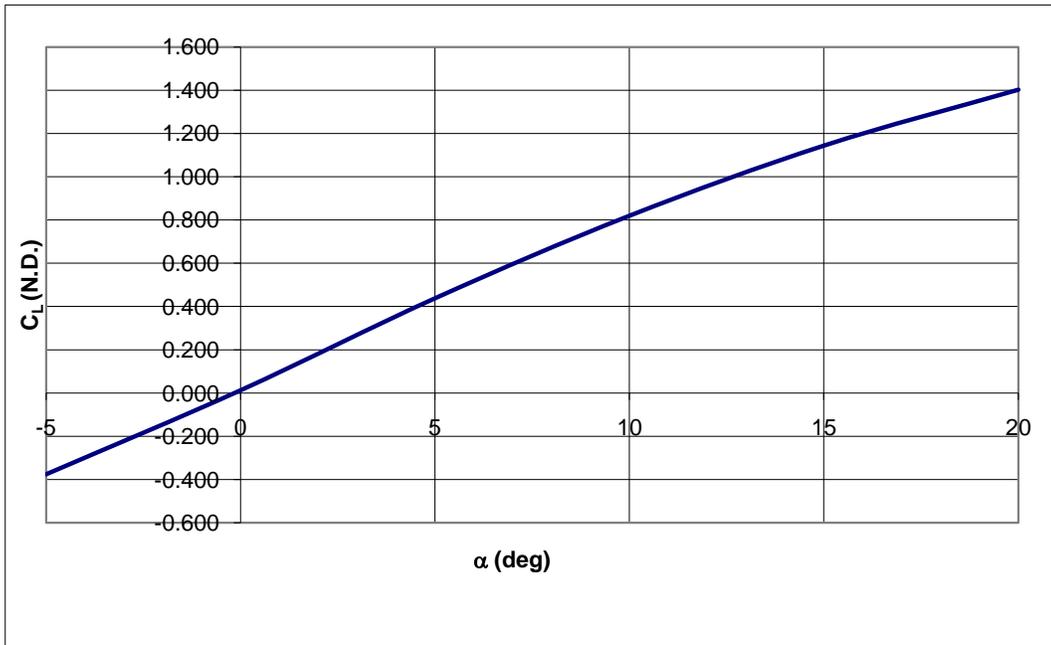
Figure 4: YAK-54 VORSTAB Lift Curve Slope
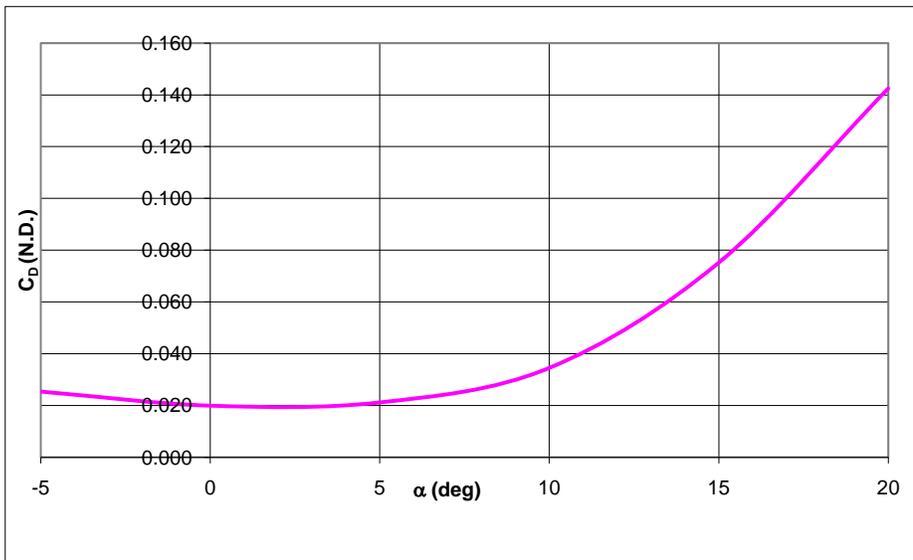
Figure 5: YAK-54 VORSTAB Drag Curve
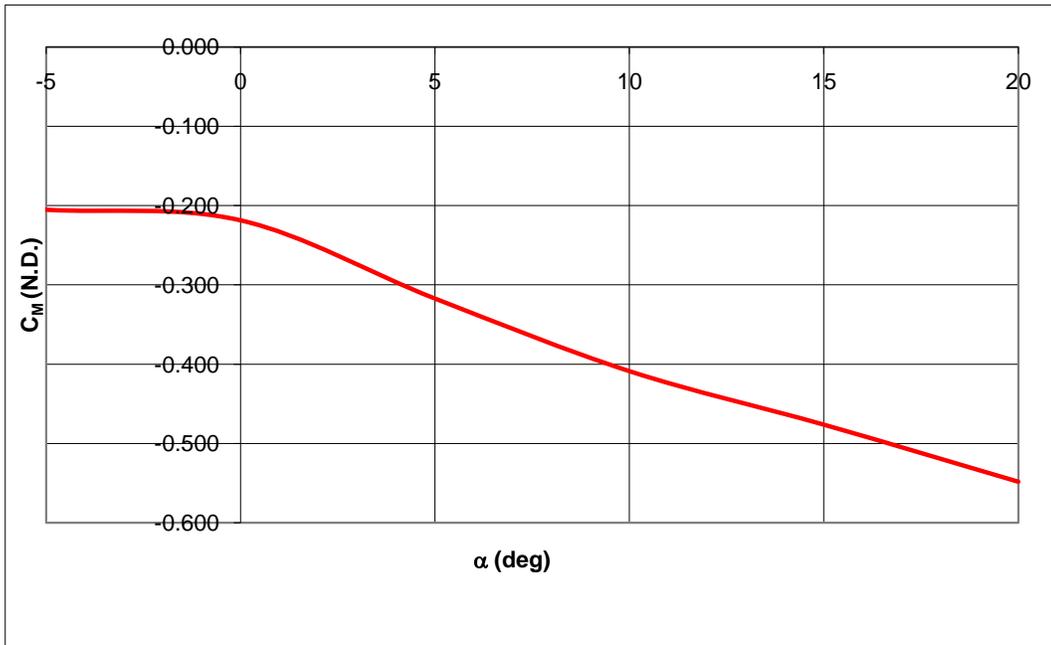
Figure 6: YAK-54 VORSTAB Pitching Moment Coefficient Curve
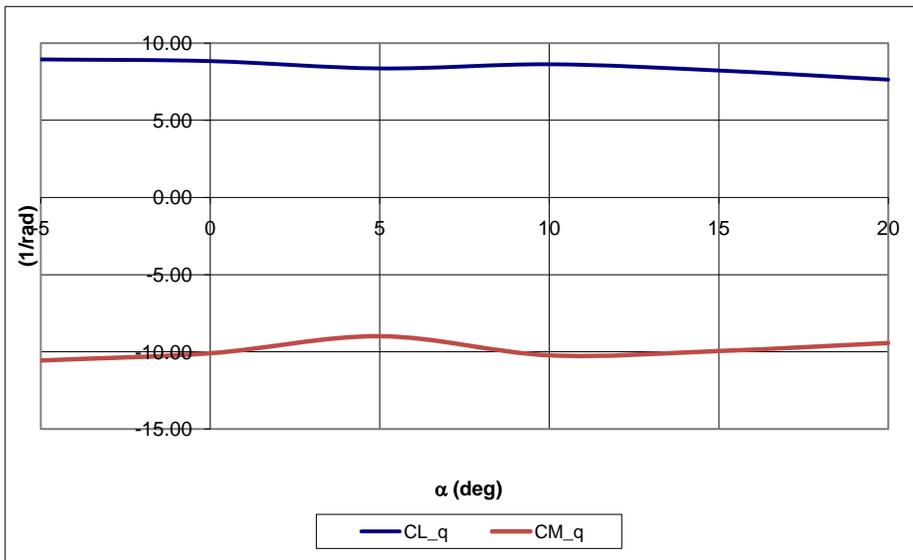
Figure 7: YAK-54 VORSTAB Longitudinal Derivatives

The longitudinal derivatives produced by VORSTAB follow the expected trends. For example, the pitching moment curve has a negative slope. This slope makes the aircraft naturally want to pitch back to the stability axes. These values were also within the range that one would expect to see. The drag, C_{Do}, is lower than the AAA results predicted. This is expected since AAA overestimates the drag at lower Reynolds number. AAA approximation was 0.0313 and VORSTAB estimates it to be 0.013, this is a significant change. The drag is known to be lower than the AAA results due the fact that AAA says the aircraft must be trimmed at a higher throttle setting, approximately 45%, and from the flight tests it is trimmed at, approximately 27% throttle setting. The magnitudes of these values might be off slightly off, but the coefficients follow the correct trend. Table 8 shows the lateral-directional derivatives due to sideslip, roll rate, and yaw rate. Figure 8 through Figure 10 depict these lateral-directional derivatives in graphical form.

Table 8: YAK-54 VORSTAB Lateral-Directional Derivatives (1/rad)

α (deg)	C_{y_β}	C_{l_β}	C_{n_β}	C_{y_p}	C_{l_p}	C_{n_p}	C_{y_r}	C_{l_r}	C_{n_r}
-5	-0.403	-0.021	0.187	-0.013	-0.213	-0.045	0.433	-0.011	-0.196
0	-0.497	-0.030	0.220	-0.046	-0.218	-0.023	0.486	0.032	-0.229
5	-0.531	-0.050	0.249	-0.016	-0.233	-0.070	0.531	0.082	-0.250
10	-0.506	-0.065	0.264	-0.018	-0.198	-0.078	0.558	0.105	-0.251
15	-0.437	-0.064	0.262	-0.010	-0.171	-0.086	0.570	0.108	-0.238
20	-0.363	-0.068	0.249	-0.001	-0.154	-0.090	0.563	0.111	-0.211
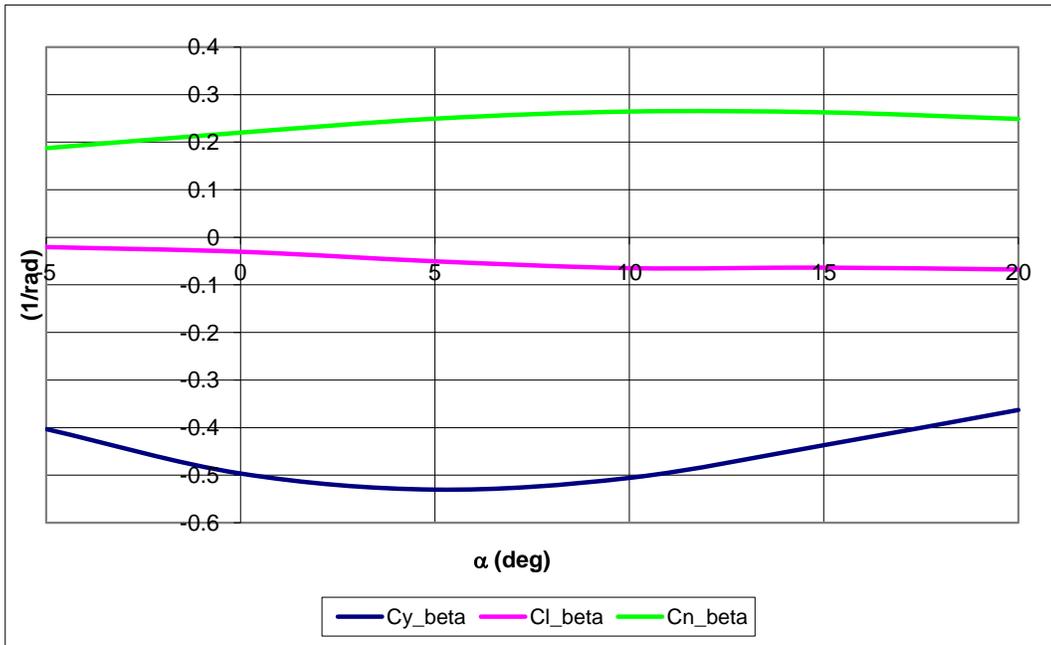
Figure 8: YAK-54 VORSTAB Lateral-Directional Derivatives due to Sideslip
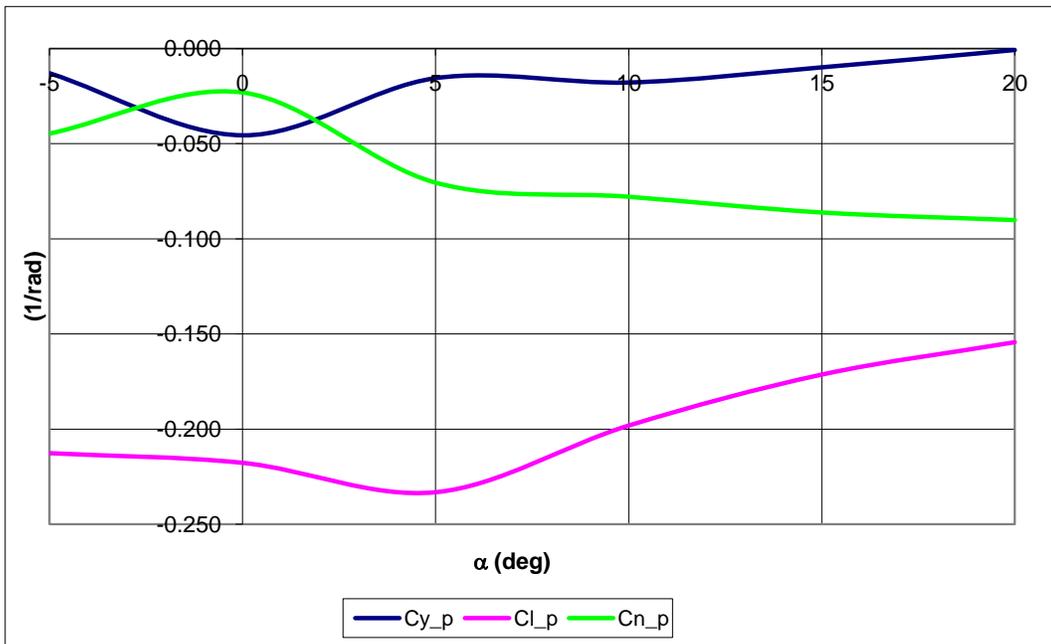
Figure 9: YAK-54 VORSTAB Lateral-Directional Derivatives due to Roll Rate
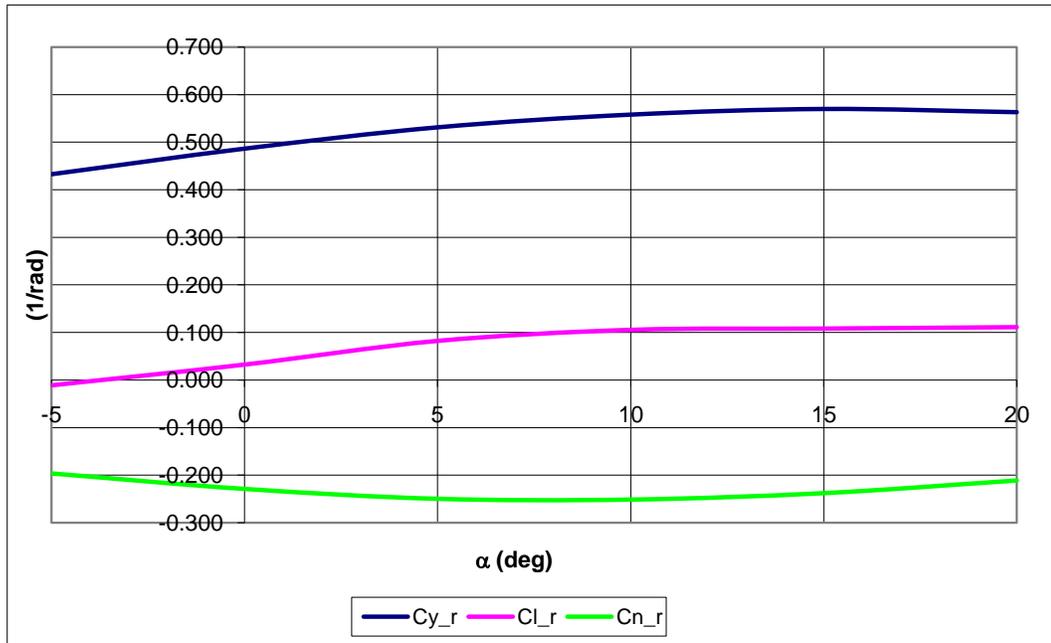
Figure 10: YAK-54 VORSTAB Lateral-Directional Derivatives due to Yaw Rate

Similar to the longitudinal derivatives, the lateral-directional derivatives follow an expected trend. All of the coefficients have the correct positive or negative value, except for rolling moment coefficient due to yaw rate at an angle of attack of -5˚. This coefficient would always be positive when the aircraft has flow that is attached to the fuselage, because the fuselage contribution outweighs the vertical tail contribution. Vertical tail contribution can be negative or positive. Again, the magnitudes might be slightly off, but the in the expected range. Both longitudinal and lateral-directional derivatives change when the control surfaces are deflected. Table 9 shows the lateral-directional derivatives due to aileron deflection, Table 10 shows the longitudinal derivatives due to elevator deflection, and Table 11 shows the lateral-directional derivatives due to rudder deflection. These control surface deflection derivatives can be seen in Figure 11 through Figure 19.

Table 9: YAK-54 VORSTAB Lateral-Directional Due to Aileron Deflection (1/rad)

α (deg)	δ_a	C_y	C_l	C_n
0	-10	0.0009	-0.0240	-0.0054
5	-10	-0.0013	-0.0221	-0.0027
10	-10	-0.0041	-0.0243	0.0003
15	-10	-0.0077	-0.0224	0.0040
20	-10	-0.0103	-0.0176	0.0073
0	-5	-0.0054	-0.0120	0.0019
5	-5	-0.0070	-0.0110	0.0035
10	-5	-0.0083	-0.0121	0.0049
15	-5	-0.0093	-0.0111	0.0061
20	-5	-0.0099	-0.0087	0.0071
0	0	0.000	0.000	0.000
5	0	0.000	0.000	0.000
10	0	0.000	0.000	0.000
15	0	0.000	0.000	0.000
20	0	0.000	0.000	0.000
0	5	-0.0033	0.0121	0.0056
5	5	-0.0029	0.0110	0.0051
10	5	-0.0026	0.0121	0.0044
15	5	-0.0022	0.0110	0.0036
20	5	-0.0010	0.0086	0.0020
0	10	-0.0213	0.0244	0.0231
5	10	-0.0189	0.0221	0.0209
10	10	-0.0178	0.0242	0.0193
15	10	-0.0164	0.0219	0.0172
20	10	-0.0125	0.0171	0.0128
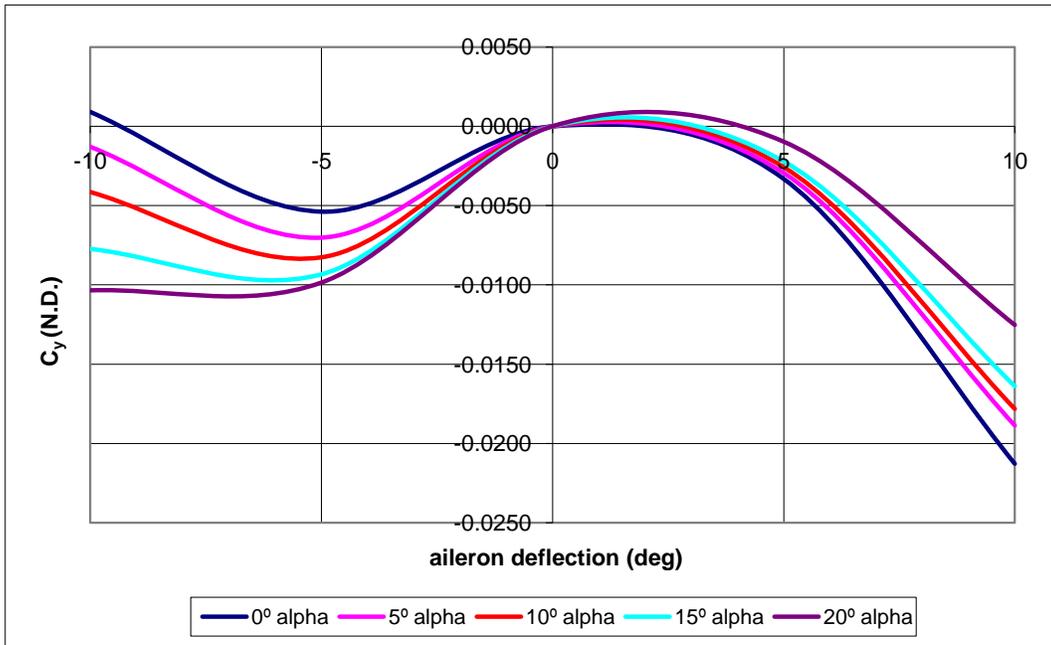
Figure 11: YAK-54 VORSTAB Sideforce Coefficient due to Aileron Deflection

Figure 12: YAK-54 VORSTAB Rolling Moment Coefficient due to Aileron Deflection

Figure 13: YAK-54 VORSTAB Yawing Moment Coefficient due to Aileron Deflection

The aileron deflection is expected to have a very small effect on the sideforce coefficient. The rolling moment controls are in close proximity to the fuselage and this can cause a rolling moment. Therefore, the VORSTAB results are not to be assumed as wrong. Conventional ailerons will usually produce a negative yawing moment, but not always. A positive aileron deflection is defined as one that produces a positive rolling moment, and this is seen in the results produced. VORSTAB shows a positive yawing moment at almost all aileron deflections. The negative yawing moment produced by the ailerons' deflection will yaw the aircraft out of an intended turn and the VORSTAB results say the opposite. Also, the yawing moment does not have symmetric results with respect to negative and positive aileron deflections. Opposite aileron deflections should result in the same magnitude, but should have opposite sign convention. VORSTAB asks for a sideslip angle to be put in the input

file and this might be the cause of the asymmetric results. Without the source code it would be difficult to determine the source for the error.   Therefore, these two asymmetrical results should be assumed wrong and ignored.

Table 10: YAK-54 VORSTAB Longitudinal Due to Elevator Deflection (1/rad)

α (deg)	δ_e	C_L	C_D	C_M
0	-12	0.0114	0.0199	-0.2153
5	-12	0.4363	0.0211	-0.3123
10	-12	0.8181	0.0350	-0.4039
15	-12	1.142	0.0757	-0.4707
20	-12	1.401	0.1430	-0.5432
0	-6	0.0121	0.0199	-0.2169
5	-6	0.4374	0.0211	-0.3148
10	-6	0.8191	0.0347	-0.4064
15	-6	1.143	0.0754	-0.4736
20	-6	1.402	0.1427	-0.5458
0	0	0.0129	0.0199	-0.2186
5	0	0.4384	0.0212	-0.3173
10	0	0.8202	0.0345	-0.4089
15	0	1.144	0.0752	-0.4764
20	0	1.403	0.1425	-0.5484
0	6	0.0136	0.0199	-0.2202
5	6	0.4394	0.0212	-0.3197
10	6	0.8213	0.0343	-0.4119
15	6	1.146	0.0749	-0.4793
20	6	1.404	0.1422	-0.5511
0	12	0.0143	0.0199	-0.2219
5	12	0.4404	0.0212	-0.3221
10	12	0.8227	0.0341	-0.4155
15	12	1.147	0.0747	-0.4821
20	12	1.405	0.1420	-0.5537
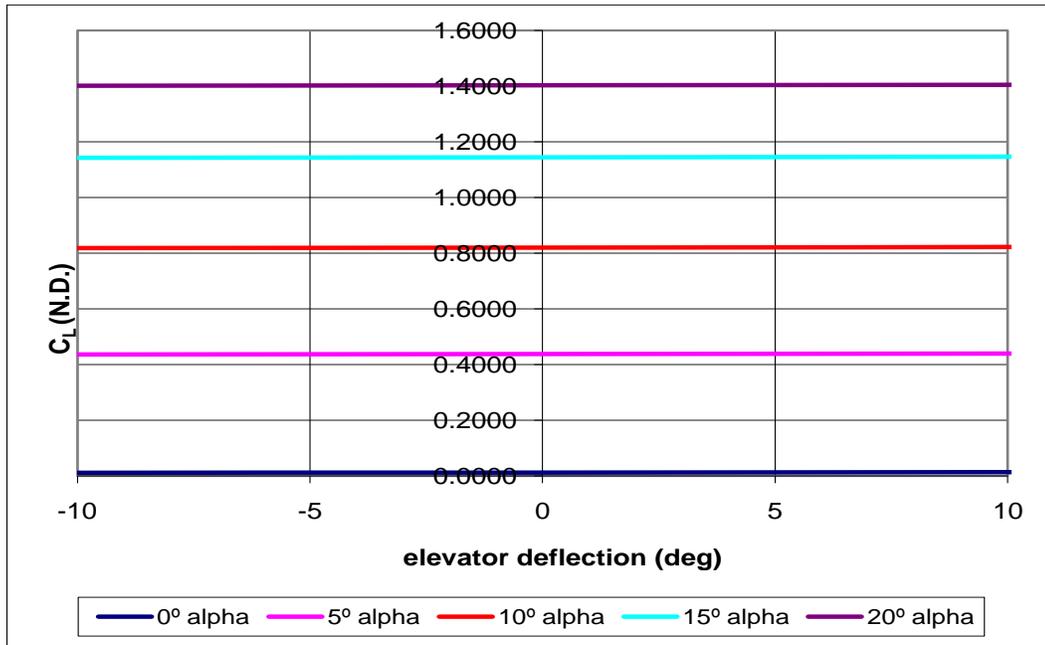
Figure 14: YAK-54 VORSTAB Lift Coefficient due to Elevator Deflection
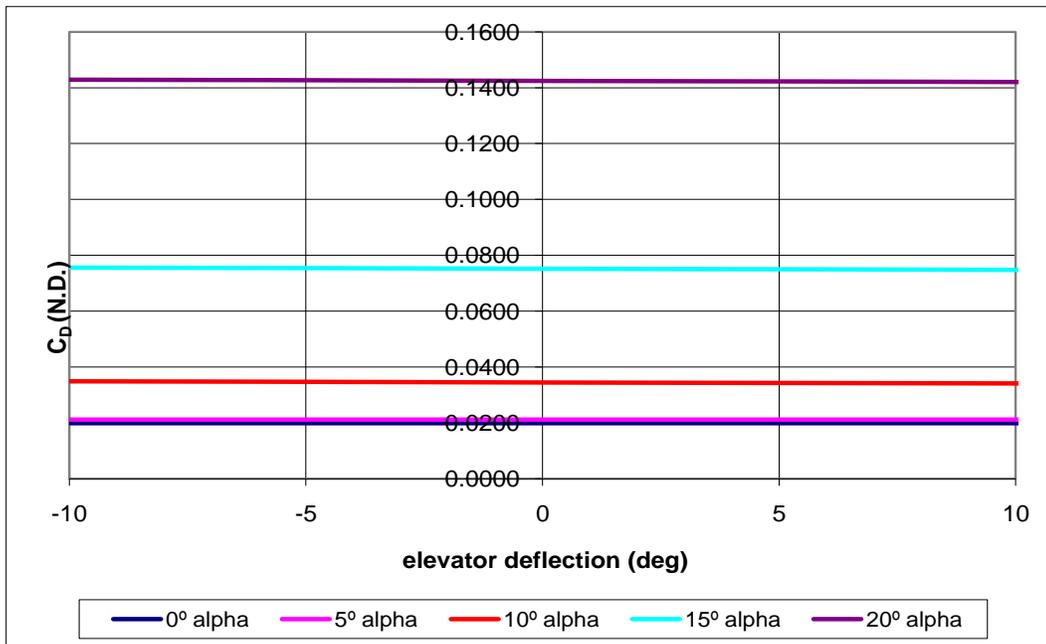
Figure 15: YAK-54 VORSTAB Drag Coefficient due to Elevator Deflection
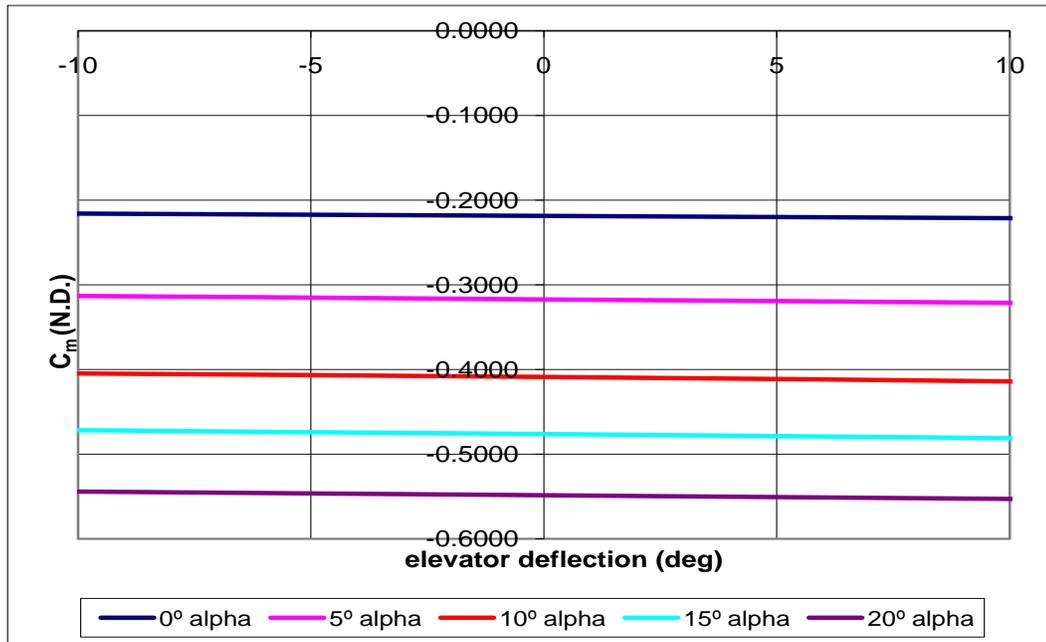
Figure 16: YAK-54 VORSTAB Pitching Moment Coefficient due to Elevator Deflection

The lift and drag coefficients are not seen to change dramatically due to elevator deflection, but this deflection will change the angle of attack. This change in angle of attack will then change the lift and drag dramatically. The pitching moment due to elevator deflection should be negative and the VORSTAB results show this. Also, the change in pitching moment seems small, but the change is large enough to change the aircraft's angle of attack.

Table 11: YAK-54 VORSTAB Lateral-Directional Due to Rudder Deflection (1/rad)

| α (deg)	δ_r	C_y	C_l	C_n
0	-10	-0.0597	-0.0033	0.0310
5	-10	-0.0591	-0.0033	0.0307
10	-10	-0.0586	-0.0032	0.0305
15	-10	-0.0576	-0.0030	0.0300
20	-10	-0.0570	-0.0029	0.0297
0	-5	-0.0300	-0.0016	0.0156
5	-5	-0.0297	-0.0017	0.0155
10	-5	-0.0295	-0.0016	0.0153
15	-5	-0.0290	-0.0015	0.0151
20	-5	-0.0287	-0.0015	0.0149
0	0	0.0000	0.0000	0.0000
5	0	0.0000	0.0000	0.0000
10	0	0.0000	0.0000	0.0000
15	0	0.0000	0.0000	0.0000
20	0	0.0000	0.0000	0.0000
0	5	0.0300	0.0016	-0.0156
5	5	0.0297	0.0017	-0.0155
10	5	0.0295	0.0016	-0.0153
15	5	0.0290	0.0015	-0.0151
20	5	0.0287	0.0015	-0.0149
0	10	0.0597	0.0033	-0.0310
5	10	0.0591	0.0033	-0.0307
10	10	0.0586	0.0032	-0.0305
15	10	0.0576	0.0030	-0.0300
20	10	0.0570	0.0029	-0.0297
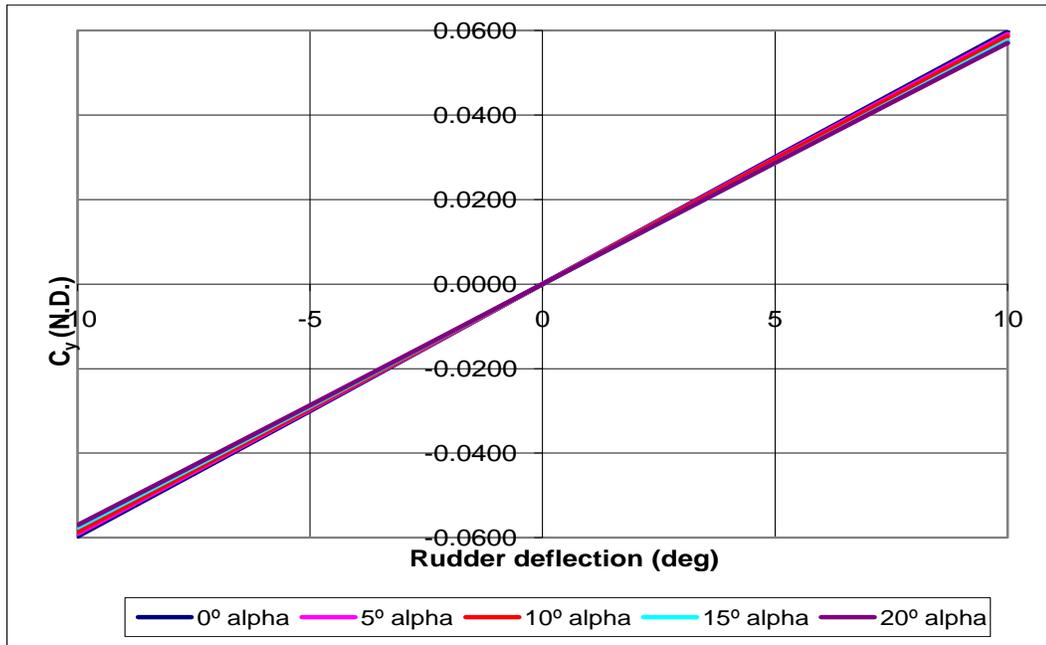
Figure 17: YAK-54 VORSTAB Sideforce Coefficient due to Rudder Deflection
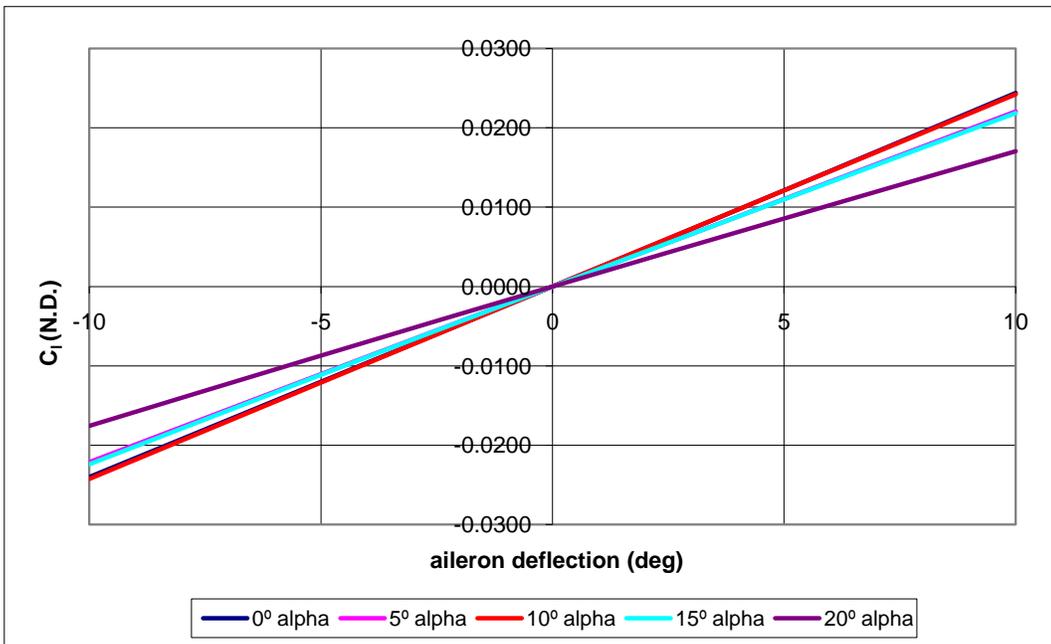

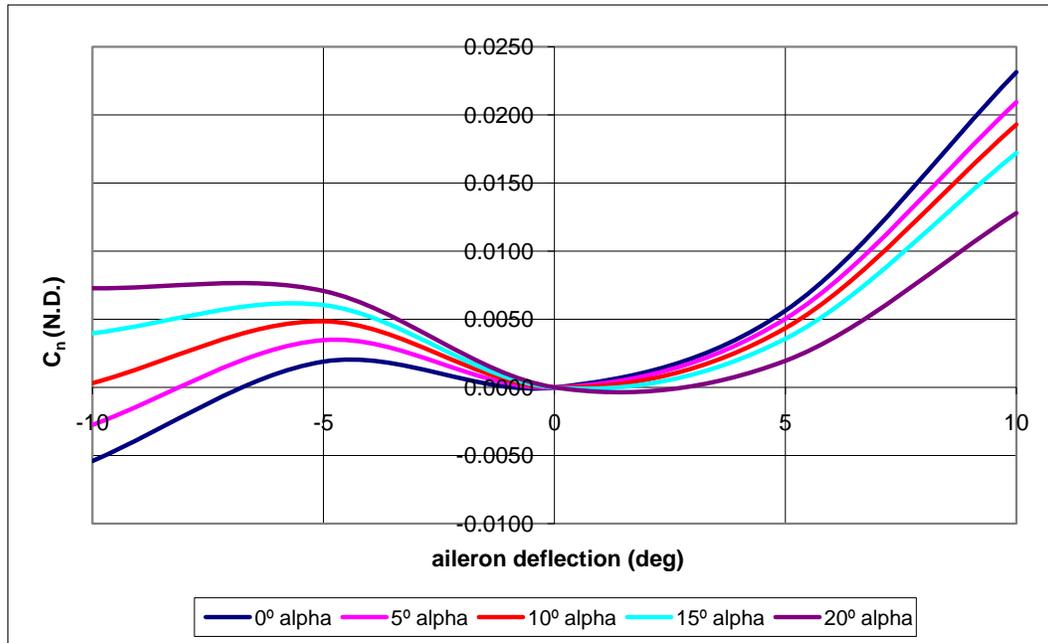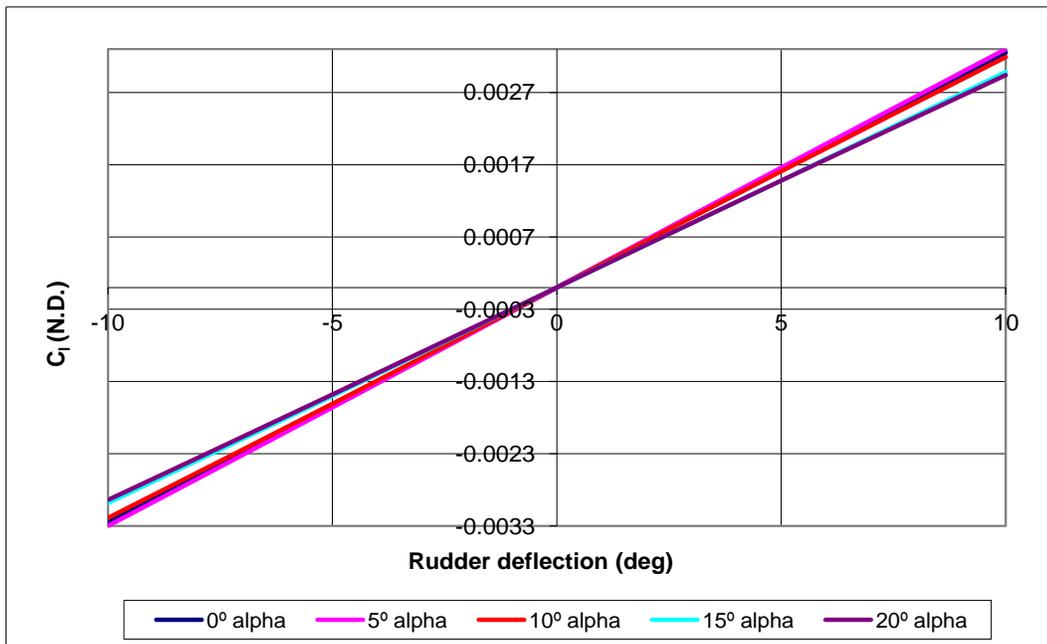**Figure 18: YAK-54 VORSTAB Rolling Moment Coefficient due to Rudder Deflection**
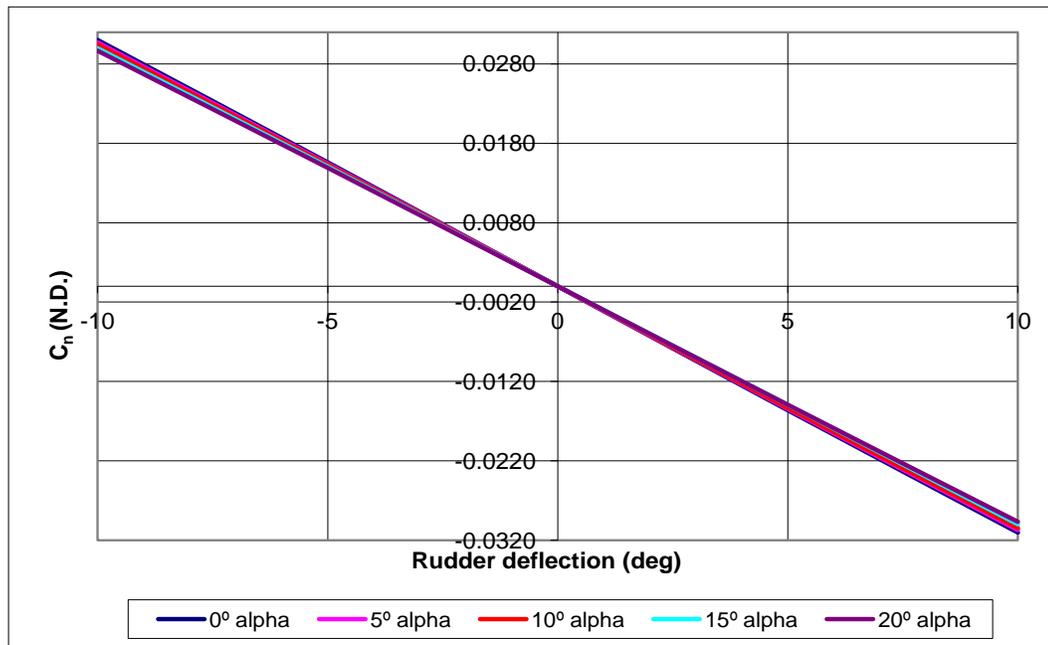
Figure 19: YAK-54 VORSTAB Yawing Moment Coefficient due to Rudder Deflection

A positive rudder defection will produce a positive sideforce as expected, and vice-versa. The rolling moment is a direct result of the sideforce, and therefore, a positive rudder deflection will also result in a positive rolling moment. A negative yawing moment is produced by a positive rudder deflection.

The VORSTAB stability requirements are shown in Table 12. As seen from this table, the YAK-54 is stable in all modes. The stability requirements were only found at the 0˚ angle of attack, and could be unstable at different positions. From reviewing the previous results from VORSTAB, it can be assumed that the aircraft is stable in all flight conditions.

Table 12: YAK-54 VORSTAB Stability Requirements

Type of Stability	Corresponding Derivatives	Criterion	Derivative (rad^{-1})	Stable/Unstable
Sideslip	$C_{y\beta}$	< 0	-0.4968	Stable
Vertical Speed	$C_{L\alpha}$	> 0	4.8762	Stable
Angle of Attack	$C_{m\alpha}$	< 0	-1.1314	Stable
Angle of Sideslip	$C_{n\beta}$	> 0	0.2200	Stable
Roll Rate	C_{lp}	< 0	-0.2178	Stable
Pitch Rate	C_{mq}	< 0	-10.090	Stable
Yaw Rate	C_{nr}	< 0	-0.2289	Stable
Lateral	$C_{l\beta}$	< 0	-0.0304	Stable

As seen from these results produced by VORSTAB, the YAK-54 is a stable aircraft with a large amount of control. This is expected since it is a remote controlled aircraft. The lift curve slope of the results was found to be 4.8762 rad^{-1}. This derivative was found from 0˚ to 5˚ angles of attack, since this was the most linear section of the curve. The aircraft is known to not stall at these angles also. Characterizing the drag and pitching moment due to angle of attack into a single number is more difficult than lift, since these two coefficients are not linear curves. The same range of angles of attack was used for the other two derivatives. The drag derivative, $C_{D\alpha}$, is 0.0144 rad^{-1} and the pitching moment derivative, $C_{m\alpha}$, is -1.1314 rad^{-1}. All other derivatives were determined at 0˚ angle of attack. The results from VORSTAB and AAA will be discussed and compared in more detail in the following section.

7.3 Method Comparison YAK-54

Both AAA and VORSTAB are considered as an accurate approximation for the control derivatives. Using a computational fluid dynamic method such as VORSTAB should produce results closer to that of the actual data than results from DATCOM and AAA. As stated previously, the VORSTAB results were found over an angle of attack range of 0˚ to 5˚. Table 13 shows the comparison data for the YAK-54 for AAA and VORSTAB. The tuned AAA results were derived after several flight tests were conducted, and the system identification warranted an improved model. These turned values were taken from Ref [14] and explanation for deriving them can be found there.

Table 13: YAK-54 AAA and VORSTAB Stability and Control Comparison

Stability and Control Derivatives					
Derivative (1/rad)	AAA	AAA Tuned	VORSTAB	% Difference AAA	% Difference AAA Tuned
$C_{L\alpha}$	4.5380	4.538	4.8762	7.45	7.45
$C_{D\alpha}$	0.0859	0.0859	0.0144	-83.24	-83.24
$C_{m\alpha}$	-0.3724	-0.3724	-1.1314	203.81	203.81
C_{Lq}	5.1509	5.1509	8.8411	71.64	71.64
C_{mq}	-8.5030	-16.1064	-10.090	18.66	-37.35
$C_{l\beta}$	-0.0229	0.022	-0.0304	32.75	-238.18
C_{lp}	-0.3839	-0.5858	-0.2178	-43.27	-62.82
C_{lr}	0.0520	0.0743	0.0323	-37.88	-56.53
$C_{y\beta}$	-0.3438	-0.2707	-0.4968	44.50	83.52
C_{yp}	0.0060	0.0194	-0.0455	-858.33	-334.54
C_{yr}	0.2349	0.2531	0.4865	107.11	92.22
$C_{n\beta}$	0.0974	0.1052	0.2200	125.87	109.13
C_{np}	-0.0172	-0.0387	-0.0231	34.30	-40.31
C_{nr}	-0.1150	-0.289	-0.2289	99.04	-20.80
$C_{L\delta e}$	0.3782	0.3782	0.0071	-98.12	-98.12
$C_{D\delta e}$	0.0000	0.0000	0.0000	0.00	0.00
$C_{m\delta e}$	-0.8766	-1.2289	-0.0158	-98.20	-98.71
$C_{l\delta a}$	0.3495	0.3707	0.1388	-60.29	-62.56
$C_{l\delta r}$	0.0172	0.0219	0.0188	9.30	-14.16
$C_{y\delta a}$	0.0000	0.0000	-0.0379	-----	-----
$C_{y\delta r}$	0.1948	0.2228	0.3441	76.64	54.44
$C_{n\delta a}$	-0.1146	-0.0088	0.0646	-156.37	-834.09
$C_{n\delta r}$	-0.0974	-0.1404	-0.1789	83.68	27.42

Several of the differences between the AAA and VORSTAB results fall within the error ranges given by Dr. Roskam. The differences that are in the 100 of percents do not fall within the error range though. The tuned AAA results improved

in some cases and not in others. These derivatives, C_{nr}, $C_{n\delta r}$, $C_{l\beta}$, C_{mq}, and $C_{m\delta e}$ were tuned from the flight test and the others were taken from the AVL model. The tuned yawing moment derivatives show an improvement in the VORSTAB results over AAA. More flight tests need to be conducted and parameter system identification need to be conducted to improve all of the derivatives.

Both methods show that the aircraft is stable. For stability and control derivatives, there are typical ranges that can be expected, and through his vast experience, Dr. Jan Roskam developed ranges for the control derivatives. These ranges are for conventional aircraft, and the ranges are a function of Mach number. Table 14 shows the Dr. Roskam, Ref. [1], typical ranges compared to the AAA and VORSTAB results.

Table 14: YAK-54 Stability and Control Derivatives Typical Ranges

Stability and Control Derivatives					
Derivative (1/rad)	VORSTAB	AAA	Typical Range	Within Range (Yes/No)	
			Dr. Roskam	VORSTAB	AAA
$C_{L\alpha}$	4.8762	4.5380	1.0 to 8.0	Yes	Yes
$C_{D\alpha}$	0.0144	0.0859	0.0 to 2.0	Yes	Yes
$C_{m\alpha}$	-1.1314	-0.3724	-4.0 to 1.0	Yes	Yes
C_{Lq}	8.8411	5.1509	0.0 to 30.0	Yes	Yes
C_{mq}	-10.09	-8.5030	-90.0 to 0.0	Yes	Yes
$C_{l\beta}$	-0.0304	-0.0229	0.1 to -4.0	Yes	Yes
C_{lp}	-0.2178	-0.3839	-0.1 to -0.8	Yes	Yes
C_{lr}	0.0323	0.0520	0.0 to 0.6	Yes	Yes
$C_{y\beta}$	-0.4968	-0.3438	-0.1 to -2.0	Yes	Yes
C_{yp}	-0.0455	0.0060	-0.3 to 0.8	Yes	Yes
C_{yr}	0.4865	0.2349	0.0 to 1.2	Yes	Yes
$C_{n\beta}$	0.2200	0.0974	0.0 to 4.0	Yes	Yes
C_{np}	-0.0231	-0.0172	-0.5 to 0.1	Yes	Yes
C_{nr}	-0.2289	-0.1150	0.0 to -1.0	Yes	Yes
$C_{L\delta e}$	0.0071	0.3782	0.0 to 0.6	Yes	Yes
$C_{D\delta e}$	0.0000	0.0000	Negligible	Yes	Yes
$C_{m\delta e}$	-0.0158	-0.8766	0.0 to -4.0	Yes	Yes
$C_{l\delta a}$	0.1388	0.3495	0.0 to 0.4	Yes	Yes
$C_{l\delta r}$	0.0188	0.0172	-0.04 to 0.04	Yes	Yes
$C_{y\delta a}$	-0.0379	0.0000	Negligible	Yes	Yes
$C_{y\delta r}$	0.3441	0.1948	0.0 to 0.5	Yes	Yes
$C_{n\delta a}$	0.0646	-0.1146	-0.08 to 0.08	Yes	Yes
$C_{n\delta r}$	-0.1789	-0.0974	-0.15 to 0.0	No	Yes

The YAK-54 VORSTAB results fall within all of the typical ranges that Dr. Roskam developed except for the yawing moment coefficient due to rudder deflection, $C_{n\delta r}$. These ranges are just estimations and many aircraft's derivatives do

not fall into the ranges. The ranges just give the designer an idea of things to expect. Also, the sideforce moment coefficient due to aileron deflection, $C_{y_{\delta a}}$, is not negligible. This can happen when the rolling moment controls are in close proximity to a vertical surface (fuselage or vertical tail). The ailerons, on the YAK-54, are in close proximity to the fuselage, and this causes the coefficient to be a non-negligible value. The AAA results all fall within the typical ranges. From these results, it is concluded that both programs obtained valid results. These results should be compared to the more flight test data to validate both software programs. A model should be created with the new flight test data and then compared to the AAA and VORSTAB results.

7.4   Linearized Model of the YAK-54

For the information and data on the state space model please refer to Appendix B.

8   MantaHawk

The MantaHawk is a remote control aircraft designed at the University of Kansas, by the AE 721 graduate design course in the fall 2009. The design team consisted of Emily Arnold, Robert Burns, Dustin Grorud, Katrina Legursky, Rick Riley, Dave Royer, and Jonathan Tom. This small UAV was developed in conjunction with the CReSIS Meridian project. MantaHawk's size and weight were well suited for a sea-born launch with a much shorter range than the other Meridian Antarctic mission. The goal of the team was to help improve the current research going on at the University of Kansas and within CReSIS itself.

After much was research conducted by the team, a wing-body configuration was chosen as the most suitable configuration for the particular mission. The design of the MantaHawk followed the Dr. Roskam method using AAA ,and AVL for some of the stability and control derivatives that AAA did not produce. Class II design resulted in an empty weight of 32 lbs for the vehicle with a design cruise speed of 70 kts. The vehicle had a payload capacity of 15 lbs plus 7 lbs of fuel. This aircraft was a prototype and had its problems. Soon after take-off, the aircraft pitched downward aggressively, and this caused the airplane to go into a nose dive. With post flight analysis, the team determined that a negative pitching moment was much higher than predicted and without pre-flight trim there was not enough control to fly. Figure 20 shows the MantaHawk designed by the AE 721 class, Ref [15]. The design and flight test of the MantaHawk can be found in Ref [15].

Figure 20: MantaHawk

8.1   AAA Modeling of the MantaHawk

Unlike the YAK-54, the MantaHawk was designed at the University of Kansas using AAA software. The MantaHawk's AAA model estimated the stability and control derivatives, but this vehicle was never a proven platform. Table 15 and Table 16 shows the stability and control derivatives produced by AAA, Ref [15]. Table 17 shows the AAA stability requirements for the MantaHawk, Ref [15].

Table 15: MantaHawk AAA Longitudinal Derivatives

Longitudinal Coefficients and Stability Derivatives-Stability Axes	
Derivatives	(1/rad)
C_{Du}	0.0000
$C_{D\alpha}$	0.0615
C_{Dq}	0.0000
C_{Txu}	0.0000
C_{Lu}	0.0021
$C_{L\alpha}$	3.9630
C_{Lq}	5.0920
C_{mu}	0.0000
$C_{m\alpha}$	-0.4034
C_{mq}	-4.7340
C_{mTu}	0.0000
$C_{mT\alpha}$	-0.2050
$C_{D\delta el}$	0.4209
$C_{L\delta el}$	0.4784
$C_{m\delta el}$	-1.0630

Table 16: MantaHawk AAA Lateral-Directional Derivatives

Lateral-Directional Coefficients and Stability Derivatives-Stability Axes	
Derivatives	(1/rad)
$C_{l\beta}$	-0.0817
C_{lp}	-0.4892
C_{lr}	0.0407
$C_{y\beta}$	-0.1877
C_{yp}	-0.1249
C_{yr}	0.0897
$C_{n\beta}$	0.0359
$C_{nT\beta}$	0.0007
C_{np}	-0.0169
C_{nr}	-0.0219
$C_{y\delta el}$	0.0012
$C_{l\delta el}$	0.3588
$C_{n\delta el}$	-0.0055

Table 17: MantaHawk AAA Stability Requirements

Type of Stability	Corresponding Derivatives	Criterion	Derivative (rad^{-1})	Stable/Unstable
Sideslip	$C_{y\beta}$	< 0	-0.1877	Stable
Vertical Speed	$C_{L\alpha}$	> 0	3.9630	Stable
Angle of Attack	$C_{m\alpha}$	< 0	-0.4034	Stable
Angle of Sideslip	$C_{n\beta}$	> 0	0.0359	Stable
Roll Rate	C_{lp}	< 0	-0.4892	Stable
Pitch Rate	C_{mq}	< 0	-4.7340	Stable
Yaw Rate	C_{nr}	< 0	-0.0219	Stable
Lateral	$C_{l\beta}$	< 0	-0.0817	Stable

According to AAA, the MantaHawk is stable in all modes and should not have a problem in flight. These results gave the flight test team confidence going into the

first flight. Shortly after liftoff, the aircraft nosed into the ground. The wreck raised concern and prompted a VORSTAB model to be produced to determine if the vehicle was actually stable in all modes.

8.2   VORSTAB Modeling of the MantaHawk

The MantaHawk was a flying wing that used three different airfoil shapes throughout the wing. There were also large wingtips that were used to help prevent wingtip vortices and wingtip stall. Since it was a flying wing, the VORSTAB model did not include a fuselage, but rather just one lifting surface and one control surface. A symmetrical deflection of the control surface, elevon, imitates an elevator input, and an asymmetrical deflection imitates a rudder or aileron input. The VORSTAB input file for the MantaHawk can be found in Appendix A. Table 18 shows the longitudinal derivatives for the MantaHawk. Figure 21 through Figure 25 depict Table 18 in graphical form.

Table 18: MantaHawk VORSTAB Longitudinal Derivatives (1/rad)

α (deg)	C_L	C_D	C_m	C_{Lq}	C_{Dq}	C_{mq}
-5	-0.1683	0.0119	-0.0167	1.9478	0.0000	-1.6498
0	0.0377	0.0068	0.0006	1.9645	0.0000	-1.6625
5	0.2603	0.0092	0.0159	1.9365	0.0000	-1.6498
10	0.4760	0.0154	0.0217	1.8694	0.0000	-1.6052
15	0.6123	0.0366	0.0271	1.7585	0.0000	-1.5442
20	0.6709	0.0763	0.0256	1.6138	0.0000	-1.4615
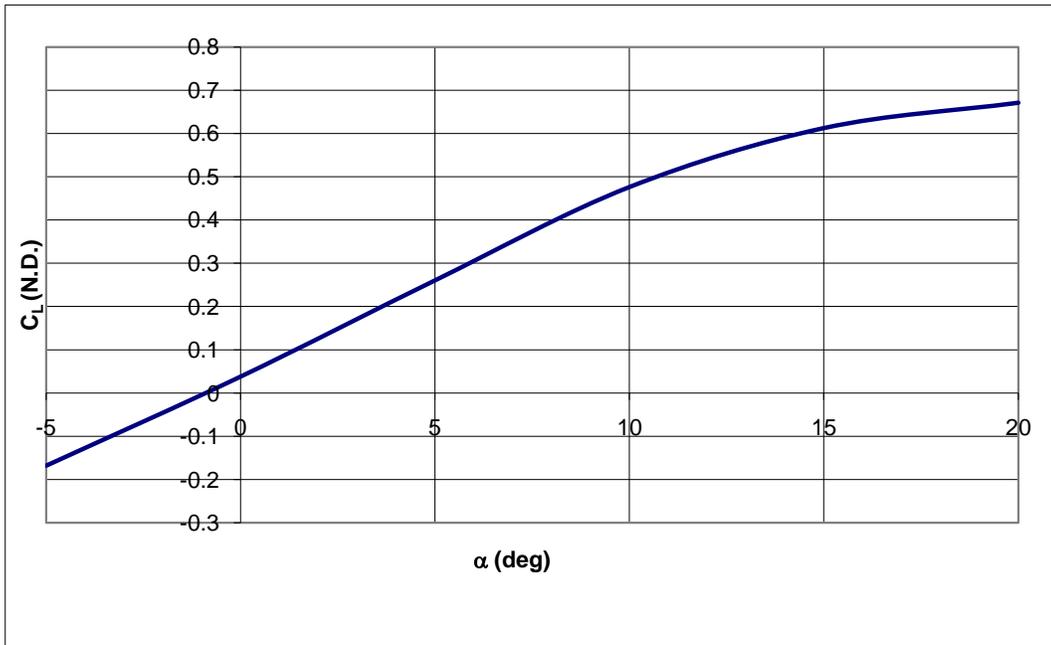
Figure 21: MantaHawk VORSTAB Lift Coefficient
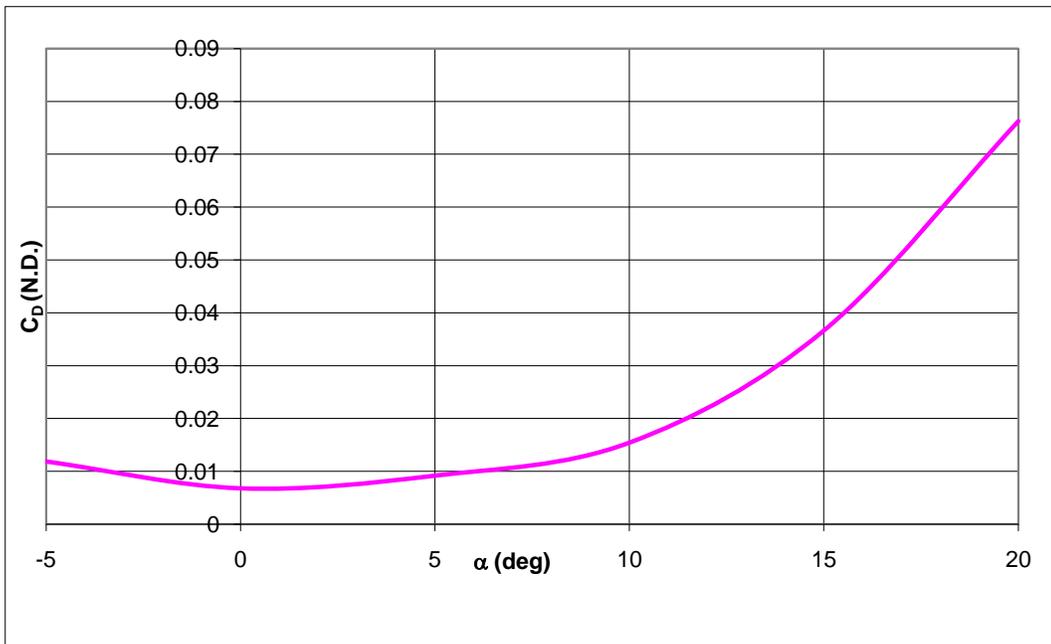
Figure 22: MantaHawk VORSTAB Drag Coefficient
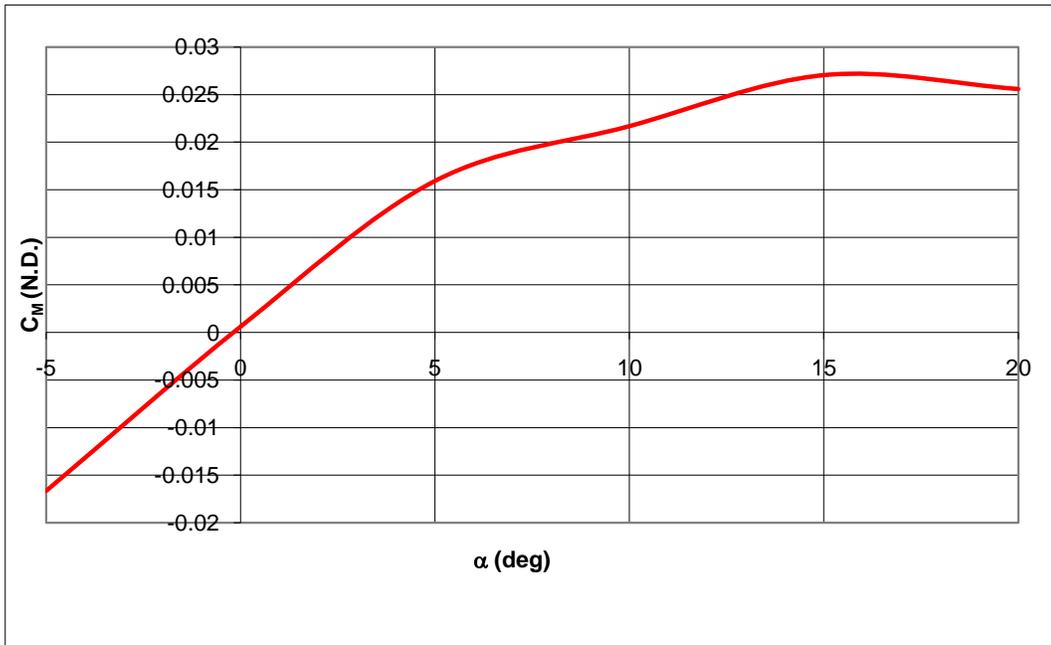
Figure 23: MantaHawk VORSTAB Pitching Moment Coefficient
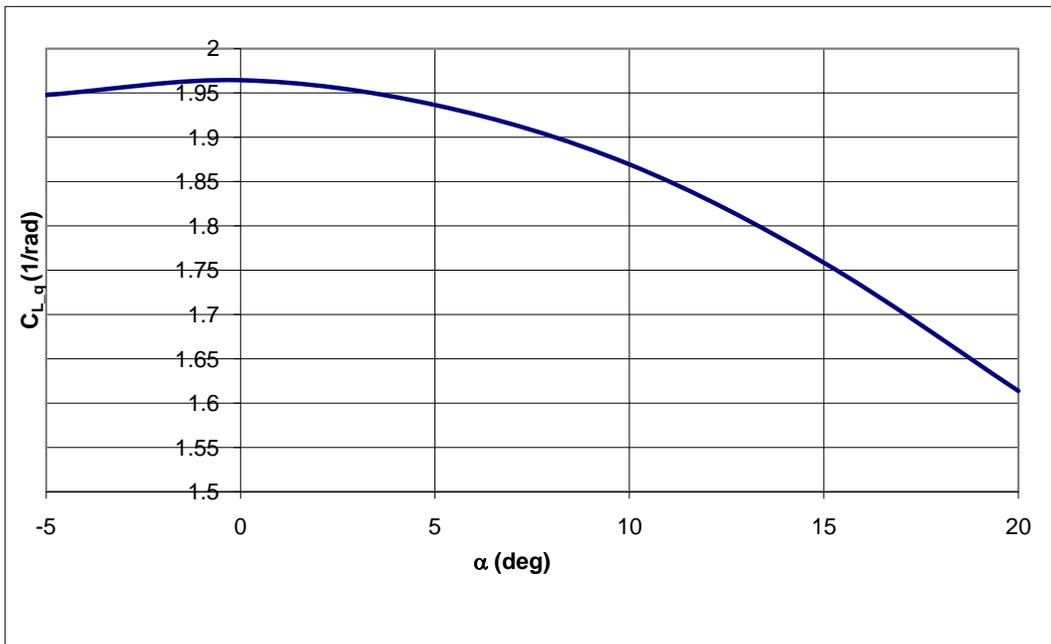
Figure 24: MantaHawk VORSTAB Lift Coefficient due to Pitch Rate
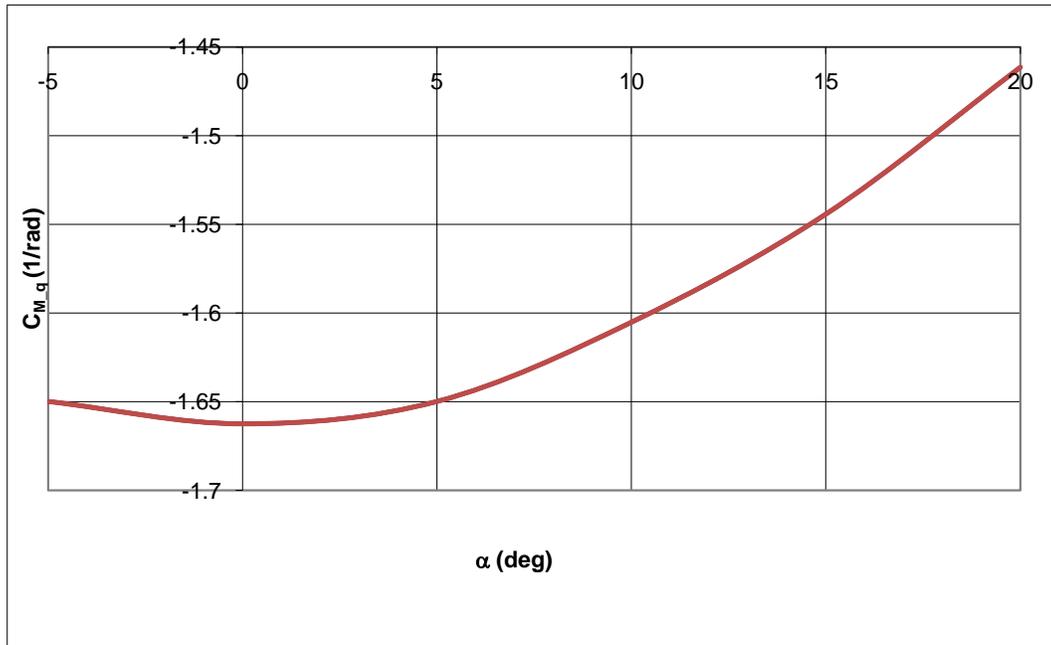
Figure 25: MantaHawk VORSTAB Pitching Moment Coefficient due to Pitch Rate

As seen from the pitching moment curve, there is a positive slope. This means that the aircraft is naturally unstable. When the aircraft is pitched upward, it will not pitch back downward, but rather continue pitching upward. The other longitudinal derivatives were as expected. With this information the flight test team would have exercised more caution during the testing of the vehicle. The drag, C_{Do}, estimated by VORSTAB was 0.0068 and AAA estimated it to be 0.022. This is also a very significant difference and should be investigated. In reality, the drag is most likely between these two software programs. VORSTAB only determines the pressure drag and not the viscous drag. This is why the VORSTAB drag results are lower than what flight test data should show. The overall lift coefficient for the aircraft is rather small, but the drag is very low for this aircraft. Pitching moment coefficient due to pitch rate is typically large, because it is proportional to the square

of the moment arm of the horizontal tail. The MantaHawk is a flying wing, so the

moment arm is not as large as a conventional aircraft and this is why the derivative is

not very large. Table 19 shows the lateral-directional derivatives. Figure 26 through

Figure 28 depicts these derivatives in graphical form.

Table 19: MantaHawk VORSTAB Lateral-Directional Derivatives (1/rad)

α (deg)	$C_{y\beta}$	$C_{l\beta}$	$C_{n\beta}$	C_{yp}	C_{lp}	C_{np}	C_{yr}	C_{lr}	C_{nr}
-5	-0.098	-0.016	0.021	-0.082	-0.287	0.072	0.036	-0.011	-0.004
0	-0.117	-0.048	0.018	-0.054	-0.287	-0.0003	0.047	0.020	-0.008
5	-0.090	-0.082	0.009	0.071	-0.283	-0.057	0.053	0.055	-0.003
10	-0.034	-0.107	-0.002	0.061	-0.261	-0.0996	0.061	0.084	0.006
15	0.033	-0.091	-0.011	0.033	-0.165	-0.086	0.056	0.078	0.016
20	0.060	-0.064	-0.015	0.004	-0.083	-0.065	0.056	0.054	0.020
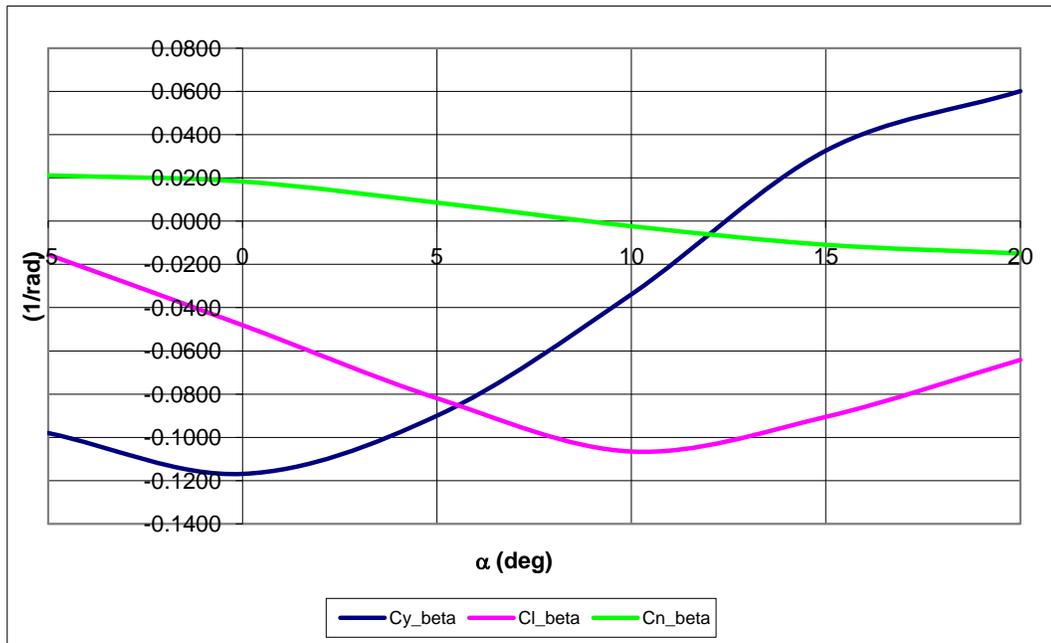
Figure 26: MantaHawk VORSTAB Lateral-Directional Derivatives due to Sideslip
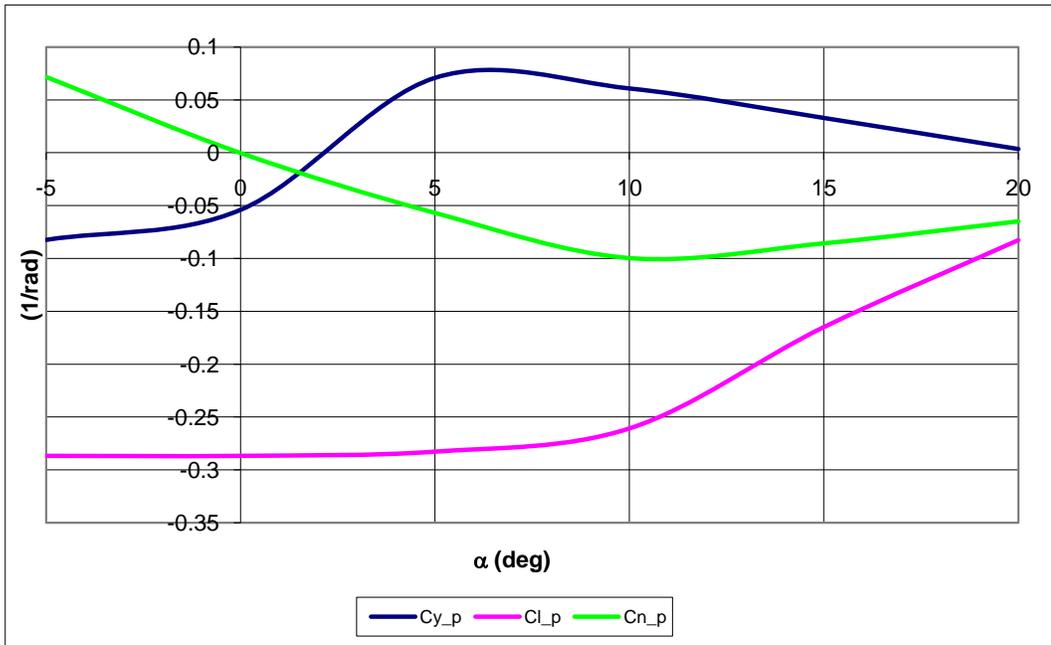
Figure 27: MantaHawk VORSTAB Lateral-Directional Derivatives due to Roll Rate
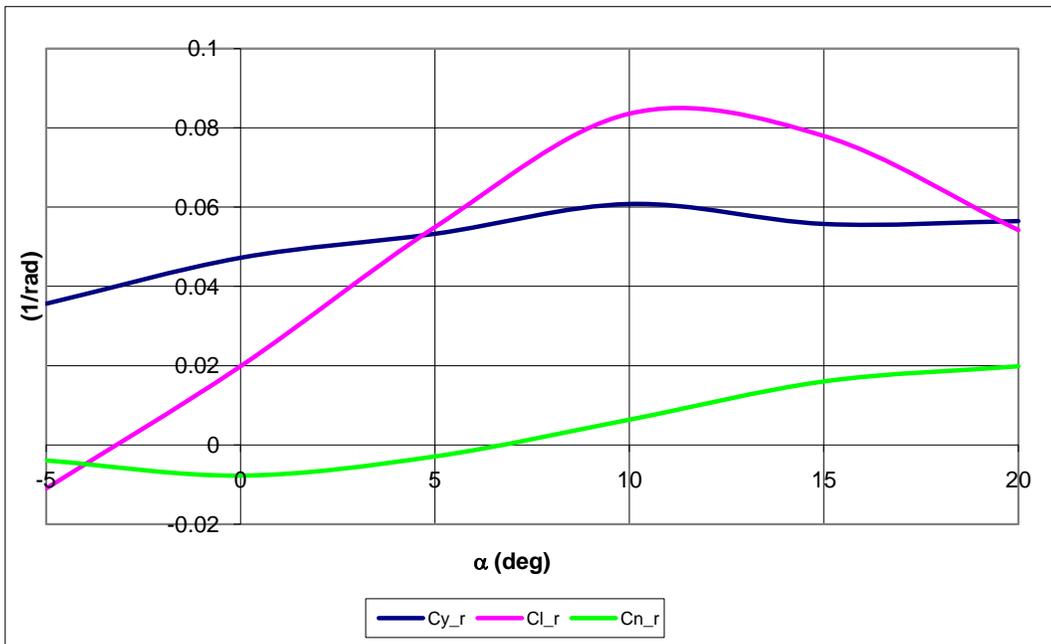
Figure 28: MantaHawk VORSTAB Lateral-Directional Derivatives due to Yaw Rate

At high angles of attack, aircrafts do not always follow the expected trends for the derivatives. This is observed on several of these derivatives. The sideforce coefficient due to sideslip is typically negative due to the defined positive angle of sideslip. VORSTAB estimates that at high angles of attack this derivative becomes positive. The yawing moment due to sideslip should be positive for the same reasons as sideforce should be negative. This derivative becomes negative at high angles of attack. Due to the definition of sideforce coefficient due to roll rate it would be assumed that the derivative should be negative, but at high angles of attack the moment arm will change signs. This will result in the derivative changing signs to positive. It can be expected for the sign to change for the yawing moment derivative due to roll rate as the angle of attack changes from positive to negative. The effect of this derivative is rather small on the airplane dynamic stability, and since this is the case the sign convention does not matter. Yawing moment coefficient due to yaw rate changes signs due to the fact that as the angle of attack increase the moment arm goes from positive to negative. All other derivatives were as expected.

With the control surfaces deflected, the longitudinal and lateral-directional derivatives change. Table 20 shows the effects of an elevator input sent to the elevons on the longitudinal derivatives. This type of input results in a symmetrical deflection of the elevons. Table 21 shows the effects of the aileron or rudder input sent to the elevons on the lateral directional derivatives. There is a resulting asymmetrical deflection of the elevons. An asymmetrical deflection imitates an

aileron and a rudder input both. All values are given in radians. Graphically, these

tables are shown in Figure 29 through Figure 34.

Table 20: MantaHawk VORSTAB Longitudinal Derivatives due to Symmetrical Deflection

α (deg)	δ_{el} (deg)	C_L	C_D	C_m
0	-12	-0.0896	0.0125	0.0561
5	-12	0.1251	0.0107	0.0827
10	-12	0.3413	0.0127	0.0888
15	-12	0.5118	0.0252	0.0806
20	-12	0.6034	0.0534	0.0602
0	-6	-0.0250	0.0088	0.0267
5	-6	0.1930	0.0091	0.0477
10	-6	0.4132	0.0126	0.0529
15	-6	0.5705	0.0296	0.0485
20	-6	0.6432	0.0622	0.0407
0	0	0.0377	0.0068	0.0006
5	0	0.2603	0.0092	0.0159
10	0	0.4760	0.0154	0.0217
15	0	0.6123	0.0366	0.0271
20	0	0.6709	0.0763	0.0256
0	6	0.1079	0.0085	-0.0298
5	6	0.3354	0.0109	-0.0201
10	6	0.5317	0.0215	-0.0025
15	6	0.6433	0.0484	0.0120
20	6	0.6871	0.0939	0.0154
0	12	0.1840	0.0126	-0.0687
5	12	0.3969	0.0158	-0.0476
10	12	0.5768	0.0299	-0.0210
15	12	0.6643	0.0645	0.0004
20	12	0.7001	0.1117	0.0086
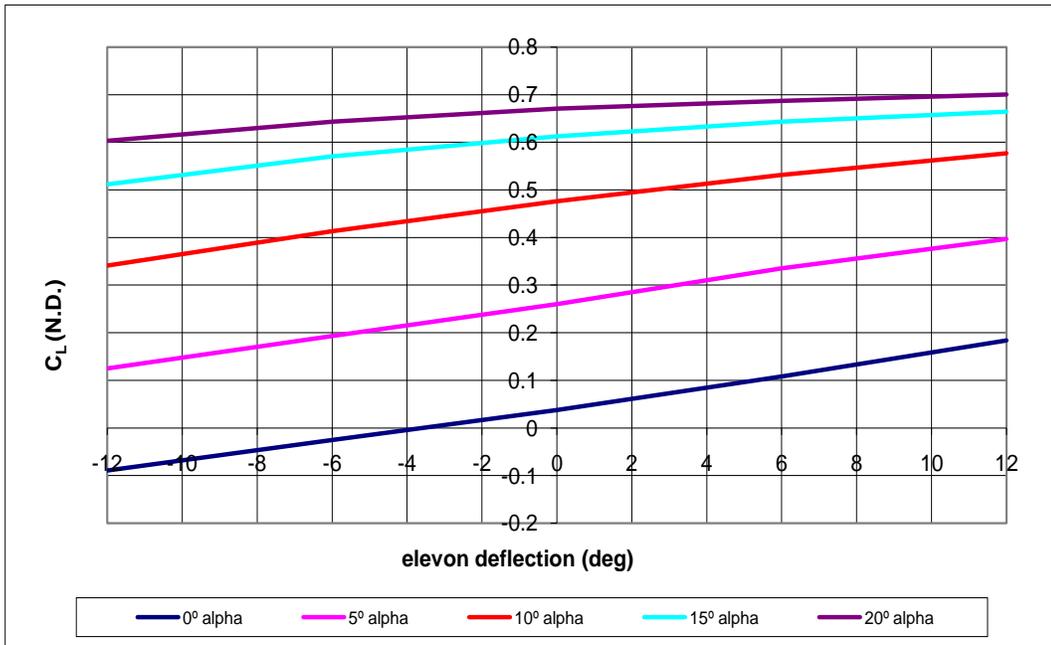
Figure 29: MantaHawk VORSTAB Lift Coefficient due to Symmetrical Deflection
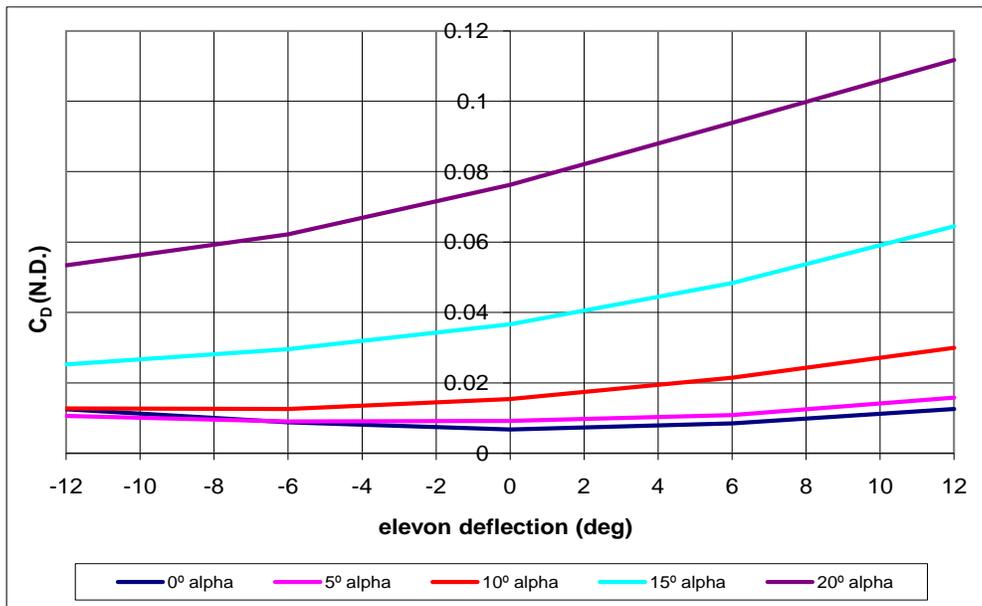
Figure 30: MantaHawk VORSTAB Drag Coefficient due to Symmetrical Deflection
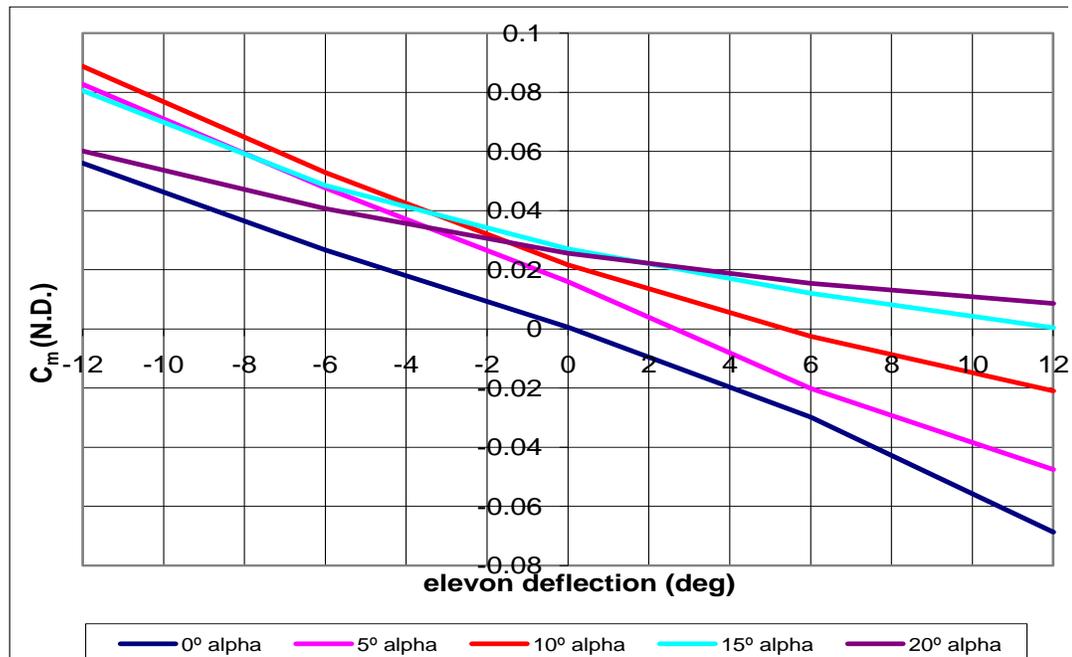
Figure 31: MantaHawk VORSTAB Pitching Moment Coefficient due to Symmetrical Deflection

These three longitudinal derivatives due to the elevator input have a value and sign convention that is expected. A large symmetrical elevon deflection would increase the magnitude of the pitching moment and as a result the lift and drag would also increase. These trends are observed in the VORSTAB results.

Table 21: MantaHawk VORSTAB Lateral-Directional Derivatives due to Asymmetrical Deflections

α (deg)	δ_el (deg)	C_y	C_l	C_n
0	-10	-0.0062	-0.0304	-0.0010
5	-10	-0.0050	-0.0301	-0.0011
10	-10	-0.0021	-0.0296	-0.0024
15	-10	0.0003	-0.0287	-0.0035
20	-10	0.0020	-0.0273	-0.0043
0	-5	-0.0033	-0.0152	0.0001
5	-5	-0.0023	-0.0151	-0.0003
10	-5	-0.0008	-0.0149	-0.0010
15	-5	0.0003	-0.0144	-0.0015
20	-5	0.0011	-0.0137	-0.0019
0	0	0.0000	0.0000	0.0000
5	0	0.0000	0.0000	0.0000
10	0	0.0000	0.0000	0.0000
15	0	0.0000	0.0000	0.0000
20	0	0.0000	0.0000	0.0000
0	5	0.0032	0.0152	-0.0008
5	5	0.0017	0.0152	-0.0001
10	5	0.0004	0.0149	0.0005
15	5	-0.0005	0.0144	0.0009
20	5	-0.0008	0.0129	0.0010
0	10	0.0059	0.0304	-0.0021
5	10	0.0029	0.0304	-0.0007
10	10	0.0006	0.0298	0.0004
15	10	-0.0007	0.0279	0.0010
20	10	-0.0010	0.0230	0.0008
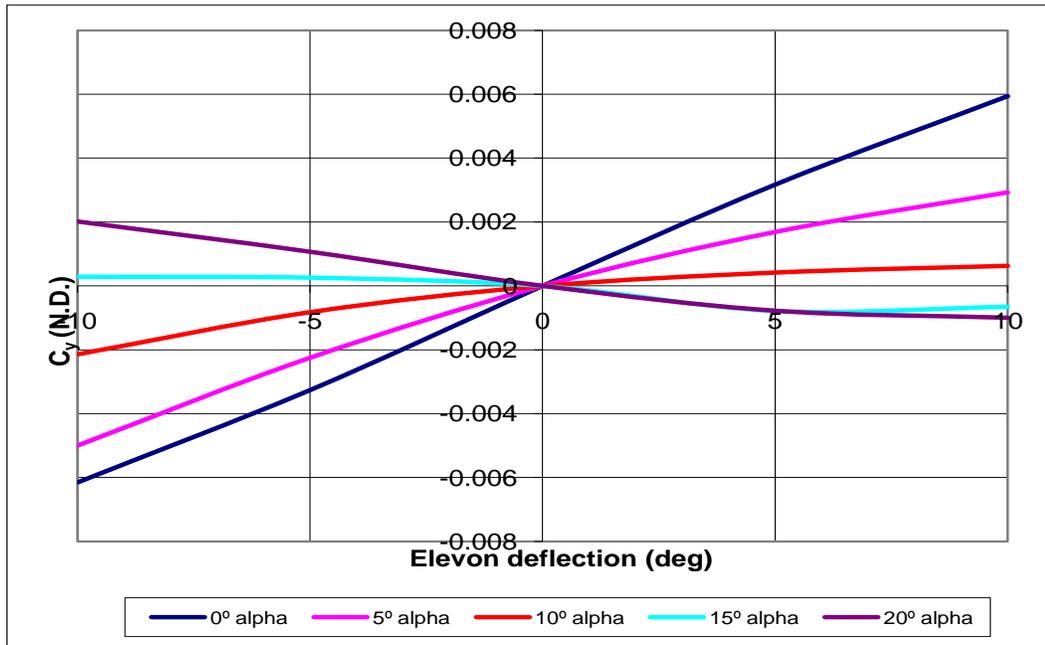
Figure 32: MantaHawk VORSTAB Sideforce Coefficient due to Asymmetrical Deflection
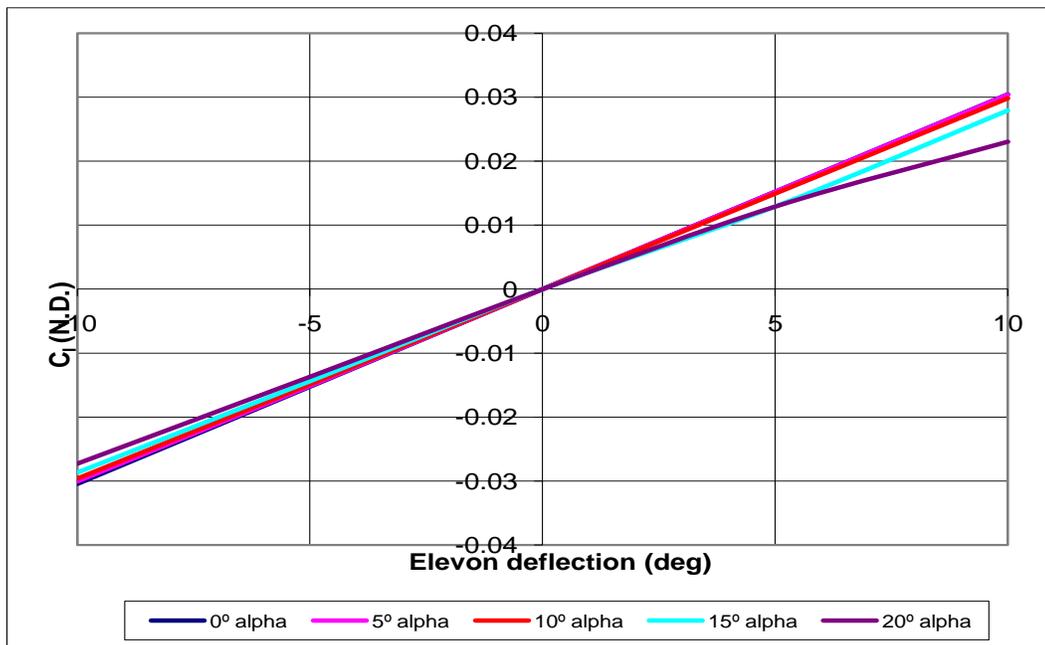
Figure 33: MantaHawk VORSTAB Rolling Moment Coefficient due to Asymmetrical Deflection
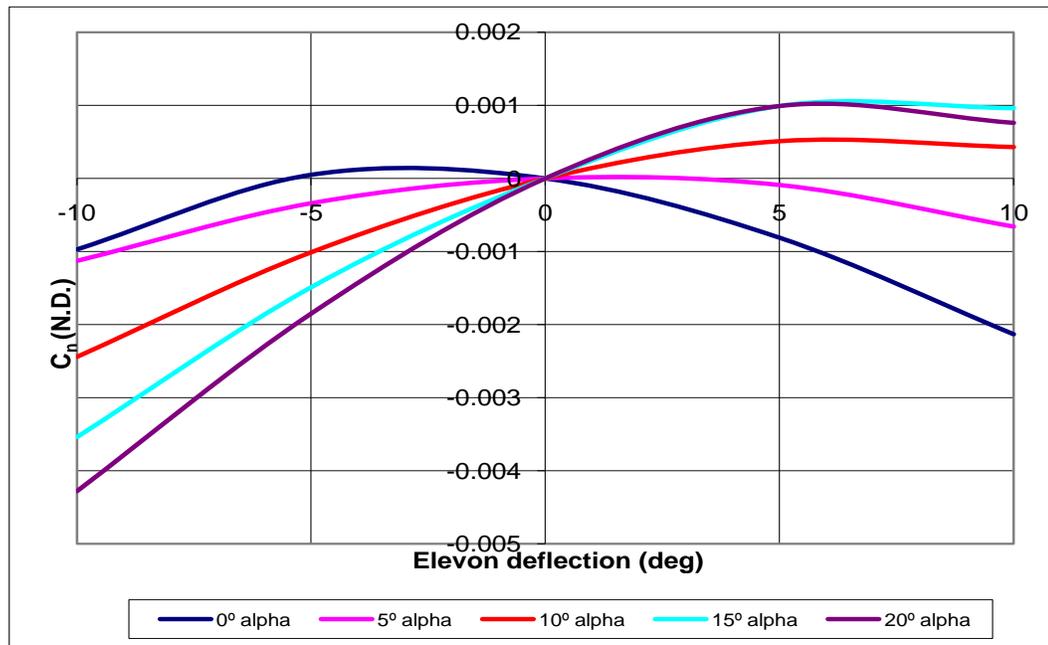
Figure 34: MantaHawk VORSTAB Yawing Moment Coefficient due to Asymmetrical Deflection

A positive aileron/rudder input should result in a positive sideforce. At high angles of attack this is not seen in the VORSTAB results. At extreme angles of attack the forces and moments are usually not what is expected or desired, unless the aircraft is designed to fly at these angles. The MantaHawk was not designed to fly at these angles though. Similar to the sideforce, a positive asymmetrical elevon deflection will result in a positive rolling moment. Typically, a positive rudder input will result in a negative yawing, and a positive aileron input will result in a negative yawing moment but can be positive. At low angles of attack the yawing moment is negative, as expected, but at higher angles it becomes positive. This is most likely due to the change in drag over the airfoils at extreme angles of attack. The result of this positive

value will actually help the intended turn. Table 22 shows the stability requirements for the MantaHawk.

Table 22: MantaHawk VORSTAB Stability Requirements

Type of Stability	Corresponding Derivatives	Criterion	Derivative (rad^{-1})	Stable/Unstable
Sideslip	$C_{y\beta}$	< 0	-0.1146	Stable
Vertical Speed	$C_{L\alpha}$	> 0	2.5500	Stable
Angle of Attack	$C_{m\alpha}$	< 0	0.1756	Unstable
Angle of Sideslip	$C_{n\beta}$	> 0	0.0172	Stable
Roll Rate	C_{lp}	< 0	-0.2866	Stable
Pitch Rate	C_{mq}	< 0	-1.6625	Stable
Yaw Rate	C_{nr}	< 0	-0.0077	Stable
Lateral	$C_{l\beta}$	< 0	-0.0458	Stable

Like the YAK-54, the MantaHawk's stability requirements were determined at 0˚ angle of attack. At other angles of attack, the aircraft may become unstable in modes other than angle of attack stability. The vertical speed and angle of attack stability requirements were both found over the angle of attack range of 0˚ to 5˚ from the VORSTAB results. As seen from the AAA data, it was predicted that the aircraft was stable in all modes and VORSTAB predicted an unstable mode.

8.3 Method Comparison MantaHawk

The results from AAA and VORSTAB are different in the terms that $C_{m\alpha}$ is unstable as predicted by VORSTAB. AAA's results say that the MantaHawk is stable in all modes. A comparison of the two methods can be seen in Table 23.

Table 23: MantaHawk AAA and VORSTAB Comparison

Stability and Control Derivatives			
Derivative (1/rad)	AAA	VORSTAB	% Difference
$C_{L\alpha}$	3.9630	2.5500	-35.65
$C_{D\alpha}$	0.0615	0.0275	-55.28
$C_{m\alpha}$	-0.4034	0.1756	-143.53
C_{Lq}	5.0920	1.9645	-61.42
C_{mq}	-4.7340	-1.6625	-64.88
$C_{l\beta}$	-0.0817	-0.0458	-43.94
C_{lp}	-0.4892	-0.2866	-41.41
C_{lr}	0.0407	0.0199	-51.11
$C_{y\beta}$	-0.1877	-0.1146	-38.95
C_{yp}	-0.1249	-0.0539	-56.85
C_{yr}	0.0897	0.0472	-47.38
$C_{n\beta}$	0.0359	0.0172	-52.09
C_{np}	-0.0169	-0.0003	-98.22
C_{nr}	-0.0219	-0.0077	-64.84
$C_{D\delta el}$	0.4209	0.0168	-96.01
$C_{L\delta el}$	0.4784	0.6703	40.11
$C_{m\delta el}$	-1.0630	-0.2908	-72.64
$C_{l\delta el}$	0.3588	0.1745	-51.37
$C_{y\delta el}$	0.0012	0.0363	2925.00
$C_{n\delta el}$	-0.0055	-0.0093	69.09

VORSTAB produces results that are lower than most of the AAA derivatives. This means that the aircraft is not going to have as much control as expected. Most of the differences between AAA and VORSTAB fall within the error ranges that Dr. Roskam describes that AAA will have. Pitching moment coefficient due to angle of attack has the largest variance and this is the most critical derivative, since this was

the unstable mode. VORSTAB should be used as a method for checking if there is a possibility for one of the modes to be unstable. Even if VORSTAB is incorrect this will give designers a chance to plan the flight test with this possibility.

The same typical ranges that applied to the YAK-54 apply to the MantaHawk as well. These ranges again were developed by Dr. Roskam, Ref [5], for what approximately an aircraft can expect the control derivatives to be. These ranges are for conventional aircrafts, and the ranges are a function of Mach number. Table 24 shows the VORSTAB MantaHawk results compared to typical ranges from Dr. Roskam, Ref [5].

Table 24: MantaHawk Stability and Control Derivatives Typical Ranges

Derivative (1/rad)	VORSTAB	AAA	Typical Ranges Dr. Roskam	Within Range (Yes/No) VORSTAB	AAA
$C_{L\alpha}$	2.55	3.963	1.0 to 8.0	Yes	Yes
$C_{D\alpha}$	0.0275	0.0615	0.0 to 2.0	Yes	Yes
$C_{m\alpha}$	0.1756	-0.4034	-4.0 to 1.0	No	Yes
C_{Lq}	1.9645	5.092	0.0 to 30.0	Yes	Yes
C_{mq}	-1.6625	-4.734	-90.0 to 0.0	Yes	Yes
$C_{l\beta}$	-0.0458	-0.0817	0.1 to -4.0	Yes	Yes
C_{lp}	-0.2866	-0.4892	-0.1 to -0.8	Yes	Yes
C_{lr}	0.0199	0.0407	0.0 to 0.6	Yes	Yes
$C_{y\beta}$	-0.1146	-0.1877	-0.1 to -2.0	Yes	Yes
C_{yp}	-0.0539	-0.1249	-0.3 to 0.8	Yes	Yes
C_{yr}	0.0472	0.0897	0.0 to 1.2	Yes	Yes
$C_{n\beta}$	0.0172	0.0359	0.0 to 4.0	Yes	Yes
C_{np}	-0.0003	-0.0169	-0.5 to 0.1	Yes	Yes
C_{nr}	-0.0077	-0.0219	0.0 to -1.0	Yes	Yes
$C_{L\delta e}$	0.6703	0.4784	0.0 to 0.6	No	Yes
$C_{D\delta e}$	0.0168	0.4209	Negligible	No	No
$C_{m\delta e}$	-0.2908	-1.0630	0.0 to -4.0	Yes	Yes
$C_{l\delta a}$	0.1745	0.3588	0.0 to 0.4	Yes	Yes
$C_{l\delta r}$	0.1745	0.3588	-0.04 to 0.04	No	Yes
$C_{y\delta a}$	0.0363	0.0012	Negligible	No	No
$C_{y\delta r}$	0.0363	0.0012	0.0 to 0.5	Yes	Yes
$C_{n\delta a}$	-0.0093	-0.0055	-0.08 to 0.08	Yes	Yes
$C_{n\delta r}$	-0.0093	-0.0055	-0.15 to 0.0	Yes	Yes

Not all of the control derivatives fall within the expected ranges. This does not necessarily mean that the aircraft is unstable. These are estimated ranges and an unconventional aircraft will not necessarily fall in the range. Also, the rudder

deflection and aileron deflection control derivatives are the same because there is only one input for those control surfaces. The input simulates both a rudder input and an aileron input. This means that the control derivatives might fall into the range for the rudder or aileron deflection, but not the other deflection. For example, the rolling moment coefficient due to aileron deflection falls into the typical range Dr. Roskam gives, but it does not fall into the typical range for the rudder deflection. The drag coefficient due to elevator deflection is usually ignored. Therefore, there is no cause for alarm that there is an increase in drag when the control surfaces are deflected. As stated earlier, the MantaHawk is unstable in the pitching mode, and this is observed since the pitching moment coefficient due to change in angle of attack, $C_{m\alpha}$, does not fall into the typical range Dr. Roskam describes.

8.4 Linearized Model of the MantaHawk

For the information and data on the state space model please refer to Appendix B.

9   Meridian UAV

The Center for Remote Sensing of Ice Sheets (CReSIS) is a science and technology center established by the National Science Foundation (NSF) in 2005. The foundation has the mission of developing new technologies and computer models to measure and predict the response of sea level change to the mass balance of ice sheets in Greenland and Antarctica. CReSIS is developing sophisticated sensors and a long-duration un-inhabitant aerial vehicle (UAV), called the Meridian.

The KUAE, in close collaboration with national and international partners, has designed and developed the Meridian UAV for the Center for Remote Sensing of Ice Sheets (CReSIS). The Meridian has a gross takeoff weight of 1,100 lbs, a wingspan of 26.4 ft, and a range of 950 nautical miles. Vehicle cruise speed is 100-120 kts, endurance exceeds 9 hours, and available payload exceeds 120 lbs and 300W consumed power. As such, this is an extraordinarily valuable scientific research platform, since most civilian UAV research currently limits payloads to a few pounds and a fraction of the power. Added benefits of greater than two cubic feet of payload volume and eight wing hard points provide a sensor platform with little competition. This data was taken from Ref [16]. Table 25 shows some of the important salient characteristics and Figure 35 shows the design of the Meridian UAV both from Ref [17]. Information about the design on the Meridian can also be found in Ref [17].

Table 25: Meridian Characteristics

Characteristic	Wing	V-Tail
Area	69.6 ft^2	10 ft^2
Span	26.4 ft	5.9 ft
MGC	31.7 ft	1.75 ft
Aspect Ratio	10	3.5
Quarter Chord Sweep Angle	0 deg	26.3 deg
Taper Ratio	1	0.5
Thickness Ratio	18%	12%
Dihedral Angle	5 deg	50 deg
Incidence Angle	0 deg	0 deg
Aileron Chord Ratio	0.24	
Aileron Span Ratio	0.60-1.00	
Flap Chord Ratio	0.2	
Flap Span Ratio	0.10-0.599	

Characteristic	Fuselage
Maximum Length	14.8 ft
Maximum Height	2.9 ft
Maximum Width	3.5

Figure 35: Unigraphics CAD Model of the Meridian UAV

The design of the Meridian was completed using AAA and Dr. Roskam's method. The AAA software was also used to find the stability and control derivatives of the Meridian. The tail of the Meridian is unconventional and uses a v-tail. It is also a fully moving tail.

9.1 <u>AAA Modeling of the Meridian</u>

Similar to the YAK-54 and MantaHawk, the AAA file produced stability and control derivatives for the Meridian UAV. The longitudinal derivatives are found in Table 26 and the lateral-directional derivatives are found in Table 27, both Ref [18]. As seen in Table 28 the aircraft is found to be stable in all modes.

Table 26: Meridian AAA Longitudinal Derivatives

Longitudinal Coefficients and Stability Derivatives-Stability Axes	
Derivatives	(1/rad)
C_{Du}	0.0000
$C_{D\alpha}$	0.1409
C_{Txu}	-0.0713
C_{Lu}	0.0109
$C_{L\alpha}$	5.1648
$C_{L\alpha dot}$	0.7407
C_{Lq}	4.6179
C_{mu}	-0.0028
$C_{m\alpha}$	-0.6207
$C_{m\alpha dot}$	-2.9826
C_{mq}	-13.973
C_{mTu}	0.0294
$C_{mT\alpha}$	-0.3419
Longitudinal Control and Hinge Moment Derivatives-Stability Axes	
Derivatives	(1/rad)
$C_{D\delta re}$	0.0117
$C_{L\delta re}$	0.4149
$C_{m\delta re}$	-1.6709

Table 27: Meridian AAA Lateral-Directional Derivatives

Lateral-Directional Coefficients and Stability Derivatives-Stability Axes	
Derivatives	(1/rad)
$C_{l\beta}$	-0.0776
C_{lp}	-0.5546
C_{lr}	0.1099
$C_{y\beta}$	-0.4789
C_{yp}	-0.1465
C_{yr}	0.3217
$C_{n\beta}$	0.1386
$C_{nT\beta}$	-0.0007
C_{np}	-0.0351
C_{nr}	-0.1338
Lateral-Directional Control and Hinge Moment Derivatives-Stability Axes	
Derivatives	(1/rad)
$C_{l\delta a}$	0.2316
$C_{l\delta re}$	-0.0253
$C_{y\delta a}$	0.0000
$C_{y\delta re}$	-0.3681
$C_{n\delta a}$	-0.0134
$C_{n\delta\rho\epsilon}$	0.1481

Table 28: Meridian AAA Stability Requirements

Type of Stability	Corresponding Derivatives	Criterion	Derivative (rad⁻¹)	Stable/Unstable
Sideslip	$C_{y\beta}$	< 0	-0.4789	Stable
Vertical Speed	$C_{L\alpha}$	> 0	5.1648	Stable
Angle of Attack	$C_{m\alpha}$	< 0	-0.6207	Stable
Angle of Sideslip	$C_{n\beta}$	> 0	0.1386	Stable
Roll Rate	C_{lp}	< 0	-0.5546	Stable
Pitch Rate	C_{mq}	< 0	-13.973	Stable
Yaw Rate	C_{nr}	< 0	-0.1338	Stable
Lateral	$C_{l\beta}$	< 0	-0.0776	Stable

9.2   VORSTAB Modeling of the Meridian

Several different Meridian VORSTAB models were created with changes to the geometry of the fuselage. The reasons for these changes were due to the fact that VORSTAB calculates such a high downwash as a result of the shape and camber of the fuselage, and these changes to the model were to improve the results. Typically, the fuselage does not result in a large amount of downwash and can almost be completely ignored.   The downwash on the Meridian fuselage is due to the large amount of convergence from the nose to the tail and the negative camber or downward swoop of the empennage. From this downwash, the effectiveness of the tails is almost blanketed out.   In reality, there is not as much downwash as VORSTAB is predicting due to the fact that the flow will separate from the fuselage.

9.2.1   Model 1: Half Scale Model of Meridian

The first model created was of the exact shape of the entire Meridian, but scaled down to half of the size. This is a requirement for VORSTAB that the largest

radius of the fuselage be no larger than 1, for any unit system. The downwash was so large for this model that VORSTAB did not obtain any valid results. Table 29 shows the longitudinal derivatives obtained, and Table 30 shows the lateral-directional derivatives. As seen from the results, there is negative lift and zero drag at multiple angles of attack. These results were known to be invalid.

Table 29: Meridian VORSTAB Model 1 Longitudinal Derivatives (1/rad)

α (deg)	C_L	C_D	C_m	C_{Lq}	C_{mq}
-5	-2.863	0.1402	0.9534	33.592	-17.037
0	-3.1363	0	1.3823	34.603	-17.109
5	-3.6006	0	0.2483	35.110	-17.069
10	-2.8592	0	-1.5042	35.041	-16.463
15	-2.882	0	-1.1976	34.609	-16.118
20	-2.6188	0	-1.5477	33.746	-15.799

Table 30: Meridian VORSTAB Model 1 Lateral-Directional Derivatives (1/rad)

α (deg)	$C_{y\beta}$	$C_{l\beta}$	$C_{n\beta}$	C_{yp}	C_{lp}	C_{np}	C_{yr}	C_{lr}	C_{nr}
-5	-17.49	-16.48	10.04	-3.735	6.656	2.925	-2.917	-1.700	1.357
0	-1.203	2.280	2.412	-0.215	1.161	1.129	-4.541	-0.659	2.095
5	-0.588	0.655	2.364	-1.738	0.581	2.120	-6.194	-0.602	2.787
10	9.515	-2.671	-2.697	-1.041	-0.041	1.589	-8.032	-0.489	3.677
15	12.611	-3.054	-3.485	-2.411	-0.072	2.185	-10.99	-0.510	5.079
20	12.672	-3.177	-3.183	-2.825	-0.052	2.210	-13.07	-0.523	5.717

After several discussions with Dr. Lan about the possible cause for the problem, he offered advice on what he believed to be the problem and how it could possibly be fixed. VORSTAB predicts that all of the flow over the top of the fuselage will become downwash, but in reality not all of it will. There will be some flow separation that does not result in downwash. The v-tail are in the path of this flow wake and rendering them ineffective. In the VORSTAB output file, the downwash

on the fuselage can be seen as extremely high pressure on the upper surface. Dr. Lan recommended changing the fuselage to help eliminate some of the downwash and obtain valid results. The VORSTAB input file can be found in Appendix A.

9.2.2   Model 2: Larger Empennage

The best way to help eliminate some of the downwash was to eliminate the large amount of convergence, and also, to estimate the cross-sections of the fuselage with a circular cross-section. This method replaced the fuselage body with a fuselage wake surface. Having circular cross-sections allowed for much faster modifications to the model. The forward section of the fuselage size did not change and the aft sections radius was increased. The size of the increase of the aft fuselage sections was changed multiple times. The final increase was to approximately half of the forward section size. Table 31 shows the diameter used for this approximation as well as the right side view of the fuselage diameter for the first model. Both models are to half scale. Figure 36 shows the increase in size of the empennage.

Table 31: Fuselage Diameter for Meridian Models 1 and 2

| Station	x (ft)	Model 1 Diameter (ft)	Model 2 Diameter (ft)
1	0	0	0
2	0.3458	0.3225	0.3225
3	0.75	0.5183	0.5183
4	0.7917	0.5183	0.5183
5	1.042	0.9879	0.9879
6	1.321	1.238	1.238
7	1.608	1.317	1.317
8	2.058	1.375	1.375
9	2.438	1.388	1.388
10	2.883	1.376	1.376
11	3.521	1.292	1.292
12	4.146	1.118	1.118
13	4.642	0.9458	0.9458
14	5.25	0.7542	0.7542
15	5.771	0.6125	0.7542
16	6.592	0.4525	0.7542
17	7.463	0.4121	0.7542
18	8.125	0.3325	0.6708
19	8.563	0.0417	0.5042
20	8.604	0	0.2042
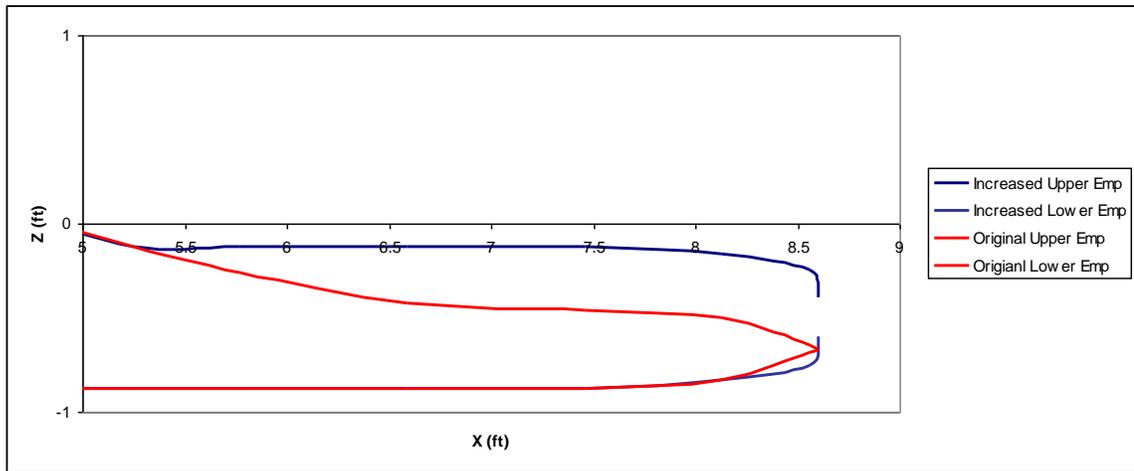
Figure 36: Meridian Empennage Models 1 and 2

Model 2's results were much better than the first model, but the drag was very high. The high drag was a result of a few different things. Increasing the fuselage size added some to the drag. Also, there is still camber in the empennage that results in some downwash that increases the drag. For this model the drag should be ignored. Like all VORSTAB models this model does not show that the aircraft stalls, because there is no flow separation. The input file for this model can be found in Appendix A. Table 32 shows the longitudinal derivatives and Figure 37 through Figure 40 show Table 32 in graphical form.

Table 32: Meridian VORSTAB Model 2 Longitudinal Control Derivatives and Affected by Pitch Rate

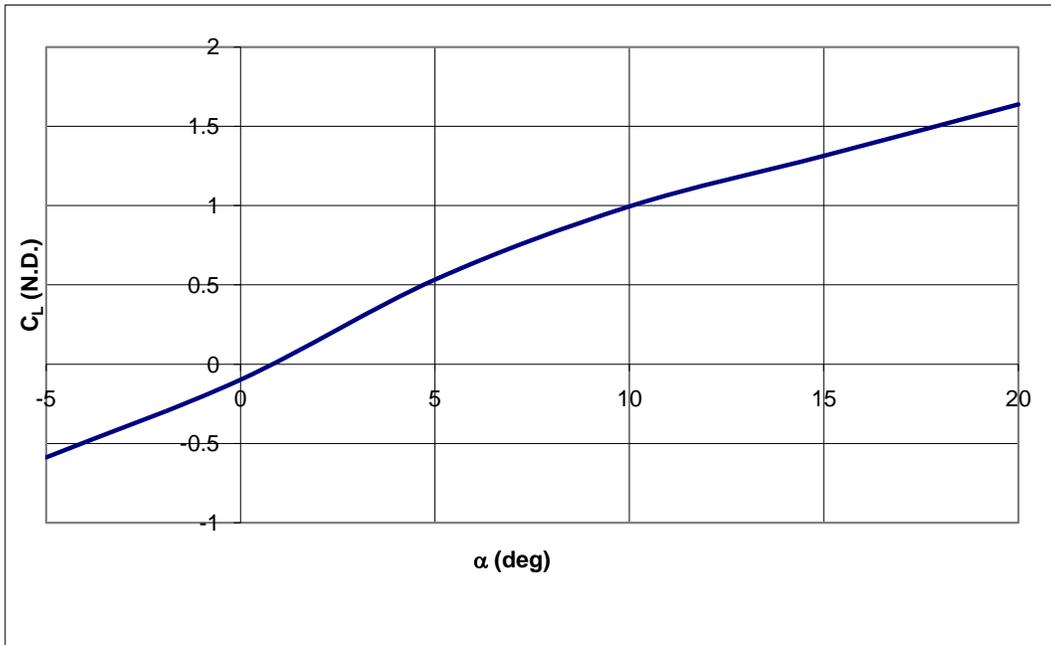| α (deg)	C_L	C_D	C_m	$C_{L,q}$	$C_{D,q}$	$C_{m,q}$
-5	-0.5876	0.4912	-0.0352	6.9660	0.0000	-8.4348
0	-0.0978	1.4931	-0.1877	7.1682	0.0000	-8.5662
5	0.5335	2.8528	-0.2621	7.2364	0.0000	-8.5967
10	0.9949	4.6480	-0.3414	7.1232	0.0000	-8.3508
15	1.3140	6.6175	-0.4179	6.7959	0.0000	-7.6702
20	1.6382	8.6688	-0.4923	6.5872	0.0000	-7.8880

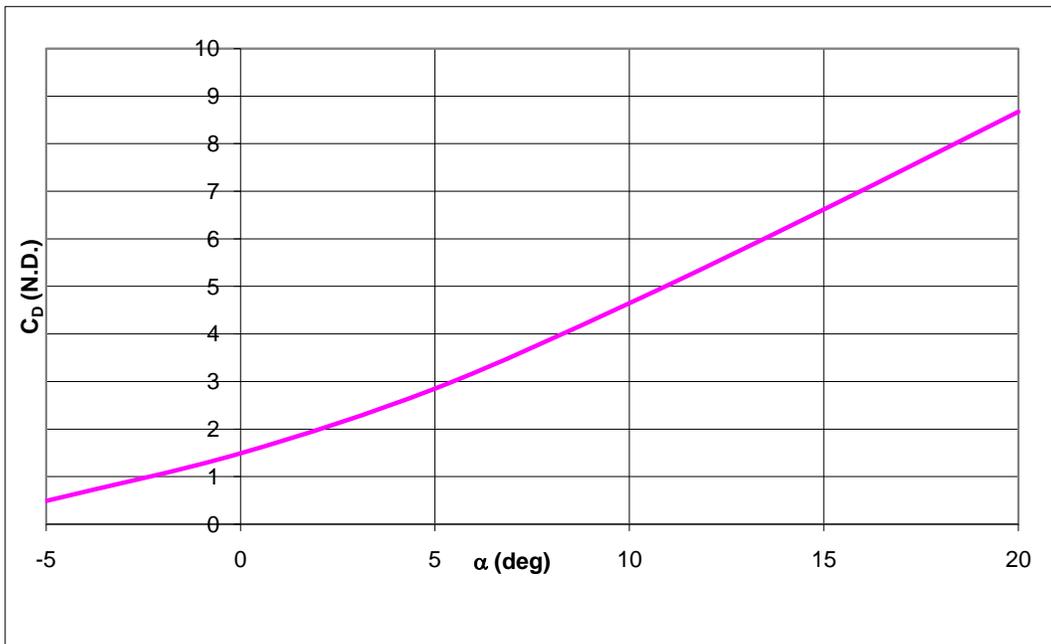**Figure 37: Meridian VORSTAB Model 2 Lift Coefficient due to Angle of Attack**

Figure 38: Meridian VORSTAB Model 2 Drag Coefficient due to Angle of Attack
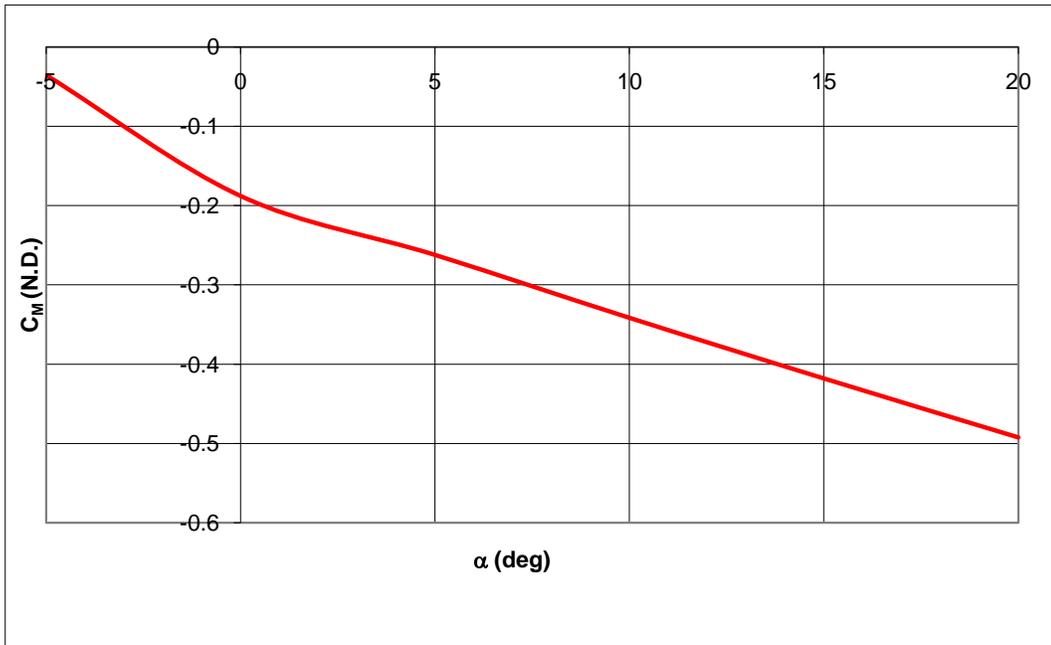
Figure 39: Meridian VORSTAB Model 2 Pitching Moment Coefficient due to Angle of Attack
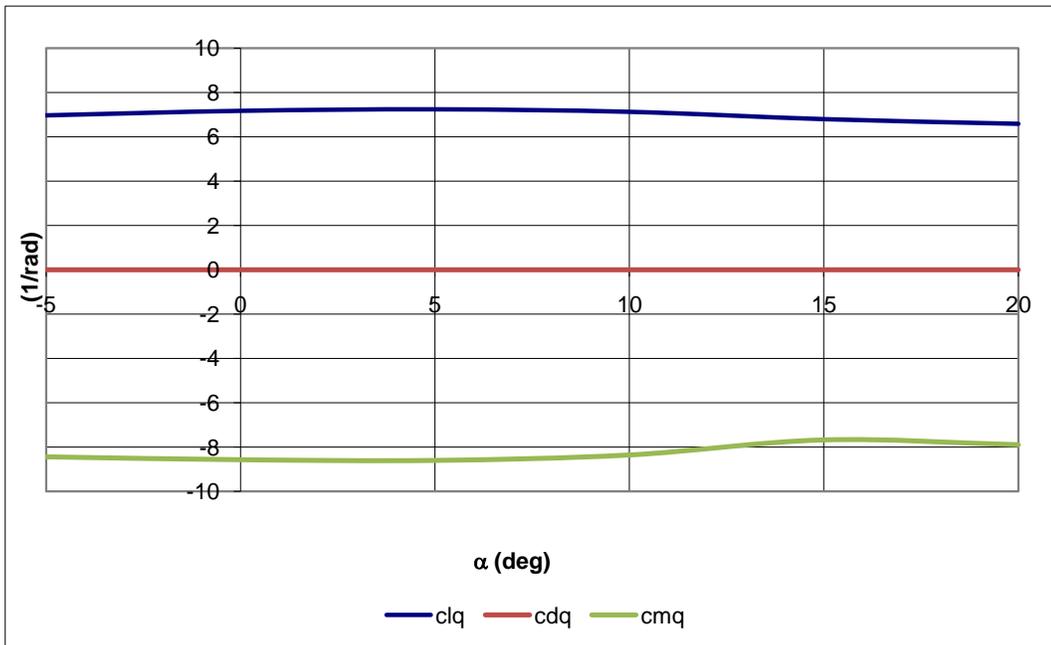

Figure 40: Meridian VORSTAB Model 2 Longitudinal Derivatives due to Pitch Rate

The lift coefficient is appropriate in magnitude, but the zero lift angle of attack is positive. For this type of aircraft, the zero lift angle of attack should be negative. This lift would result in the aircraft cruising at a positive angle of attack. It is obvious that the drag is too high. All of the other derivatives have an appropriate value and trend. For example, the pitching moment coefficient shows the aircraft is inherently stable.

The lateral-directional control derivatives due to sideslip and roll rate for Model 2 can be seen in Table 33. The graphical form of this table is shown in Figure 41 and Figure 42. Table 34 shows the lateral-directional control derivatives due to yaw rate, and Figure 43 shows this in graphical form.

Table 33: Meridian VORSTAB Model 2 Lateral-Directional Derivatives due to Sideslip and Roll Rate

α (deg)	$C_{y,\beta}$	$C_{l,\beta}$	$C_{n,\beta}$	$C_{y,p}$	$C_{l,p}$	$C_{n,p}$
-5	0.5775	-0.1071	0.0877	-0.1552	-0.4765	-0.2220
0	0.7695	-0.1083	0.0991	-0.1010	-0.2913	-0.0312
5	0.9597	-0.1283	0.0837	-0.1356	-0.4538	-0.5138
10	0.9603	-0.1203	0.0493	-0.0569	-0.2312	-0.3247
15	0.7403	-0.1146	0.0258	-0.0288	-0.1242	-0.2432
20	0.4882	-0.1077	0.0029	-0.0167	-0.0801	-0.2357
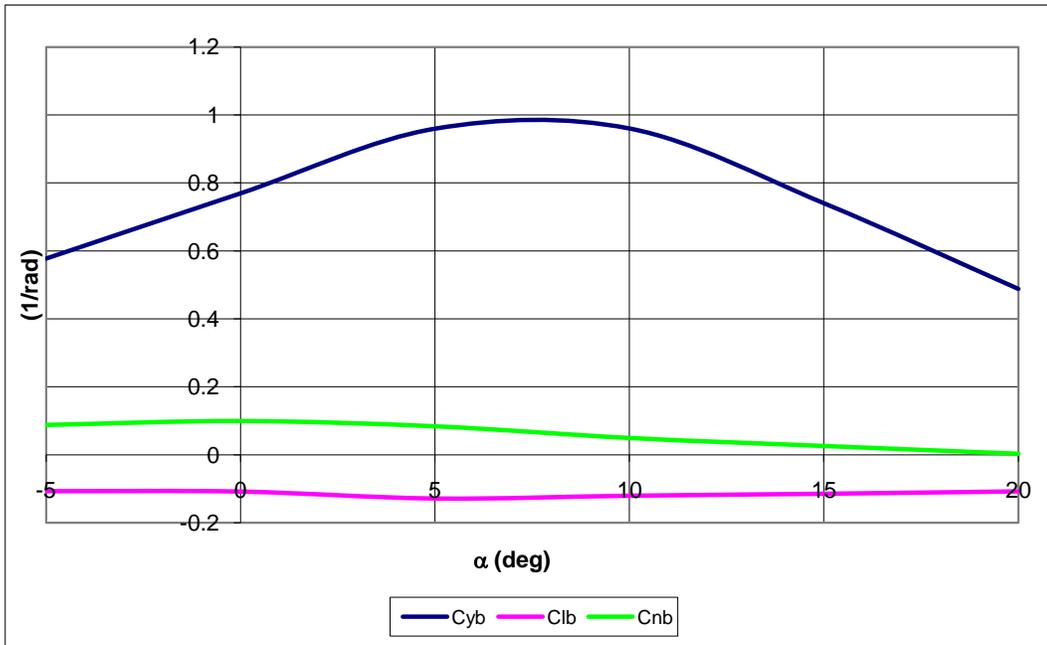
Figure 41: Meridian VORSTAB Model 2 Lateral-Directional Derivatives due to Sideslip
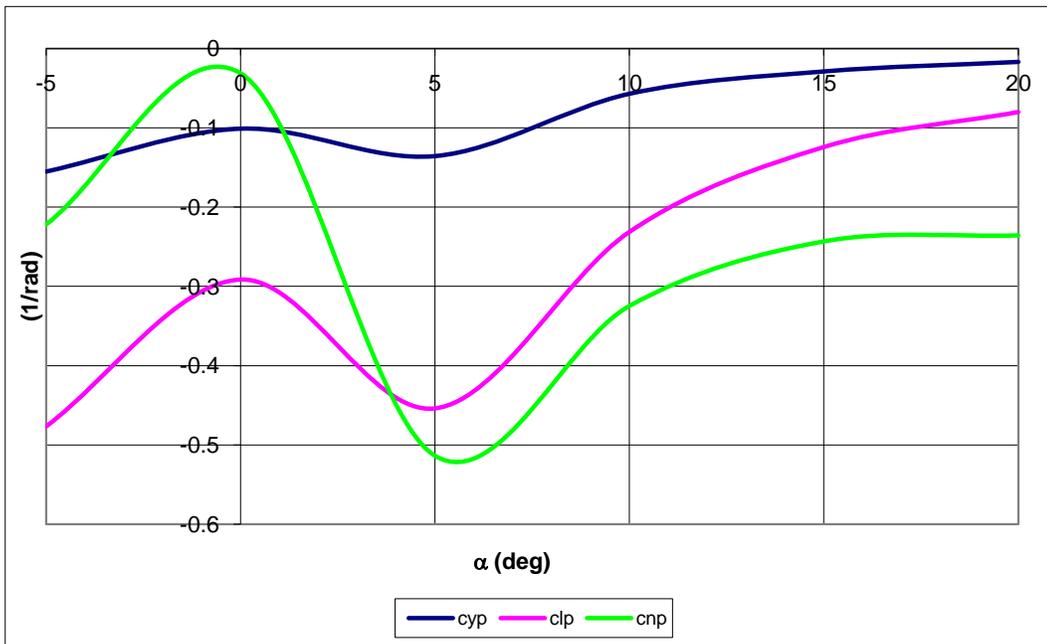
Figure 42: Meridian VORSTAB Model 2 Lateral-Directional Derivatives due to Roll Rate

Usually, the sideforce coefficient due to sideslip is negative, but the VORSTAB results show a positive value. Sideforce coefficient due to roll rate has a positive and negative typical range, but it is usually negative due to the moment arm. This is seen in the VORSTAB results. The rest of the derivatives are as expected.

Table 34: Meridian VORSTAB Model 2 Lateral-Directional Derivatives due to Yaw Rate

α (deg)	$C_{y,r}$	$C_{l,r}$	$C_{n,r}$
-5	0.1537	-0.2550	-0.0949
0	0.2091	-0.2263	-0.0748
5	0.2432	-0.1840	-0.0483
10	0.2017	-0.1126	-0.0030
15	0.1741	-0.0672	0.0244
20	0.1548	-0.0429	0.0549
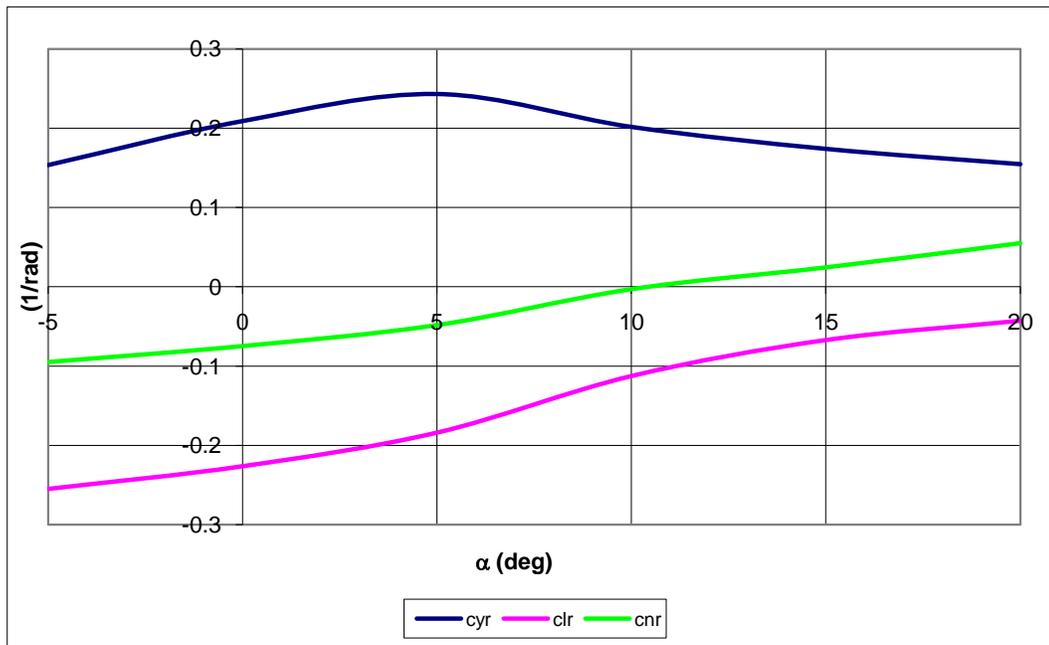
Figure 43: Meridian VORSTAB Model 2 Lateral-Directional Derivatives due to Yaw Rate

The lateral-directional derivatives due to yaw rate have values that are expected, except for the rolling moment coefficient. This derivative is normally a positive value, since the wing-fuselage contribution is always positive and outweighs the vertical tail contribution. The vertical tail contribution can be either positive or negative. This vertical tail contribution outweighs the wing-fuselage contribution for this aircraft since it has a negative value.

Deflecting the control surfaces affects the stability and control derivatives. Table 35 through Table 37 show the control derivatives due to different control surface deflections. These three tables are also graphical depicted in Figure 44 through Figure 52. The Meridian has a v-tail so there is not a conventional rudder or elevators. The v-tail imitates a rudder input with an asymmetrical deflection of the tails and imitates an elevator input with a symmetrical deflection of the tails. These types of control surfaces are called rudevators.

Table 35: Meridian VORSTAB Model 2 Lateral Directional Derivatives due to Aileron Deflection

α (deg)	δ_a	C_y	C_l	C_n
0	-10	-0.0099	-0.0460	-0.0121
5	-10	-0.0100	-0.0462	-0.0131
10	-10	-0.0091	-0.0417	-0.0122
15	-10	-0.0066	-0.0306	-0.0087
20	-10	-0.0048	-0.0222	-0.0061
0	-5	-0.0050	-0.0230	-0.0060
5	-5	-0.0050	-0.0231	-0.0066
10	-5	-0.0045	-0.0209	-0.0061
15	-5	-0.0033	-0.0153	-0.0043
20	-5	-0.0024	-0.0111	-0.0031
0	0	0.0000	0.0000	0.0000
5	0	0.0000	0.0000	0.0000
10	0	0.0000	0.0000	0.0000
15	0	0.0000	0.0000	0.0000
20	0	0.0000	0.0000	0.0000
0	5	0.0049	0.0229	0.0060
5	5	0.0050	0.0230	0.0066
10	5	0.0045	0.0208	0.0061
15	5	0.0033	0.0152	0.0043
20	5	0.0024	0.0111	0.0031
0	10	0.0098	0.0456	0.0121
5	10	0.0100	0.0458	0.0131
10	10	0.0090	0.0413	0.0122
15	10	0.0066	0.0303	0.0087
20	10	0.0047	0.0220	0.0061
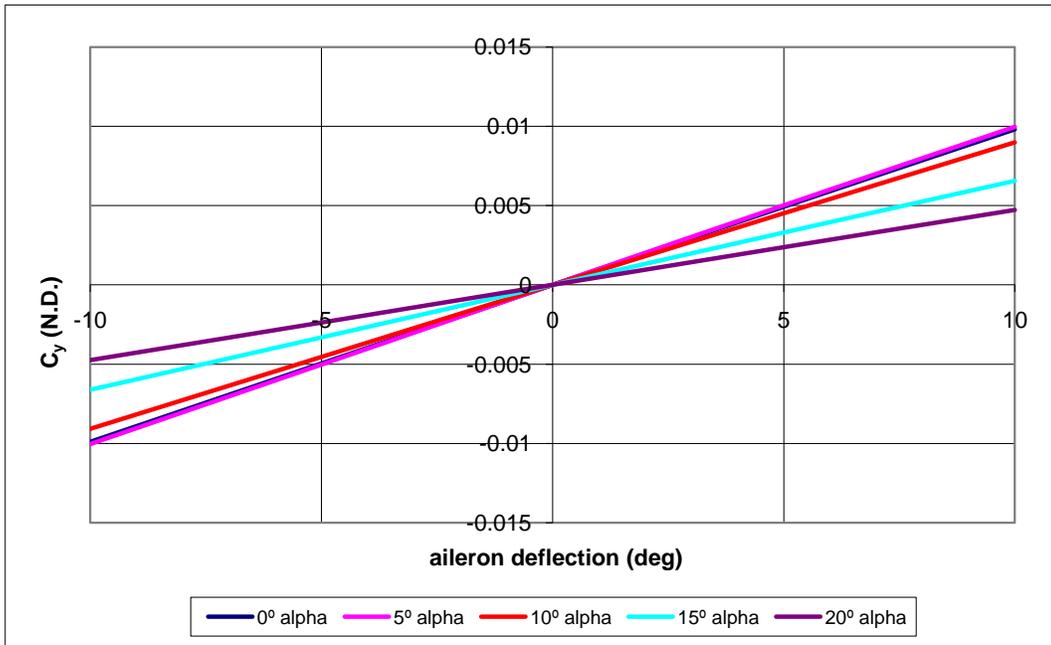
Figure 44: Meridian VORSTAB Model 2 Sideforce Coefficient due to Aileron Deflection
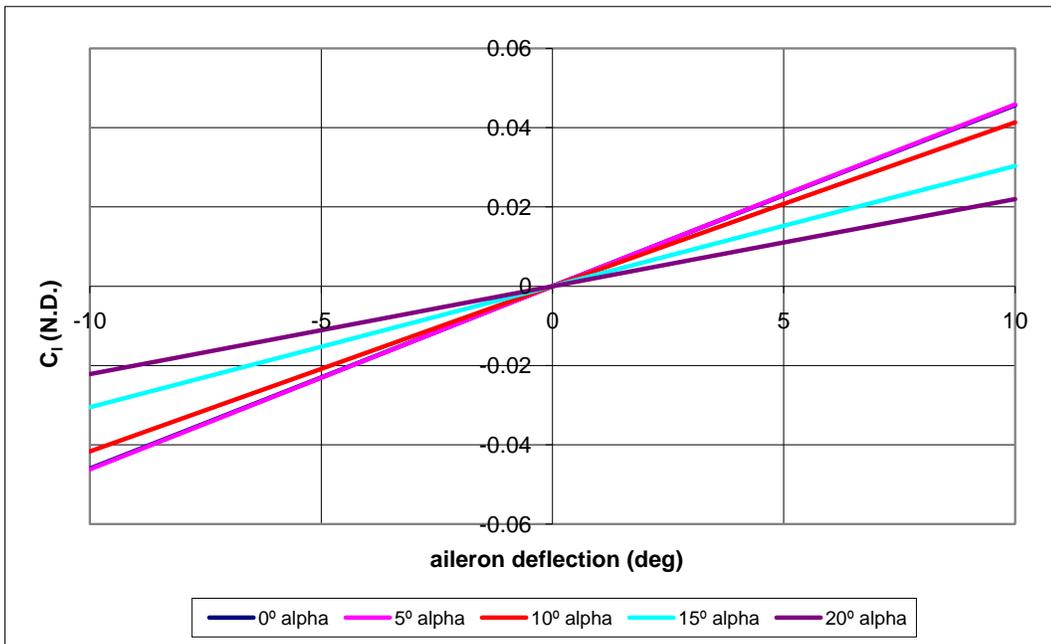
Figure 45: Meridian VORSTAB Model 2 Rolling Moment Coefficient due to Aileron Deflection
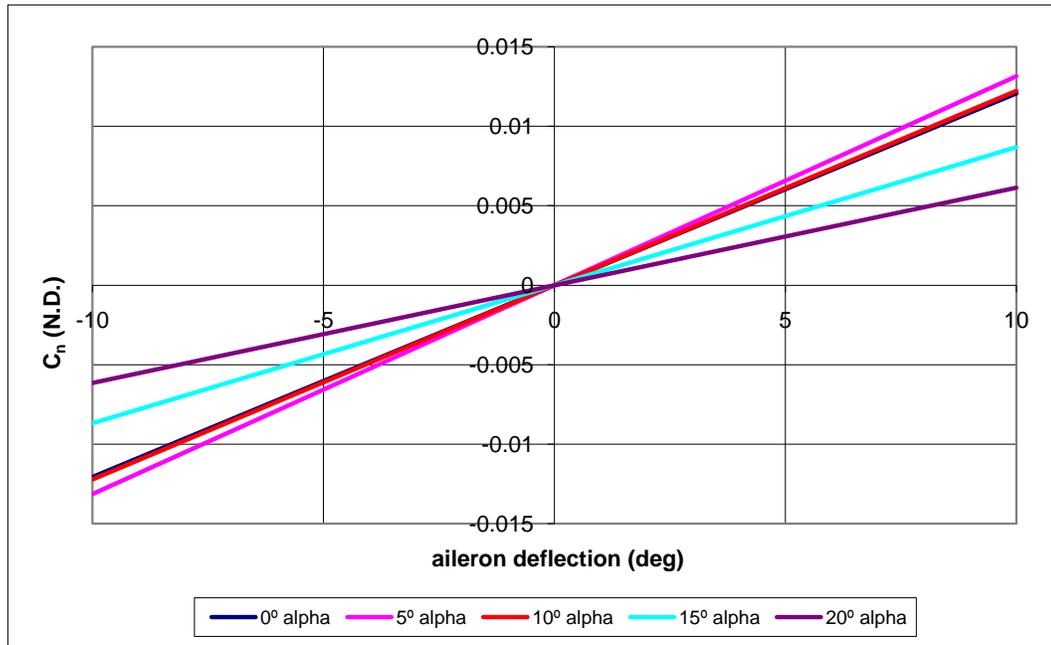
Figure 46: Meridian VORSTAB Model 2 Yawing Moment Coefficient due to Aileron Deflection

The sideforce coefficient due to aileron deflection can be normally be neglected, unless the rolling moment controls are near a vertical surface. This is not the case for the Meridian, but the contribution is very small and almost negligible. VORSTAB does not assume that it should be zero, so it will always calculate a value. Also, the yawing moment coefficient is usually negative since is tends to yaw the aircraft out of an intended turn. VORSTAB shows that this derivative actually shows that it will yaw the aircraft into the intended turn. As expected, a positive aileron deflection produces a positive rolling moment.

Table 36: Meridian VORSTAB Model 2 Longitudinal Derivatives Affected by Symmetrical Tail Deflections

α (deg)	δ_{re}	C_L	C_D	C_m
0	-12	-0.1130	1.6814	-0.1278
5	-12	0.5193	3.1227	-0.2052
10	-12	0.9911	4.8756	-0.3255
15	-12	1.2988	6.8064	-0.3564
20	-12	1.6229	8.9060	-0.4301
0	-6	-0.1009	1.5270	-0.1756
5	-6	0.5381	2.9049	-0.2805
10	-6	0.9918	4.6793	-0.3290
15	-6	1.3111	6.6600	-0.4062
20	-6	1.6353	8.7221	-0.4806
0	0	-0.0916	1.3830	-0.2122
5	0	0.5431	2.7613	-0.3009
10	0	1.0035	4.5399	-0.3764
15	0	1.3224	6.4777	-0.4515
20	0	1.6465	8.4944	-0.5257
0	6	-0.0814	1.2854	-0.2526
5	6	0.5545	2.6096	-0.3462
10	6	1.0140	4.3693	-0.4186
15	6	1.3327	6.2676	-0.4928
20	6	1.6567	8.2347	-0.5659
0	12	-0.0733	1.1596	-0.2847
5	12	0.5645	2.4716	-0.3862
10	12	1.0234	4.1793	-0.4564
15	12	1.3422	6.0375	-0.5303
20	12	1.6660	7.9323	-0.6017
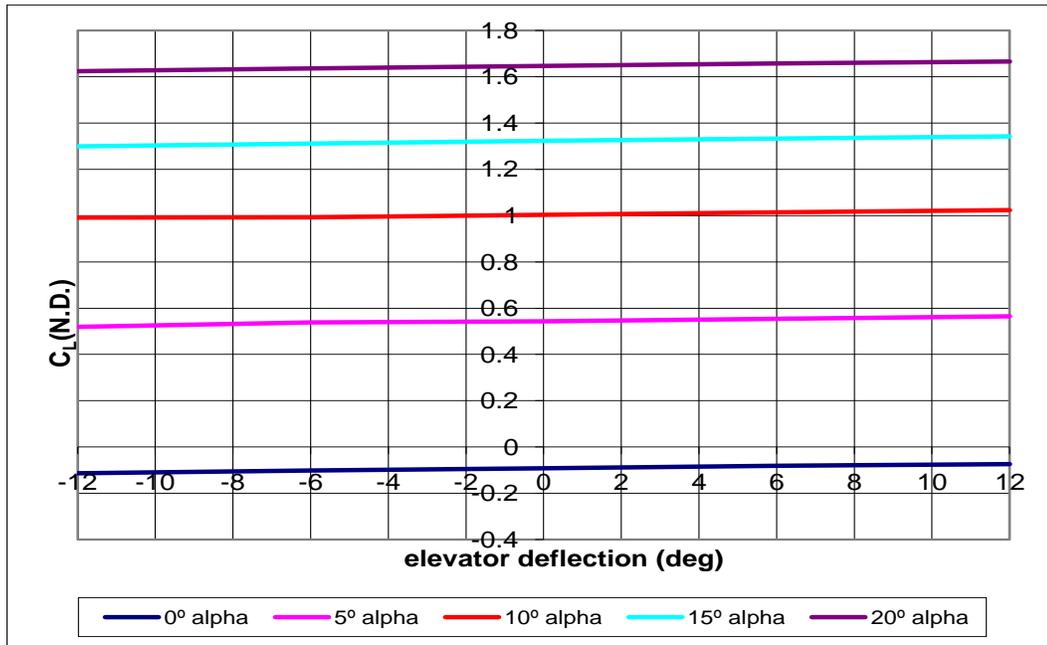
Figure 47: Meridian VORSTAB Model 2 Lift Coefficient due to Elevator Input

Figure 48: Meridian VORSTAB Model 2 Drag Coefficient due to Elevator Input
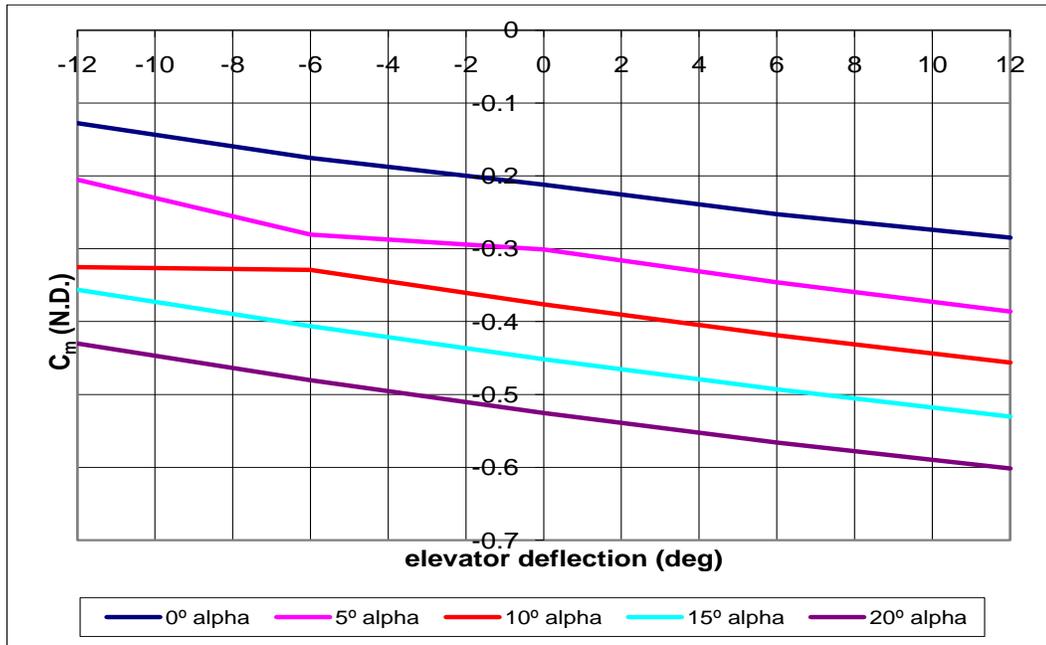
Figure 49: Meridian VORSTAB Model 2 Pitching Moment Coefficient due to Elevator Input

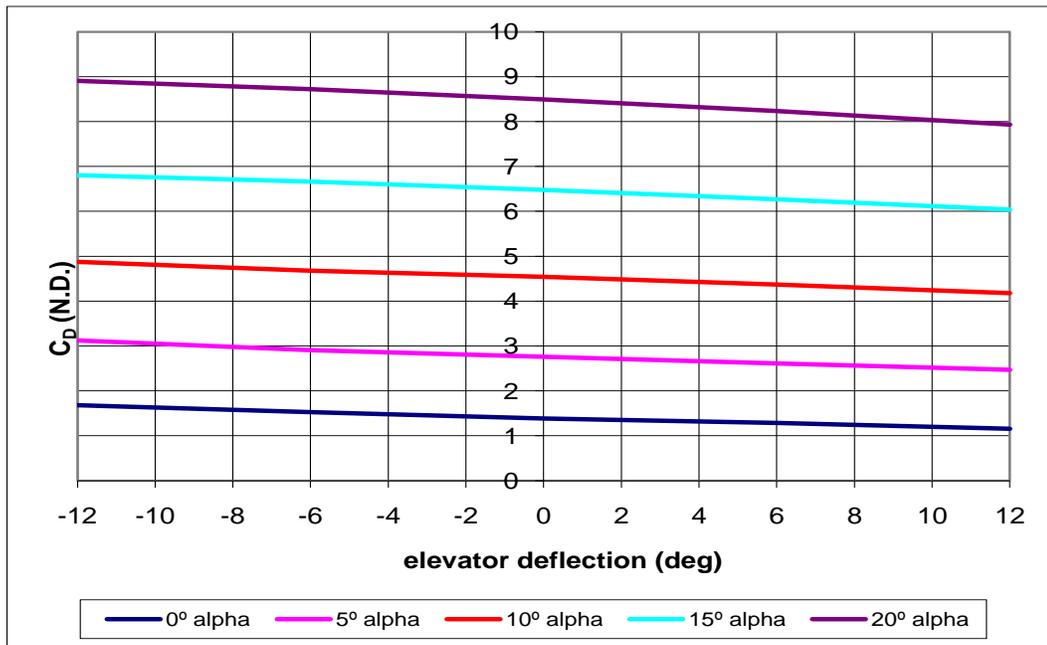A positive elevator input, shows increasing pitching moment and lift. This is expected since the elevators are used to increase the pitch and create lift. As stated earlier the drag is going to be neglected because of its high magnitude.

Table 37: Model 2 Lateral Directional Control Derivatives Affected by Asymmetrical Tail Deflection

α (deg)	δ_{re}	C_y	C_l	C_n
0	-10	-0.0236	-0.0019	0.0102
5	-10	-0.0203	-0.0022	0.0089
10	-10	-0.0162	-0.0022	0.0074
15	-10	-0.0116	-0.0022	0.0056
20	-10	-0.0101	-0.0023	0.0051
0	-5	-0.0114	-0.0010	0.0049
5	-5	-0.0103	-0.0011	0.0045
10	-5	-0.0082	-0.0011	0.0038
15	-5	-0.0059	-0.0011	0.0028
20	-5	-0.0051	-0.0011	0.0026
0	0	0.0000	0.0000	0.0000
5	0	0.0000	0.0000	0.0000
10	0	0.0000	0.0000	0.0000
15	0	0.0000	0.0000	0.0000
20	0	0.0000	0.0000	0.0000
0	5	0.0114	0.0010	-0.0049
5	5	0.0103	0.0011	-0.0045
10	5	0.0082	0.0011	-0.0038
15	5	0.0059	0.0011	-0.0028
20	5	0.0051	0.0011	-0.0026
0	10	0.0220	0.0021	-0.0094
5	10	0.0203	0.0022	-0.0089
10	10	0.0162	0.0022	-0.0074
15	10	0.0116	0.0022	-0.0056
20	10	0.0101	0.0023	-0.0051
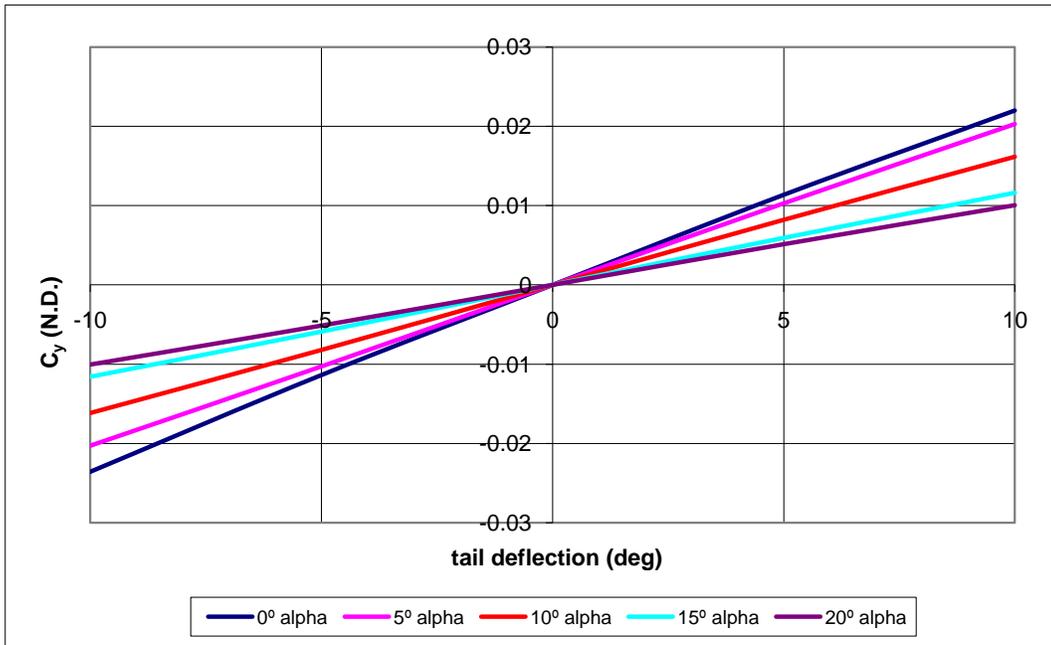
Figure 50: Meridian VORSTAB Model 2 Sideforce Coefficient due to Rudder Input
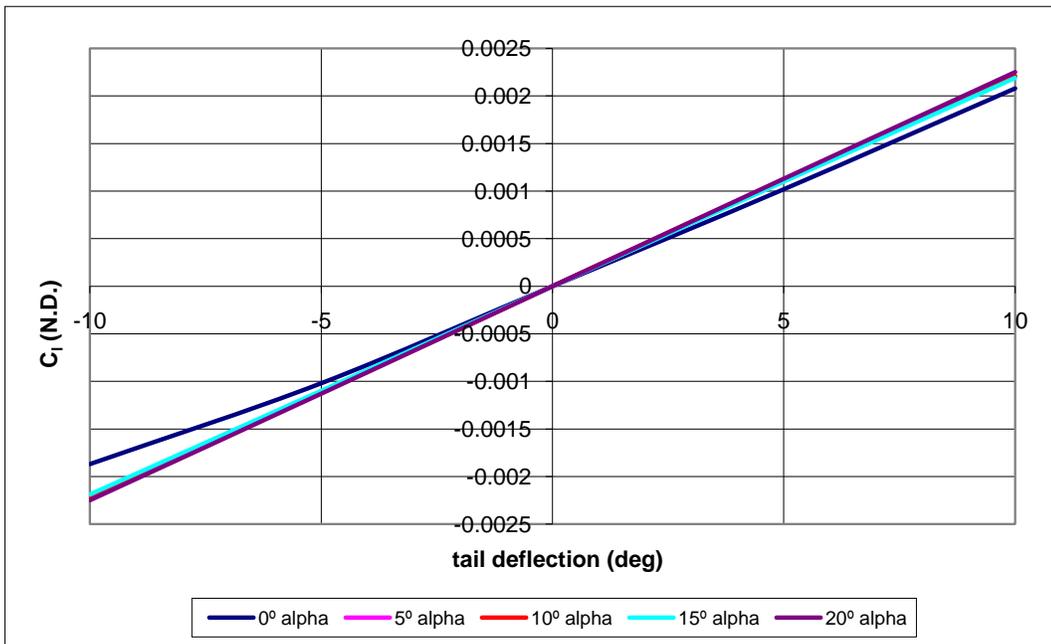
Figure 51: Meridian VORSTAB Model 2 Rolling Moment Coefficient due to Rudder Input
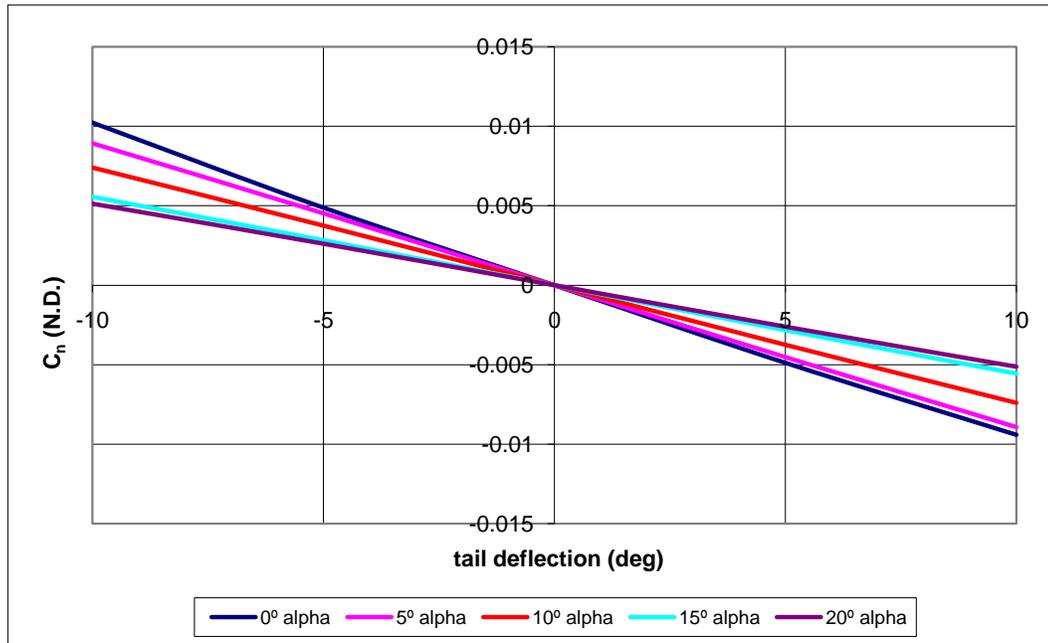
Figure 52: Meridian VORSTAB Model 2 Yawing Moment Coefficient due to Rudder Input

A positive rudder input will produce a positive sideforce, and a positive sideforce will usually generate a positive rolling moment. This type of rudder deflection will also generate a negative yawing moment. This is all seen in the VORSTAB results.

9.2.3 Model 3: Zero Camber Fuselage

The third model created was the same as the second model, but the camber was taken out of the fuselage. Removing the camber removed the amount of downwash that was produced from the large negative camber in the empennage. Having zero camber in the fuselage allows for the assumption that the downwash produced by the fuselage is negligible. The input file for this model can be found in Appendix A. Table 38 shows the longitudinal control derivatives and Figure 53

through Figure 56 depicts Table 38 in graphical form. Table 39 shows the lateral-directional control derivatives and Figure 57 through Figure 60 depicts Table 39 in graphical form.

Table 38: Meridian VORSTAB Model 3 Longitudinal Derivatives at due to Pitch Rate

α (deg)	C_L	C_D	C_m	C_{L_q}	C_{D_q}	C_{m_q}
-5	-0.7157	1.6110	0.2014	6.9744	0.0000	-8.4373
0	-0.2017	0.6312	0.0819	7.1767	0.0000	-8.5688
5	0.4238	0.0982	0.0467	7.2448	0.0000	-8.5992
10	0.9047	0.0703	-0.0596	7.1331	0.0000	-8.3595
15	1.2318	0.3564	-0.1686	6.8019	0.0000	-7.6632
20	1.5543	1.1494	-0.2437	6.5935	0.0000	-7.8832
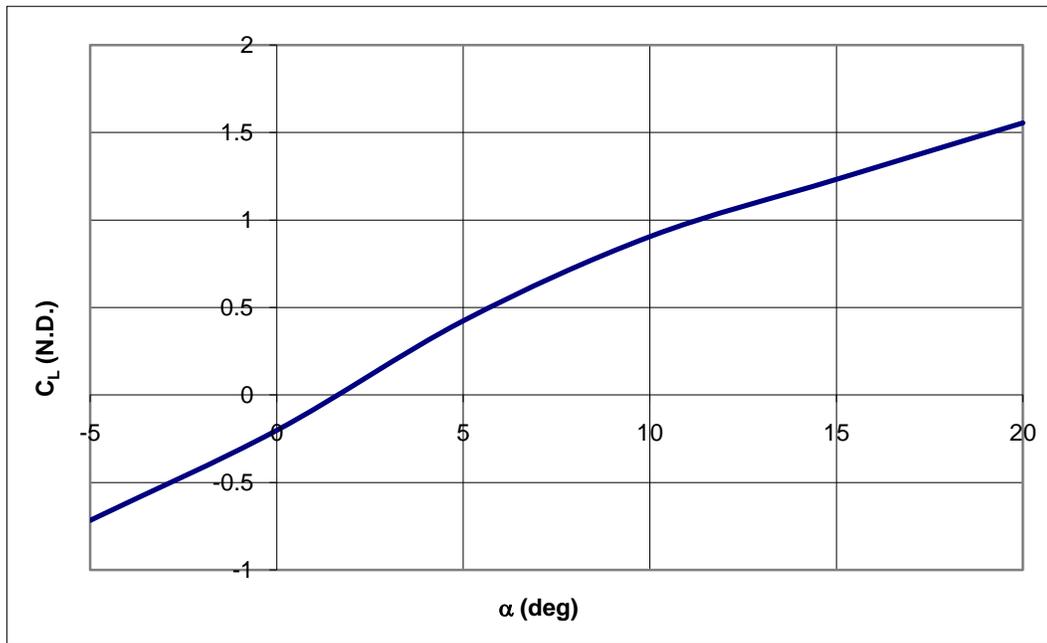
Figure 53: Meridian VORSTAB Model 3 Lift Coefficient due to Angle of Attack
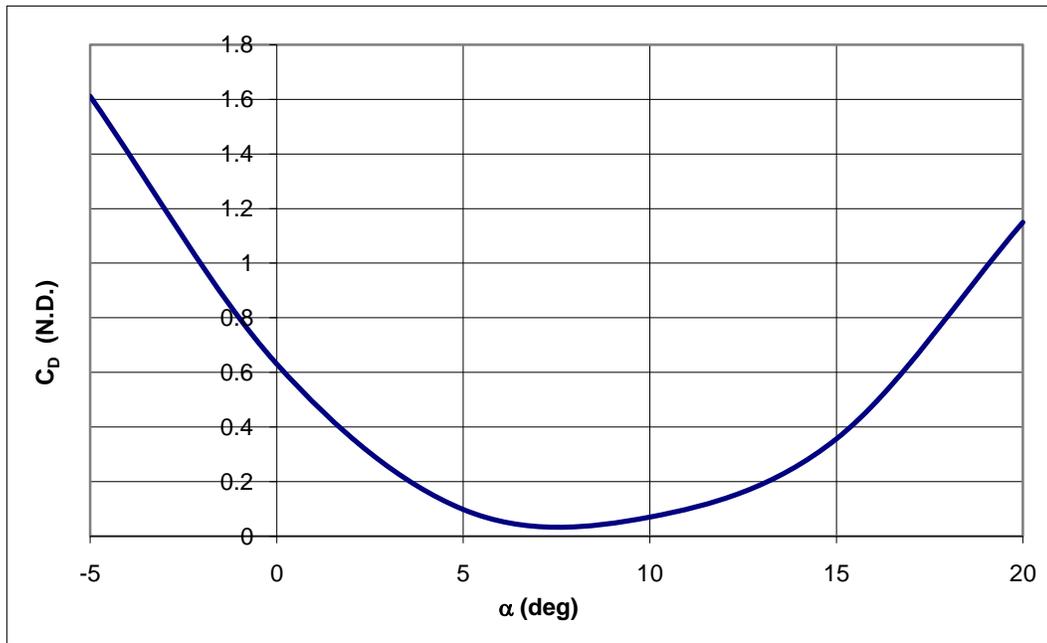
Figure 54: Meridian VORSTAB Model 3 Drag Coefficient due to Angle of Attack
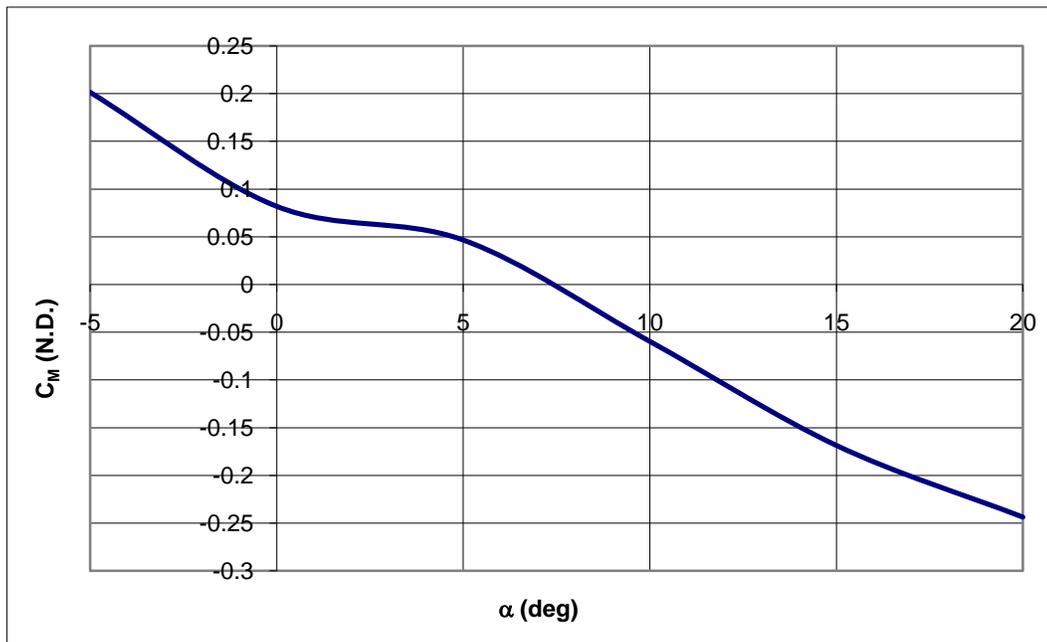
Figure 55: Meridian VORSTAB Model 3 Pitching Moment Coefficient due to Angle of Attack
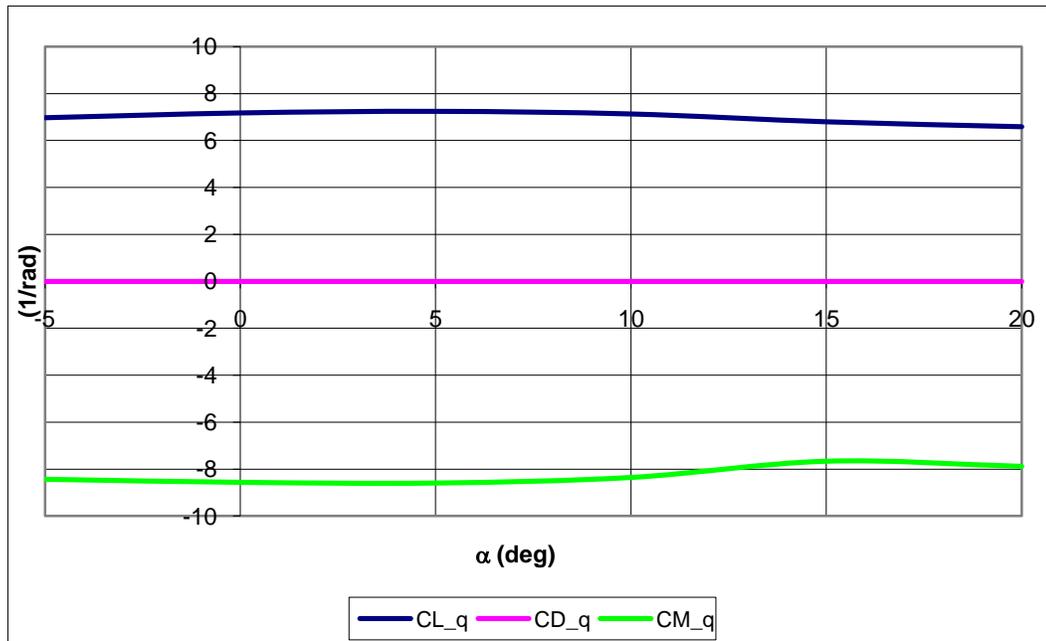
Figure 56: Meridian VORSTAB Model 3 Longitudinal Coefficients due to Pitch Rate

Similar to Model 2, these longitudinal derivatives are within the appropriate range and have the expected sign convention. The drag is still high, but is much better than the second model. Lift is negative at zero degree angle of attack, and should be positive.

Table 39: Meridian VORSTAB Model 3 Lateral-Directional Derivatives

α (deg)	$C_{y\beta}$	$C_{l\beta}$	$C_{n\beta}$	C_{yp}	C_{lp}	C_{np}	C_{yr}	C_{lr}	C_{nr}
-5	0.668	-0.104	0.051	-0.161	-0.476	-0.213	0.067	-0.260	-0.062
0	0.823	-0.103	0.077	-0.107	-0.292	-0.024	0.126	-0.232	-0.046
5	0.994	-0.123	0.071	-0.145	-0.466	-0.523	0.186	-0.195	-0.032
10	0.941	-0.119	0.069	-0.059	-0.236	-0.328	0.223	-0.118	-0.022
15	0.708	-0.116	0.056	-0.030	-0.126	-0.244	0.213	-0.069	-0.005
20	0.472	-0.108	0.032	-0.018	-0.081	-0.235	0.183	-0.045	0.026
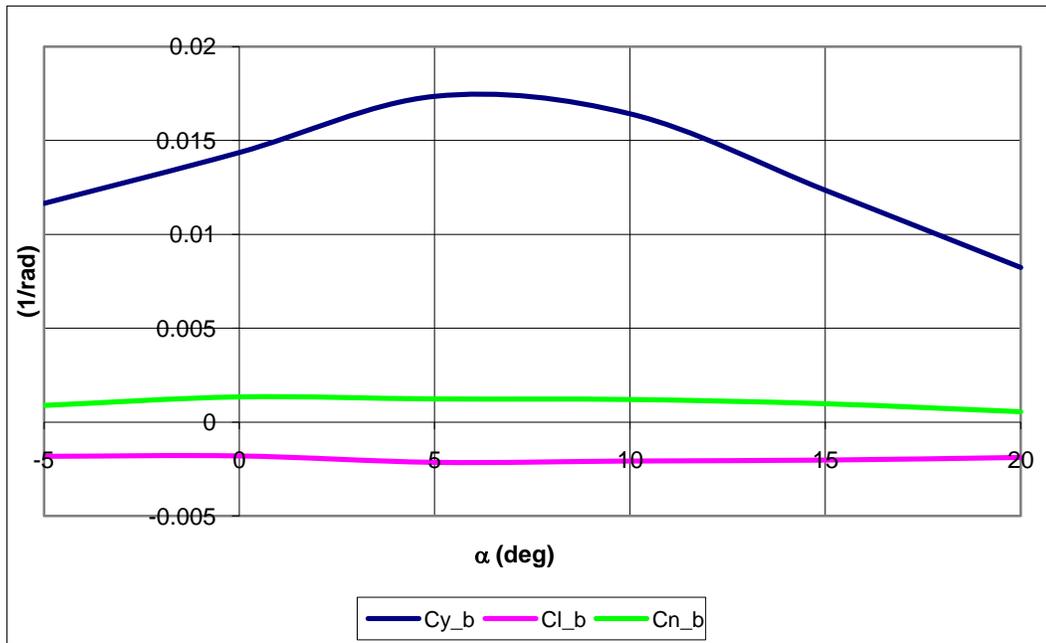
Figure 57: Meridian VORSTAB Model 3 Lateral-Directional Derivatives due to Sideslip
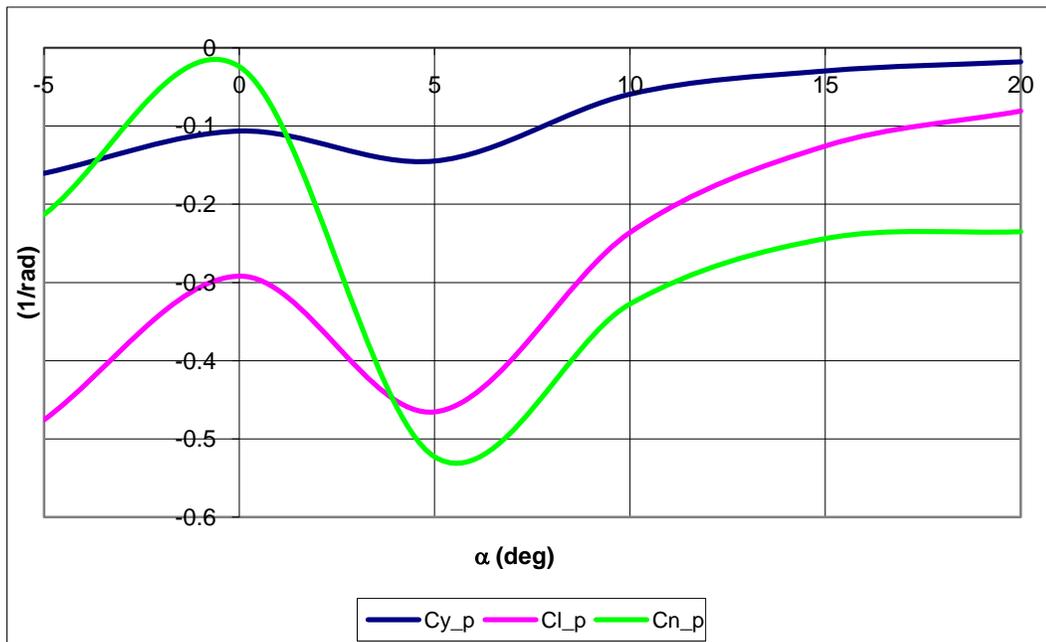
Figure 58: Meridian VORSTAB Model 3 Lateral-Directional Derivatives due to Roll Rate
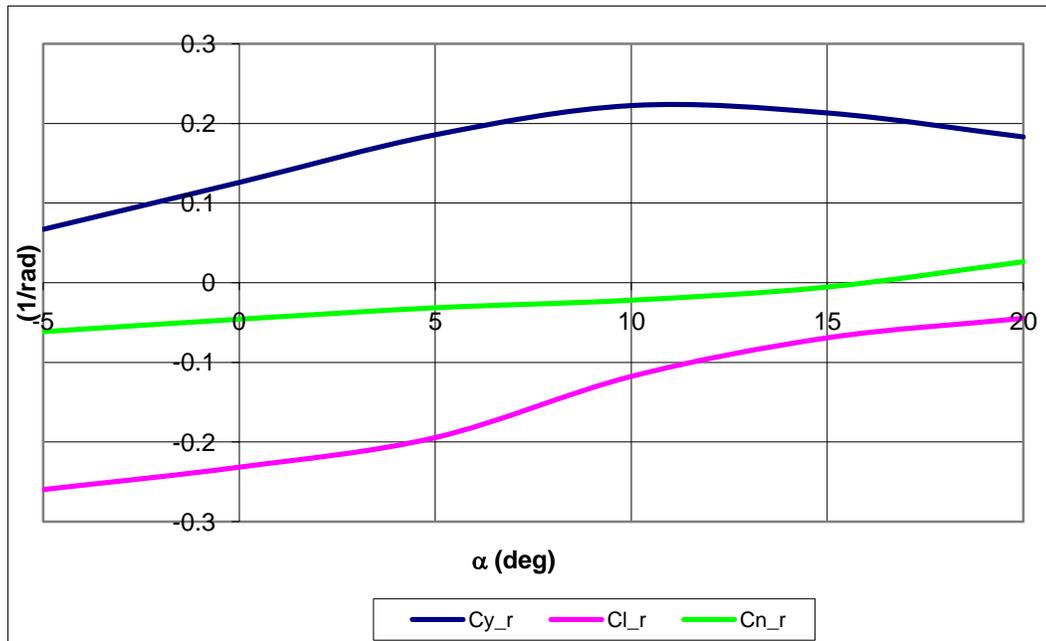
Figure 59: Meridian VORSTAB Model 3 Lateral-Directional Derivatives due to Yaw Rate

The sideforce coefficient due to sideslip is usually negative, but the VORSTAB results show a positive value. Sideforce coefficient due to roll rate has a positive and negative typical range, but it is usually negative due to the moment arm. This is seen in the VORSTAB results. The rest of the derivatives are as expected. The rolling moment and yawing moment coefficients due to roll rate have extreme fluctuations from one angle of attack to another. This does not necessarily mean that it is wrong, but rather the angle of attack has a large influence on the control of the aircraft.

The control surface deflections affect the stability and control derivatives in both the longitudinal mode and the lateral-directional mode. Table 40 shows the affects of the aileron on the lateral-directional derivatives, Table 41 shows the affect of a symmetrical tail deflection on the longitudinal derivatives, and Table 42 shows

the affect of an asymmetrical tail deflection on the lateral-directional derivatives. These tables are depicted in Figure 60 through Figure 68.

Table 40: Meridian VORSTAB Model 3 Lateral-Directional Derivative due to Aileron Deflection

α (deg)	δ_a (deg)	C_y	C_l	C_n
0	-10	-0.0099	-0.0460	-0.0120
5	-10	-0.0099	-0.0462	-0.0131
10	-10	-0.0090	-0.0420	-0.0124
15	-10	-0.0066	-0.0310	-0.0089
20	-10	-0.0048	-0.0225	-0.0063
0	-5	-0.0050	-0.0230	-0.006
5	-5	-0.0050	-0.0231	-0.0066
10	-5	-0.0045	-0.0210	-0.0062
15	-5	-0.0033	-0.0155	-0.0044
20	-5	-0.0024	-0.0113	-0.0031
0	0	0.0000	0.0000	0.0000
5	0	0.0000	0.0000	0.0000
10	0	0.0000	0.0000	0.0000
15	0	0.0000	0.0000	0.0000
20	0	0.0000	0.0000	0.0000
0	5	0.0050	0.02291	0.006
5	5	0.0050	0.02302	0.00657
10	5	0.0045	0.02095	0.00619
15	5	0.0033	0.01544	0.00442
20	5	0.0024	0.01121	0.00313
0	10	0.0098	0.04558	0.012
5	10	0.0099	0.04581	0.01315
10	10	0.0090	0.04169	0.01239
15	10	0.0066	0.03071	0.00885
20	10	0.0047	0.02231	0.00627
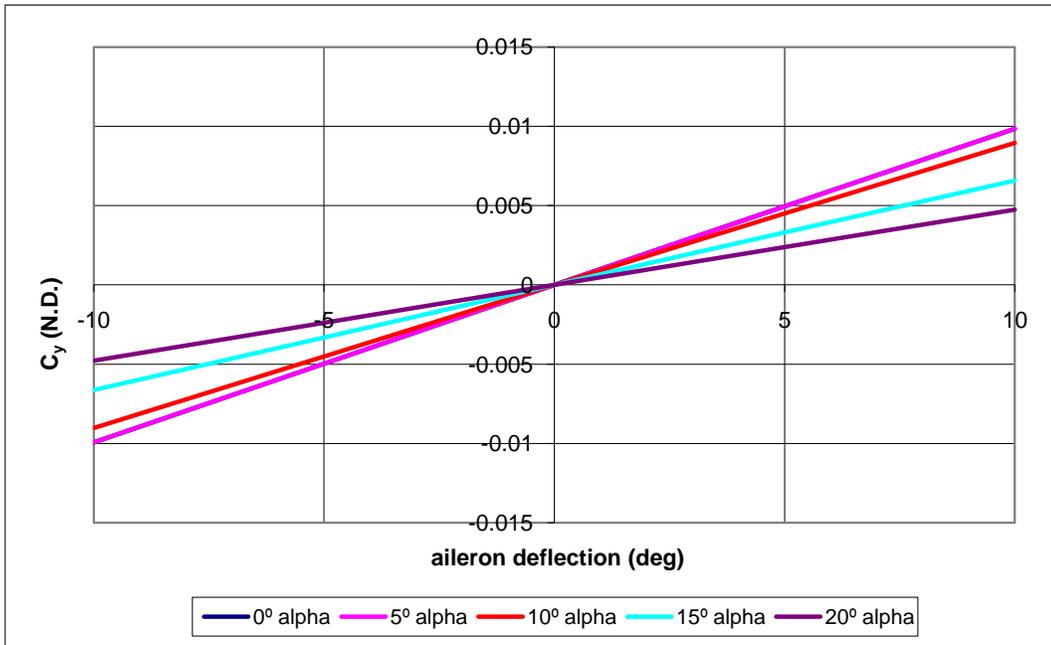
Figure 60: Meridian VORSTAB Model 3 Sideforce Coefficient due to Aileron Deflection
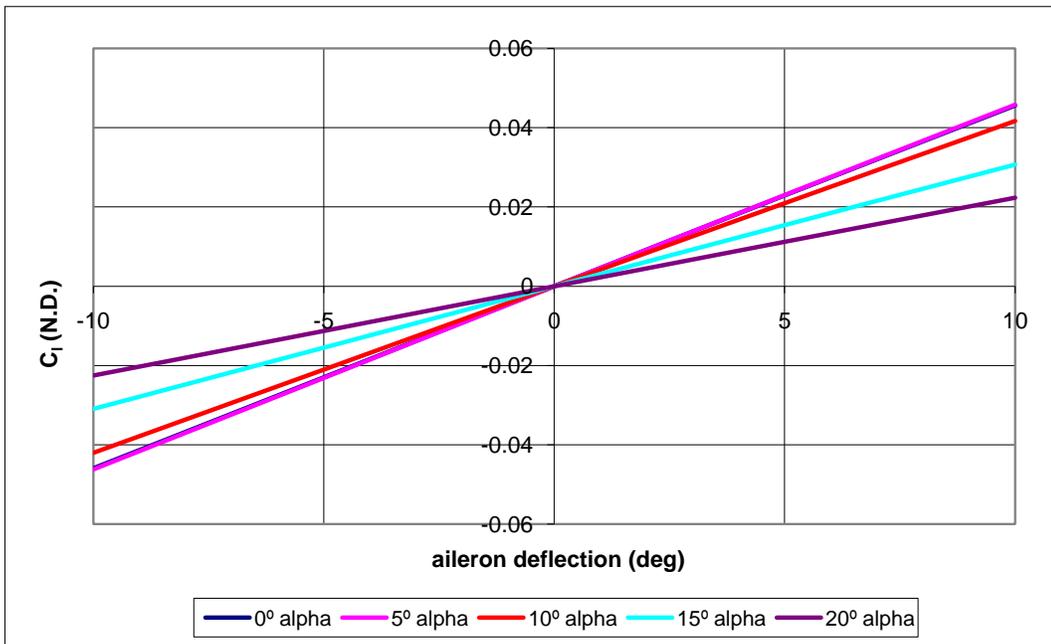
Figure 61: Meridian VORSTAB Model 3 Rolling Moment Coefficient due to Aileron Deflection

Figure 62: Meridian VORSTAB Model 3 Yawing Moment Coefficient due to Aileron Deflection

A sideforce coefficient due to aileron deflection is usually negligible, and VORSTAB shows a very small value. This is expected since there are no rolling moment controls close to a vertical surface. Positive aileron deflections result in a positive rolling moment and yawing moment.

Table 41: Meridian VORSTAB Model 3 Longitudinal Derivatives due to Symmetrical Tail Deflections

α (deg)	δ_re (deg)	C_L	C_D	C_m
0	-12	-0.2132	0.5057	0.0970
5	-12	0.4096	0.0814	0.1028
10	-12	0.8894	0.0849	0.0019
15	-12	1.2173	0.4285	-0.1098
20	-12	1.5409	1.2620	-0.1896
0	-6	-0.2042	0.5916	0.0916
5	-6	0.4230	0.0948	0.0496
10	-6	0.9016	0.0730	-0.0474
15	-6	1.2290	0.3648	-0.1572
20	-6	1.5518	1.1718	-0.2335
0	0	-0.1932	0.6789	0.0488
5	0	0.4349	0.1091	0.0024
10	0	0.9135	0.0631	-0.0956
15	0	1.2400	0.3106	-0.2016
20	0	1.5616	1.0614	-0.2731
0	6	-0.1836	0.8198	0.0111
5	6	0.4476	0.1225	-0.0482
10	6	0.9250	0.0564	-0.1420
15	6	1.2500	0.2607	-0.2421
20	6	1.5706	0.9528	-0.3088
0	12	-0.1707	0.9102	-0.0400
5	12	0.4568	0.1337	-0.0935
10	12	0.9356	0.0534	-0.1847
15	12	1.2591	0.1949	-0.2786
20	12	1.5787	0.8708	-0.3404
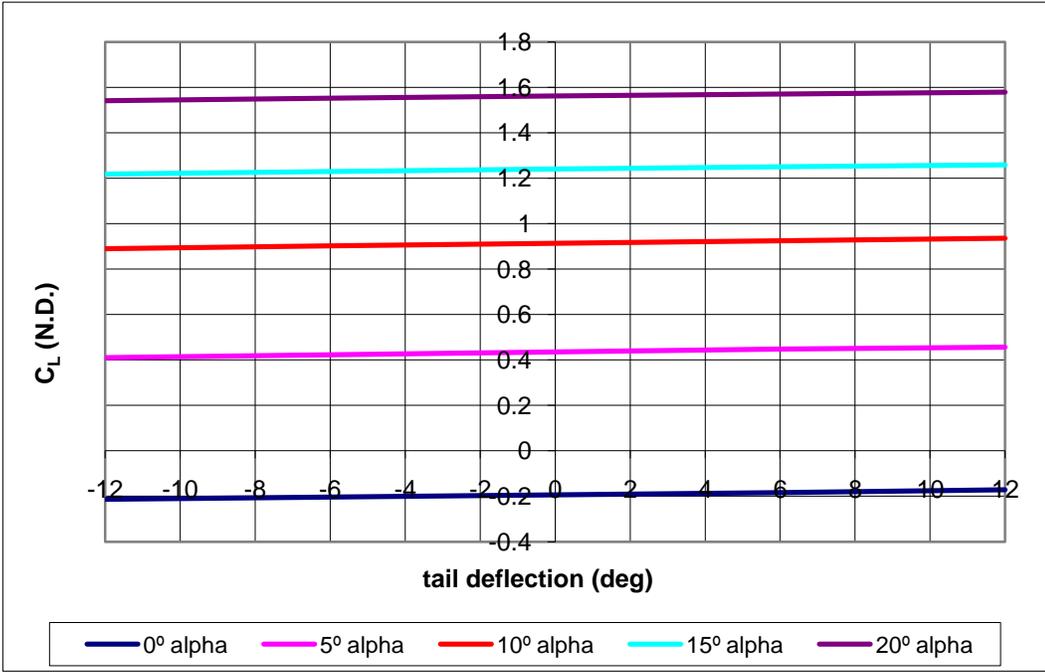
Figure 63: Meridian VORSTAB Model 3 Lift Coefficient due to Elevator Input

Figure 64: Meridian VORSTAB Model 3 Drag Coefficient at due to Elevator Input

112
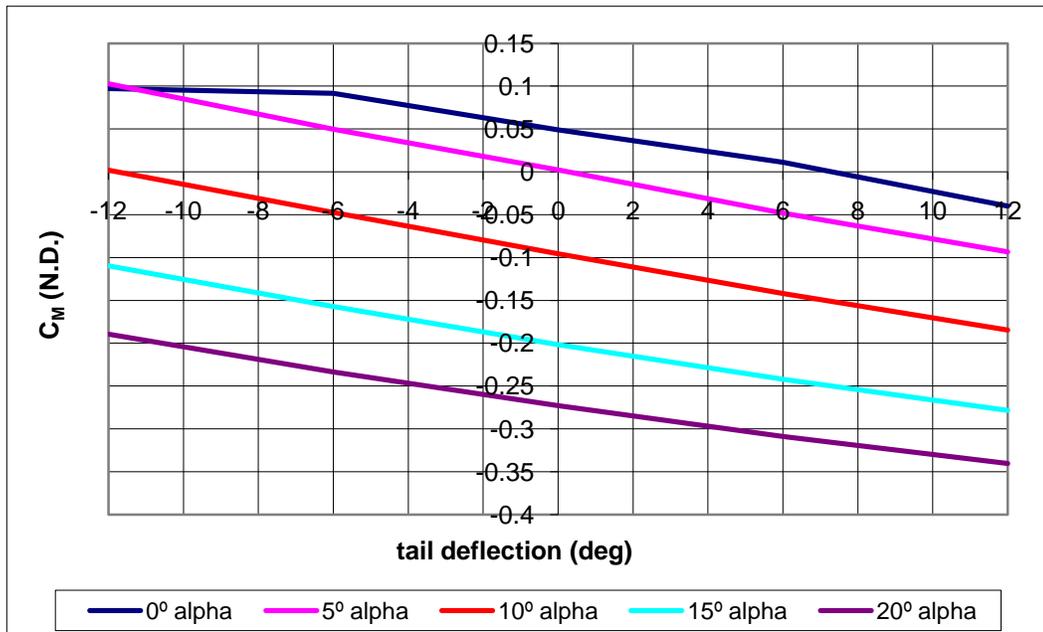
Figure 65: Meridian VORSTAB Model 3 Pitching Moment Coefficient due to Elevator Input

Elevator input deflection will increase the lift and pitching moment. This is the purpose of the positive elevator input. The drag coefficient increases on some angles of attack and decreases on the others. When the lift increases the drag should always increase. This is due to the definition of drag being a function of lift. VORSTAB shows that at angles of attack of 10° or higher the drag will decrease with positive elevator deflections. As stated previously, the drag is much higher than it should be and is not accurate.

Table 42: Meridian Model 3 Lateral-Directional Derivatives Affected by Asymmetrical Tail Deflections

α (deg)	δ_{re} (deg)	C_y	C_l	C_n
0	-10	-0.0215	-0.0021	0.0083
5	-10	-0.0226	-0.0020	0.0092
10	-10	-0.0229	-0.0018	0.0098
15	-10	-0.0162	-0.0020	0.0070
20	-10	-0.0145	-0.0022	0.0064
0	-5	-0.0109	-0.0011	0.0042
5	-5	-0.0117	-0.0010	0.0048
10	-5	-0.0109	-0.0010	0.0046
15	-5	-0.0082	-0.0010	0.0035
20	-5	-0.0073	-0.0011	0.0033
0	0	0.0000	0.0000	0.0000
5	0	0.0000	0.0000	0.0000
10	0	0.0000	0.0000	0.0000
15	0	0.0000	0.0000	0.0000
20	0	0.0000	0.0000	0.0000
0	5	0.0109	0.0011	-0.0042
5	5	0.0123	0.0009	-0.0051
10	5	0.0109	0.0010	-0.0046
15	5	0.0082	0.0010	-0.0035
20	5	0.0073	0.0011	-0.0033
0	10	0.0215	0.0021	-0.0083
5	10	0.0239	0.0019	-0.0098
10	10	0.0209	0.0020	-0.0088
15	10	0.0162	0.0020	-0.0070
20	10	0.0145	0.0022	-0.0064
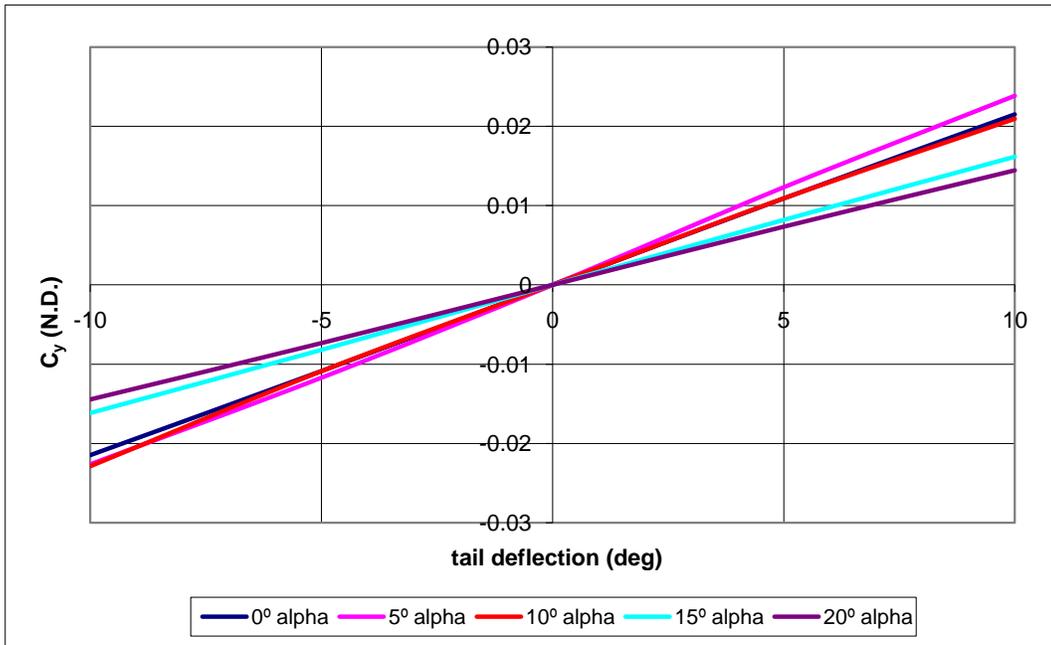
Figure 66: Meridian VORSTAB Model 3 Sideforce Coefficient due to Rudder Input

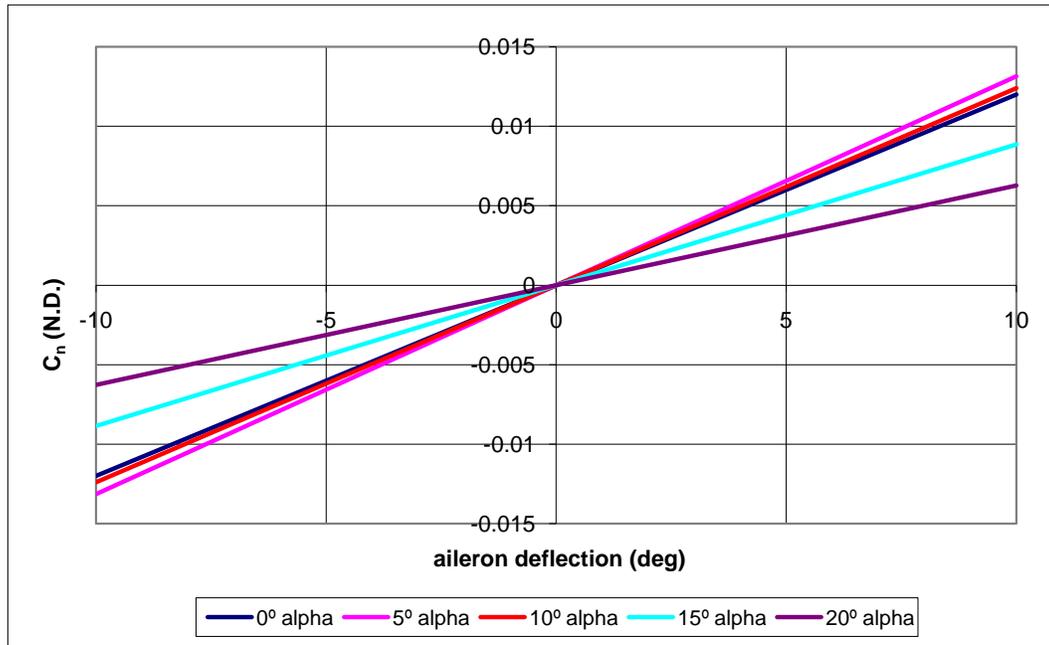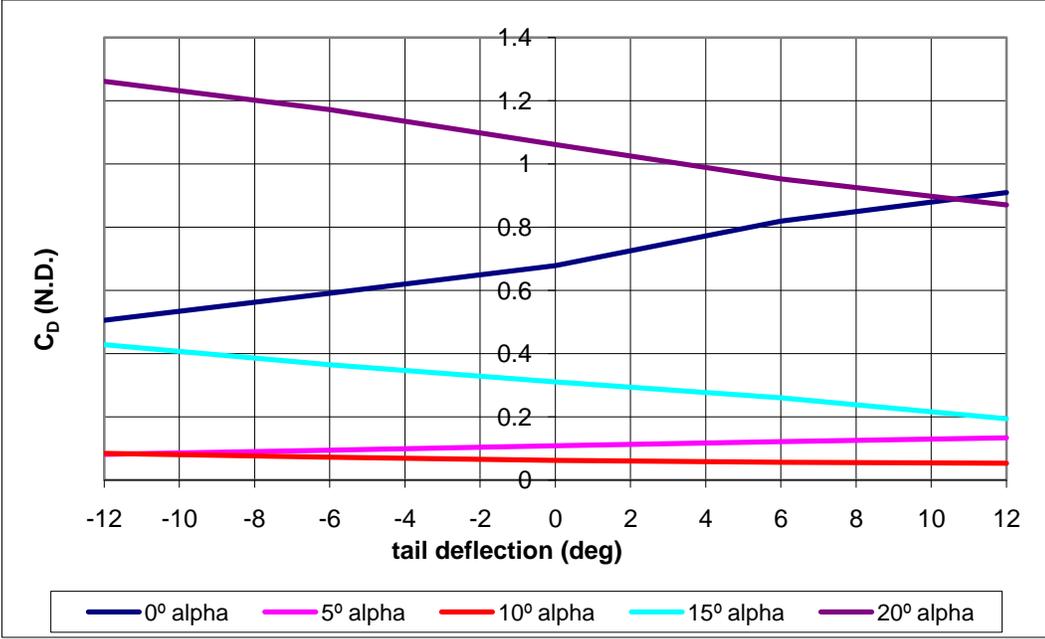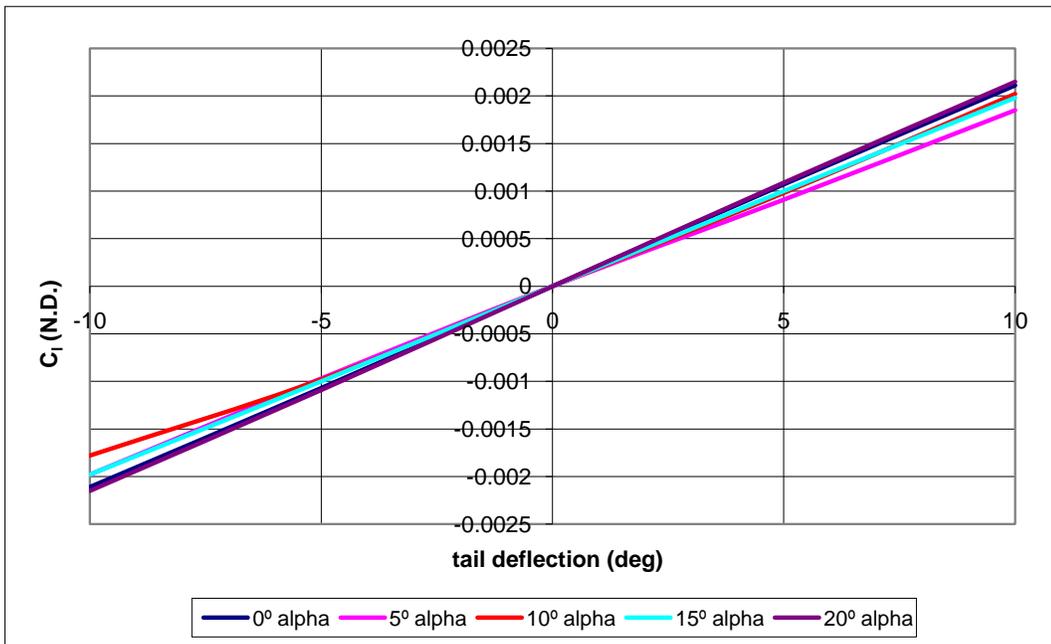**Figure 67: Meridian VORSTAB Model 3 Rolling Moment Coefficient due to Rudder Input**
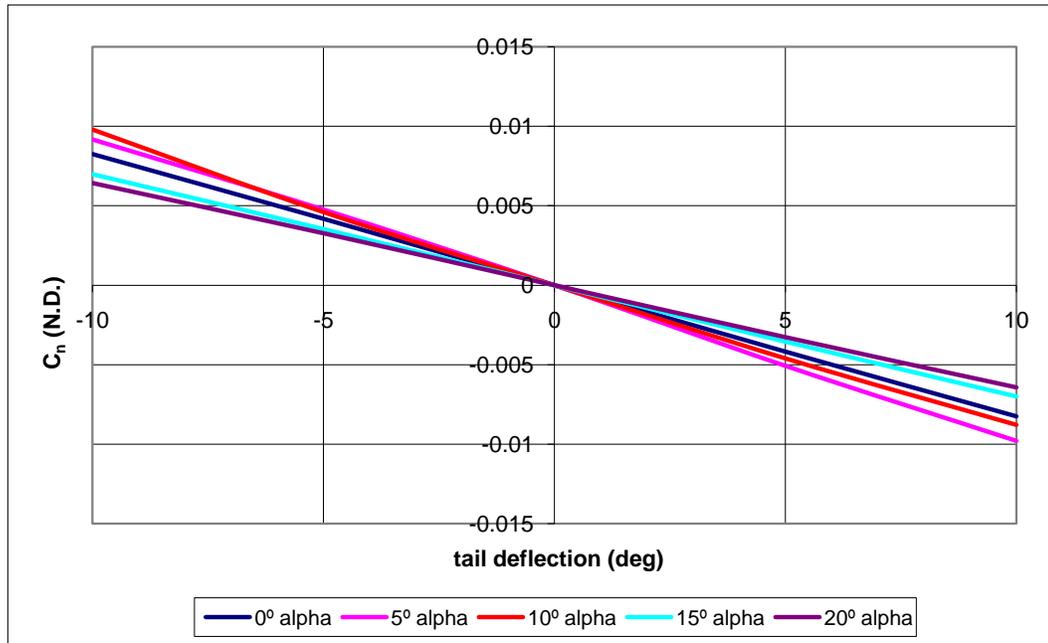
Figure 68: Meridian VORSTAB Model 3 Yawing Moment Coefficient due to Rudder Input

As expected, a positive rudder input results in a positive sideforce and rolling moment. It also results in a negative yawing moment.

9.2.4   Model 4: Wings and V-Tail

Since the problem with the downwash came from the fuselage, it was removed from the forth model. This type of model helps the designer see what effect the fuselage is having on the results. The wings and the v-tail were kept in their exact location but were extended to the centerline. Appendix A contains the input file for this model. Table 43 shows the longitudinal control derivatives, and Figure 69 through Figure 72 depicts Table 43 in graphical form.

Table 43: Meridian VORSTAB Model 4 Longitudinal Derivatives

α (deg)	C_L	C_D	C_m	C_{Lq}	C_{Dq}	C_{mq}
-5	-0.7969	0.0012	-0.0309	3.6132	0.0000	-3.7654
0	-0.3916	0.0155	-0.0995	3.7241	0.0000	-3.7942
5	0.0736	0.0244	-0.1135	3.7503	0.0000	-3.7654
10	0.6302	0.0202	-0.1031	3.6904	0.0000	-3.6798
15	0.9934	0.0431	-0.1256	3.5476	0.0000	-3.5400
20	1.2843	0.0581	-0.1517	3.3238	0.0000	-3.3255
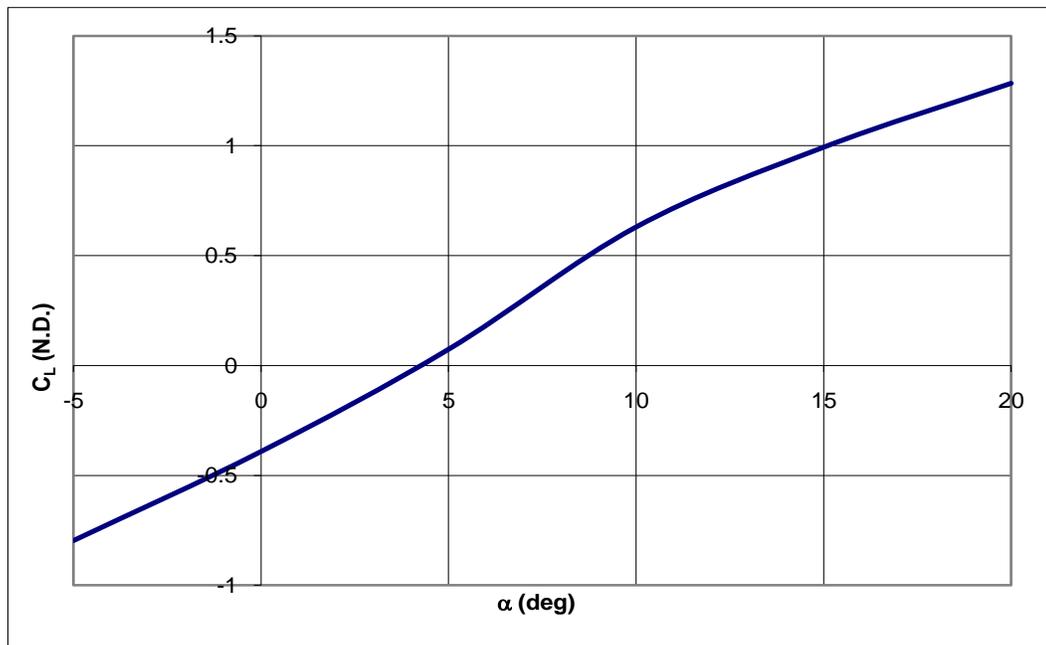
Figure 69: Meridian VORSTAB Model 4 Lift Coefficient due to Angle of Attack
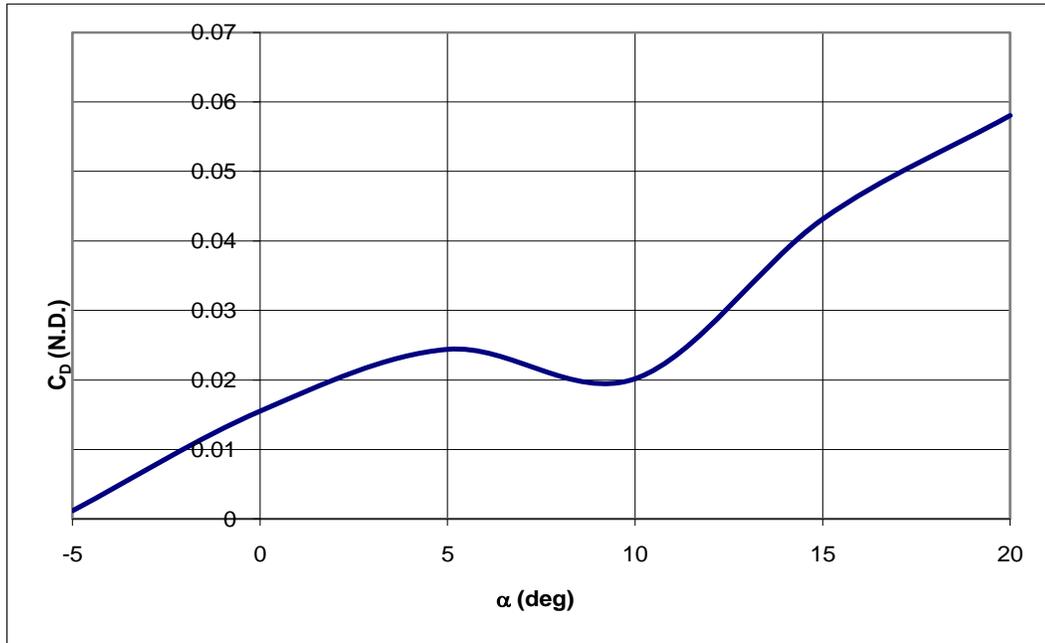
Figure 70: Meridian VORSTAB Model 4 Drag Coefficient due to Angle of Attack
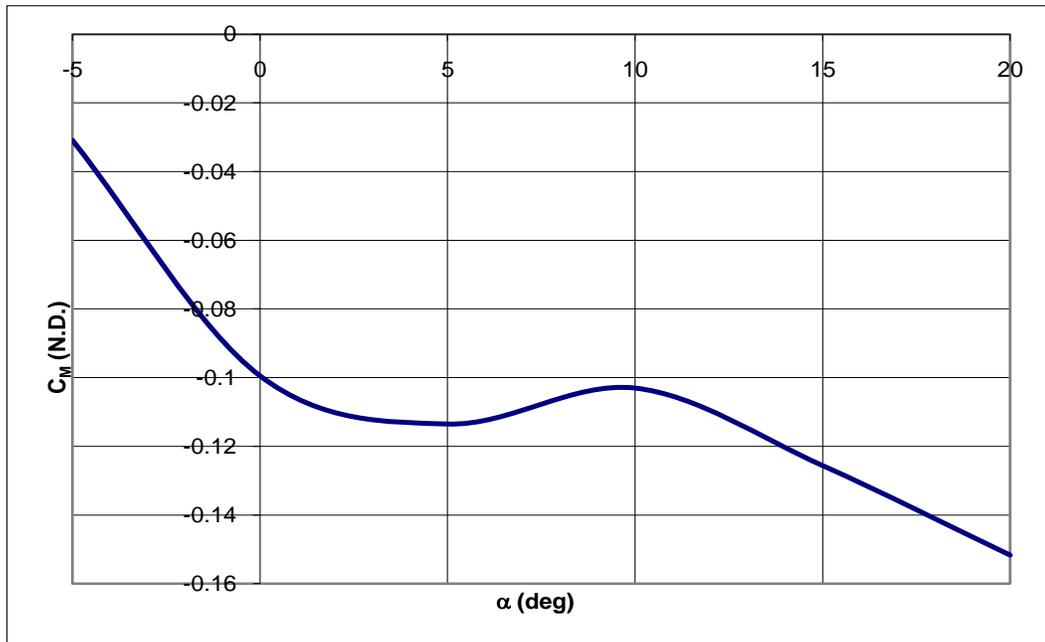
Figure 71: Meridian VORSTAB Model 4 Pitching Moment Coefficient due to Angle of Attack
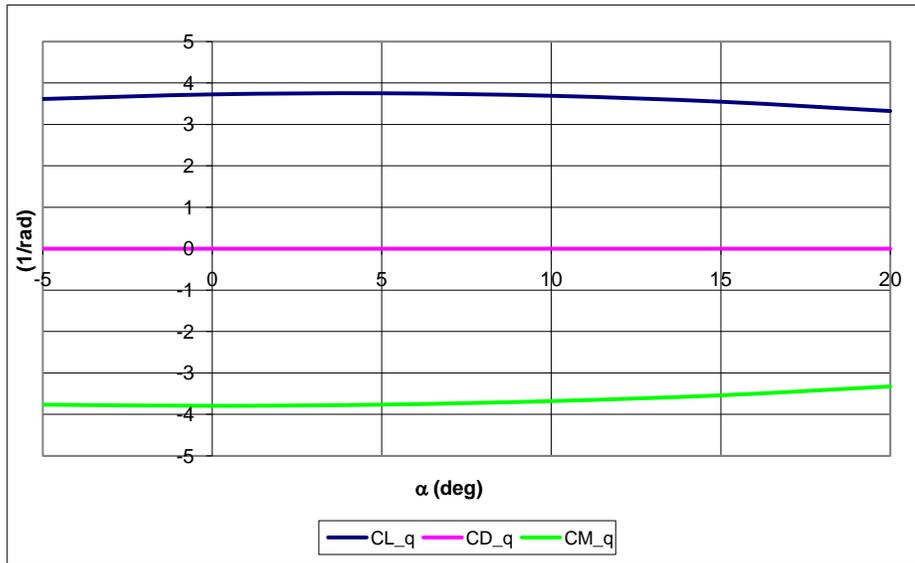
Figure 72: Meridian VORSTAB Model 4 Longitudinal Derivatives due to Pitch Rate

As seen from the pitching moment graph, the wings and tail become unstable at a certain angle of attack. This is seen by the slope of Figure 71 becoming positive. With a positive slope the aircraft wants pitch away from the stable point. The drag and lift results are as expected, except for the angle of zero lift being around 4˚. With the airfoils used on the wings and tail and their geometric configuration it would be expected that the angle of zero lift would be at a negative angle of attack. There could be many causes for these results. A possible cause is the high camber of the airfoils is producing downwash. From these results, it can be seen that the fuselage contributes significantly to the drag in the VORSTAB model. The lateral-directional control derivatives are shown in Table 44. Figure 73 through Figure 75 depicts Table 44 in graphical form.

Table 44: Meridian VORSTAB Model 4 Lateral-Directional Control Derivatives

α (deg)	$C_{y\beta}$	$C_{l\beta}$	$C_{n\beta}$	C_{yp}	C_{lp}	C_{np}	C_{yr}	C_{lr}	C_{nr}
-5	0.009	-0.0021	0.0013	-0.1703	-0.473	-0.1837	0.1107	-0.252	-0.087
0	0.011	-0.0019	0.0016	-0.1229	-0.296	0.0226	0.1291	-0.232	-0.067
5	0.014	-0.0024	0.0005	-0.1719	-0.479	-0.4940	0.1475	-0.198	-0.031
10	0.016	-0.0022	0.0006	-0.1145	-0.311	-0.3801	0.1561	-0.132	0.003
15	0.014	-0.0019	0.0006	-0.0587	-0.140	-0.2353	0.1528	-0.071	0.013
20	0.011	-0.0017	0.0005	-0.0435	-0.090	-0.2169	0.1461	-0.043	0.029
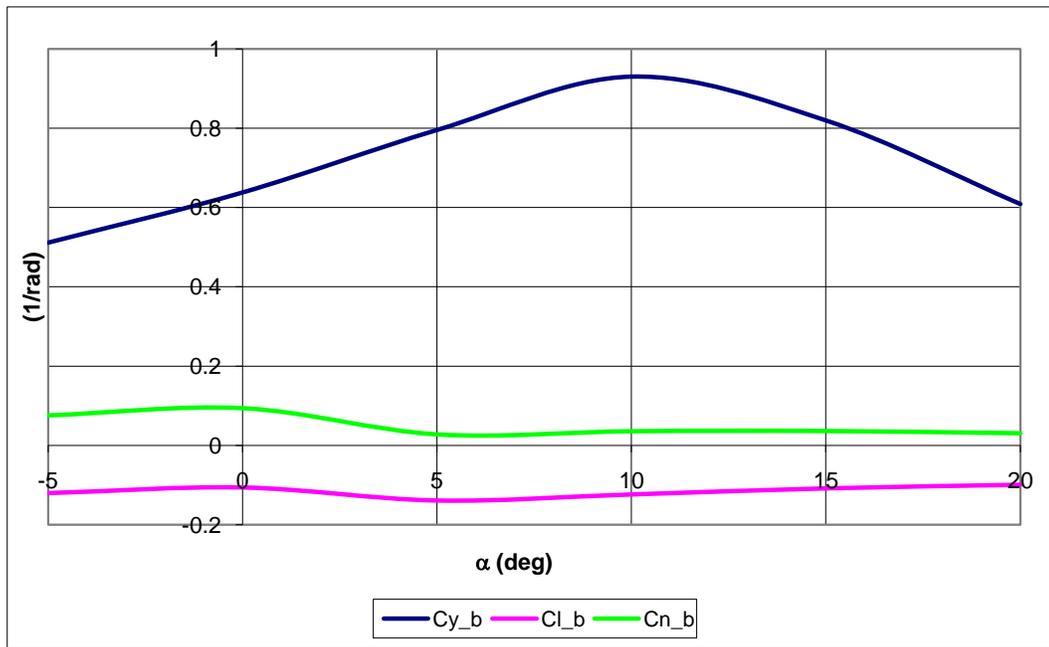
Figure 73: Meridian VORSTAB Model 4 Lateral-Directional Derivatives due to Sideslip
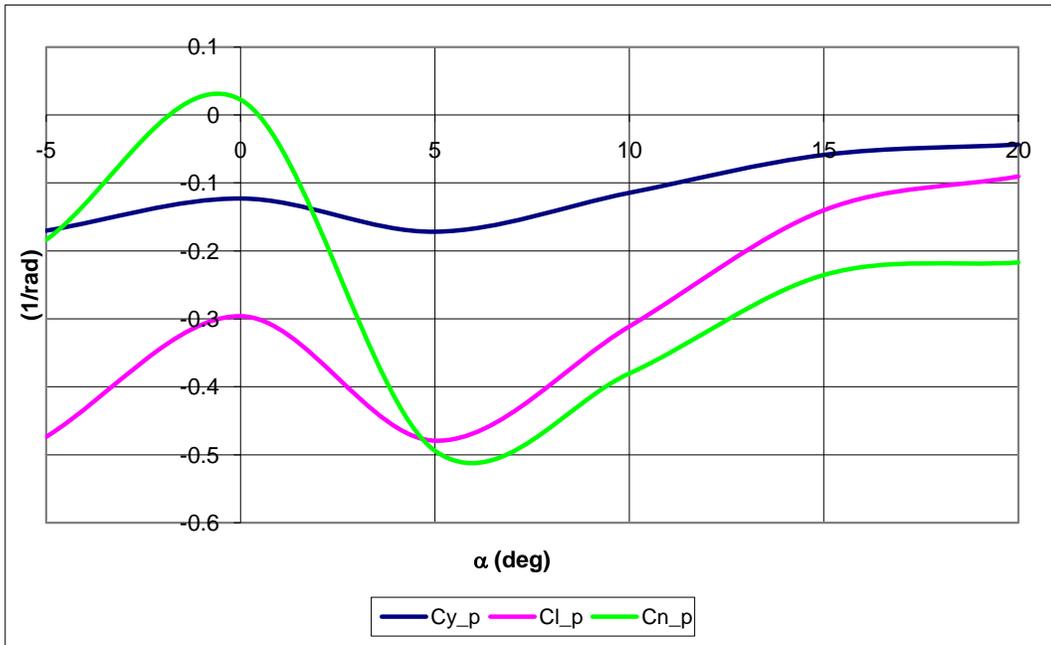
Figure 74: Meridian VORSTAB Model 4 Lateral-Directional Derivatives due to Roll Rate
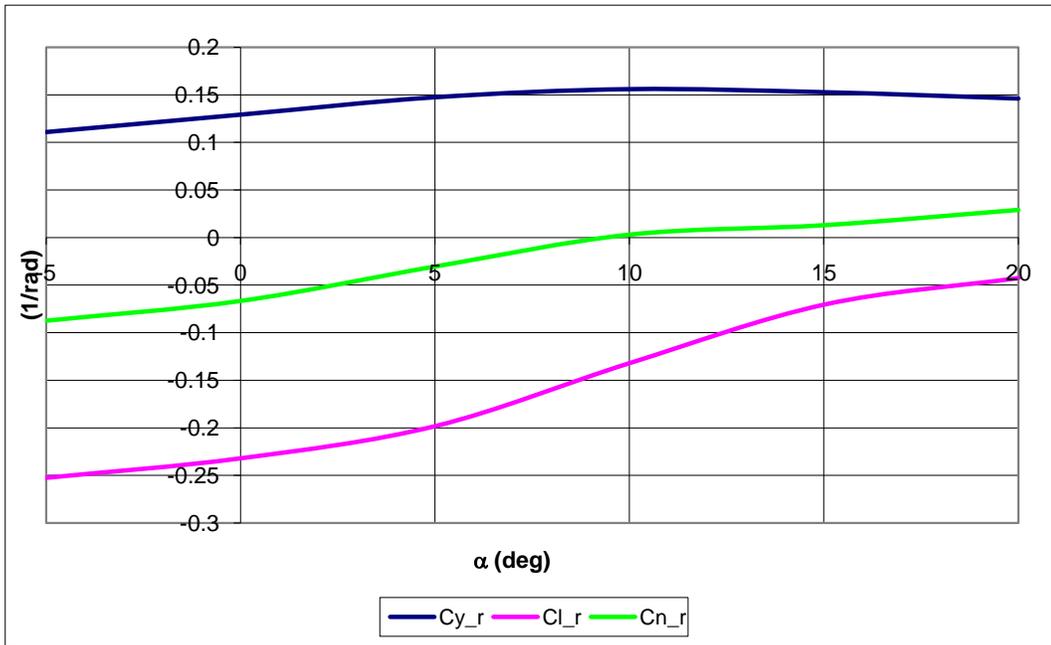
Figure 75: Meridian VORSTAB Model 4 Lateral-Directional Derivatives due to Yawing Moment

The sideforce coefficient due to sideslip, $C_{y\beta}$, is unstable at all angles of attack. This can be neglected because having the fuselage will dramatically affect this. The yawing moment coefficient due to yaw rate, C_{nr}, is also unstable at higher angles of attack. A stable aircraft should naturally want to stop yawing or slow down. When it is unstable the yawing rate increases and can lead to a spin. This will also be influenced by the fuselage and could be stable if it were present. Table 45 shows the lateral-directional derivatives due to an aileron deflection, Table 46 shows the longitudinal derivatives due to a symmetrical deflection of the rudevators, and Table 47 shows the lateral-directional derivatives due to an asymmetrical deflection of the rudevators. These tables can be seen in graphical form in Figure 76 through Figure 84.

Table 45: Meridian VORSTAB Model 4 Lateral-Directional Derivatives due to Aileron Deflection

α (deg)	δ_a (deg)	C_y	C_l	C_n
0	-10	-0.0102	-0.0456	-0.0117
5	-10	-0.0103	-0.0458	-0.0127
10	-10	-0.0100	-0.0441	-0.0131
15	-10	-0.0075	-0.0336	-0.0098
20	-10	-0.0055	-0.0247	-0.0071
0	-5	-0.0051	-0.0228	-0.0059
5	-5	-0.0052	-0.0229	-0.0064
10	-5	-0.0050	-0.0221	-0.0065
15	-5	-0.0037	-0.0168	-0.0049
20	-5	-0.0027	-0.0124	-0.0035
0	0	0.0000	0.0000	0.0000
5	0	0.0000	0.0000	0.0000
10	0	0.0000	0.0000	0.0000
15	0	0.0000	0.0000	0.0000
20	0	0.0000	0.0000	0.0000
0	5	0.0051	0.0227	0.0059
5	5	0.0051	0.0228	0.0064
10	5	0.0050	0.0220	0.0065
15	5	0.0037	0.0167	0.0049
20	5	0.0027	0.0123	0.0035
0	10	0.0101	0.0452	0.0117
5	10	0.0102	0.0454	0.0127
10	10	0.0099	0.0437	0.0131
15	10	0.0074	0.0333	0.0098
20	10	0.0054	0.0245	0.0071
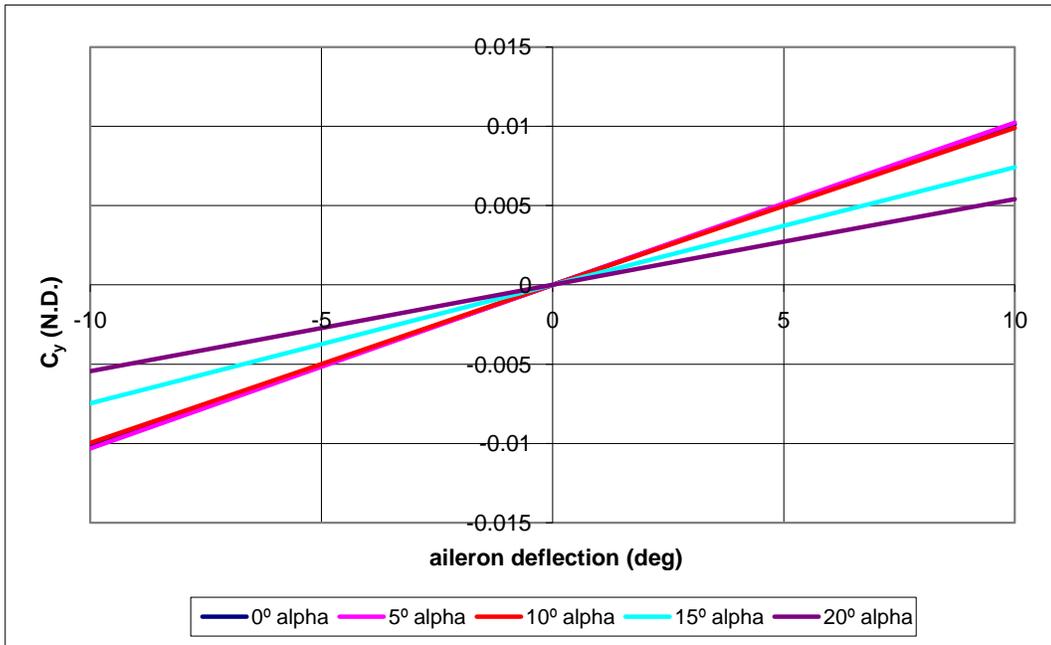
Figure 76: Meridian VORSTAB Model 4 Sideforce Coefficient due to Aileron Deflection

Figure 77: Meridian VORSTAB Model 4 Rolling Moment Coefficient due to Aileron Deflection
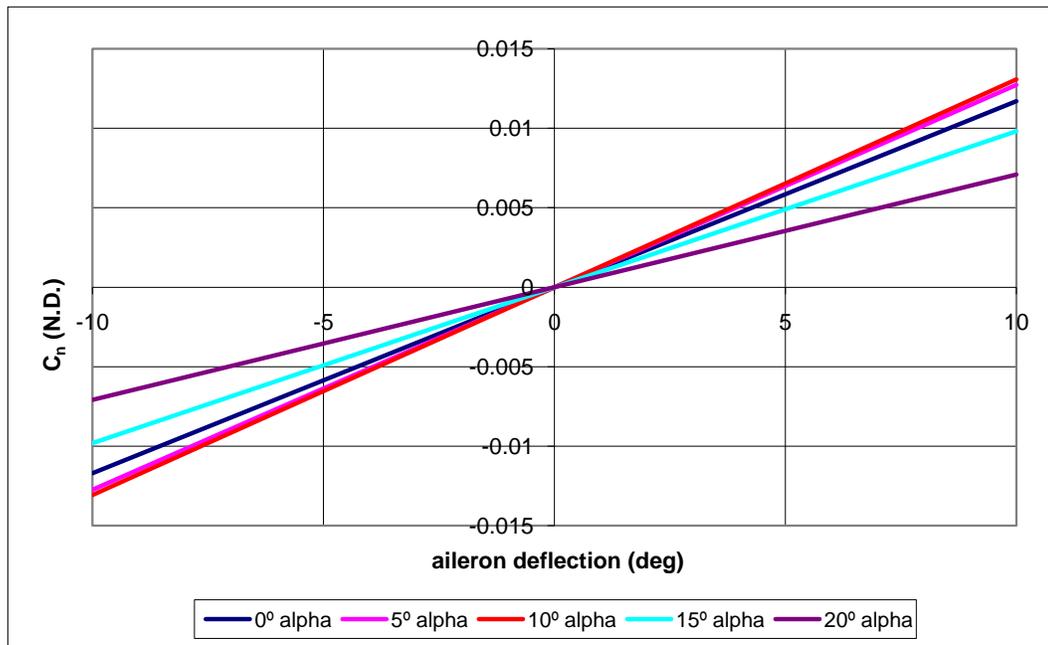
Figure 78: Meridian VORSTAB Model 4 Yawing Moment Coefficient due to Aileron Deflection

The sideforce coefficient should be very small without the fuselage present, and with it present all of the derivatives will change dramatically.

Table 46: Meridian VORSTAB Model 4 Longitudinal Derivatives due to Symmetrical Tail Deflection

α (deg)	δ_{re} (deg)	C_L	C_D	C_m
0	-12	-0.4094	0.0159	-0.0305
5	-12	0.0563	0.0244	-0.0451
10	-12	0.6136	0.0201	-0.0363
15	-12	0.9769	0.0430	-0.0588
20	-12	1.2689	0.0580	-0.0892
0	-6	-0.4007	0.0159	-0.0641
5	-6	0.0649	0.0244	-0.0791
10	-6	0.6218	0.0201	-0.0693
15	-6	0.9854	0.0431	-0.0932
20	-6	1.2769	0.0580	-0.1216
0	0	-0.3916	0.0155	-0.0995
5	0	0.0736	0.0244	-0.1135
10	0	0.6302	0.0202	-0.1031
15	0	0.9934	0.0431	-0.1256
20	0	1.2843	0.0581	-0.1517
0	6	-0.3826	0.0159	-0.1341
5	6	0.0821	0.0244	-0.1473
10	6	0.6380	0.0202	-0.1343
15	6	1.0008	0.0432	-0.1554
20	6	1.2909	0.0581	-0.1785
0	12	-0.3740	0.0160	-0.1675
5	12	0.0900	0.0245	-0.1784
10	12	0.6450	0.0202	-0.1621
15	12	1.0072	0.0433	-0.1816
20	12	1.2965	0.0581	-0.2012
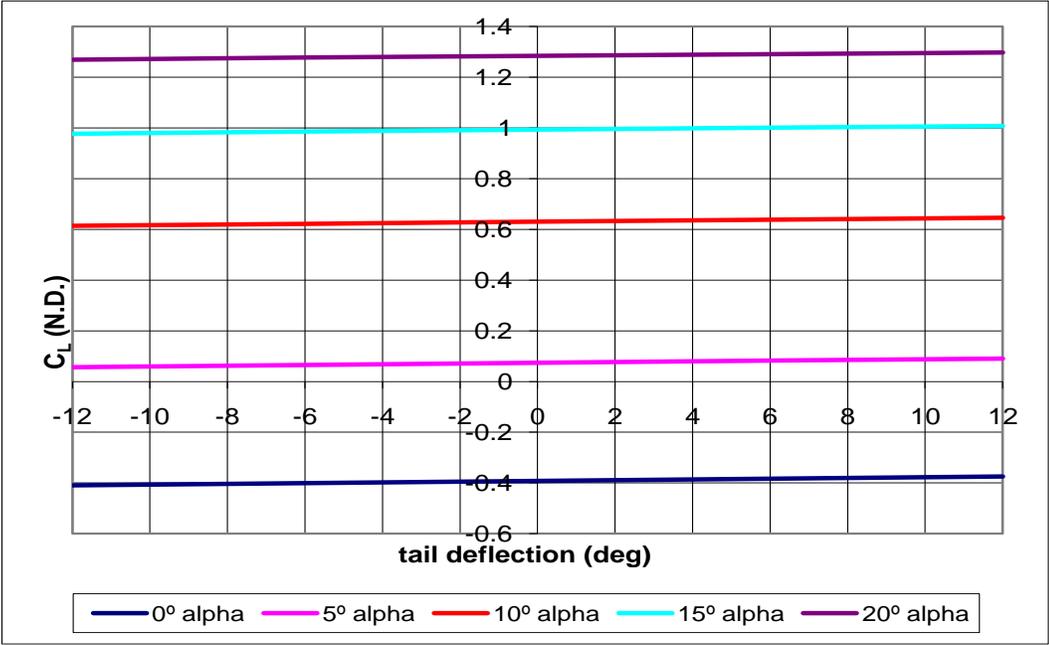
Figure 79: Meridian VORSTAB Model 4 Lift Coefficient due to Elevator Input
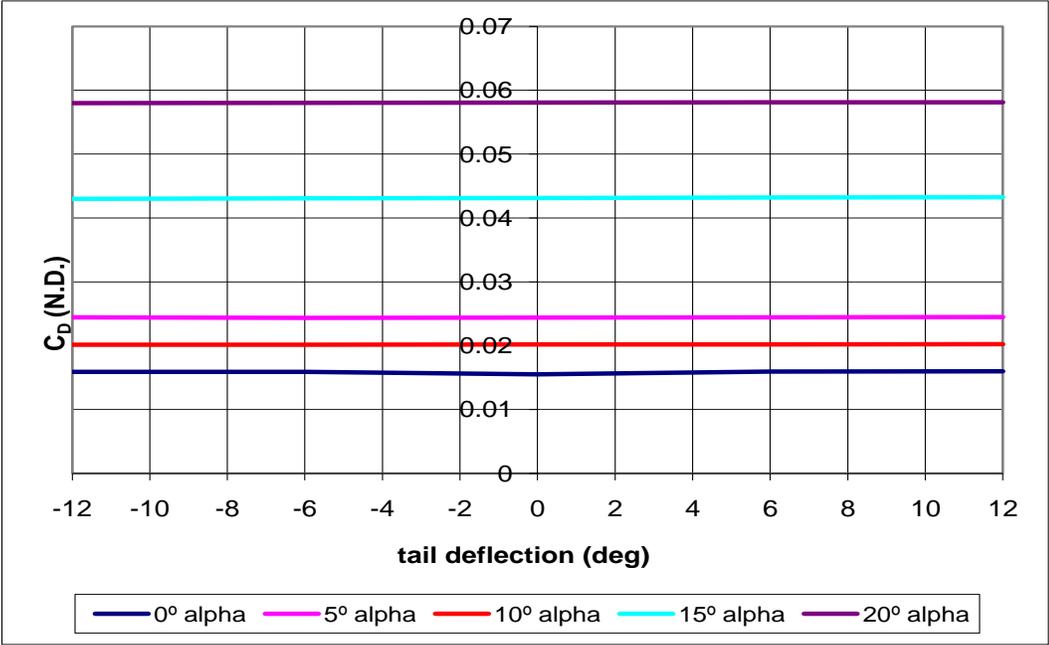
Figure 80: Meridian VORSTAB Model 4 Drag Coefficient due to Elevator Input

127
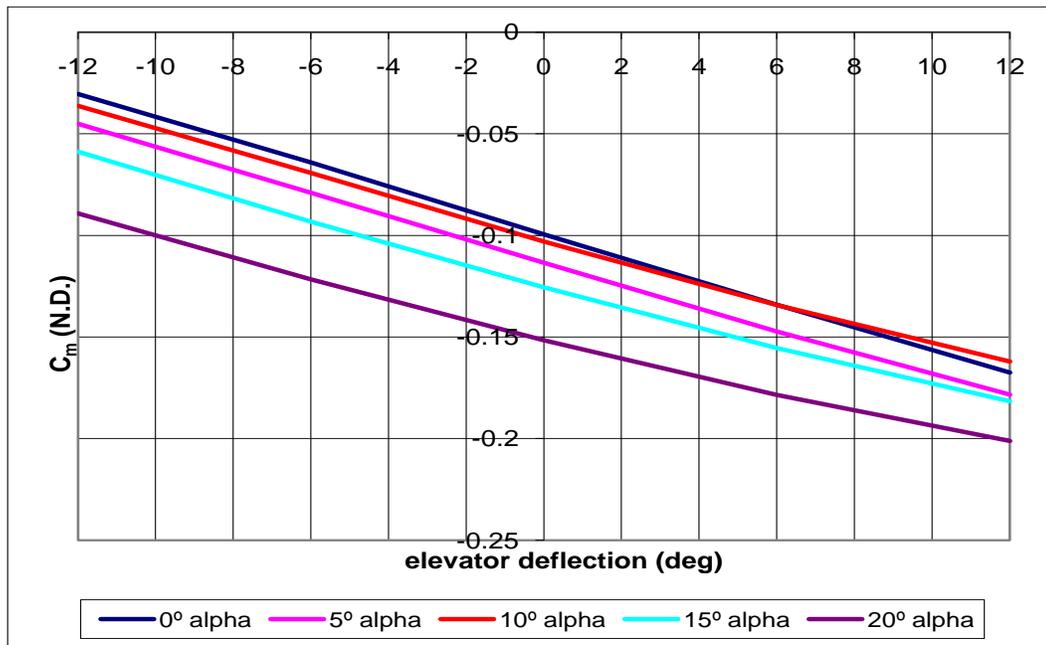
Figure 81: Meridian VORSTAB Model 4 Pitching Moment Coefficient due to Elevator Input

The lift and pitching moment both increase with a positive pitching moment, as expected. Drag stays rather steady when in reality it will change a small amount.

Table 47: Meridian VORSTAB Model 4 Lateral-Directional Derivatives due to Asymmetrical Deflection

| α (deg)	δ_{re} (deg)	C_y	C_l	C_n
0	-10	-0.0246	-0.0032	0.0102
5	-10	-0.0251	-0.0031	0.0106
10	-10	-0.0252	-0.0029	0.0107
15	-10	-0.0218	-0.0032	0.0092
20	-10	-0.0198	-0.0031	0.0084
0	-5	-0.0127	-0.0016	0.0053
5	-5	-0.0129	-0.0015	0.0054
10	-5	-0.0119	-0.0016	0.0050
15	-5	-0.0110	-0.0016	0.0047
20	-5	-0.0100	-0.0016	0.0043
0	0	0.0000	0.0000	0.0000
5	0	0.0000	0.0000	0.0000
10	0	0.0000	0.0000	0.0000
15	0	0.0000	0.0000	0.0000
20	0	0.0000	0.0000	0.0000
0	5	0.0128	0.0016	-0.0053
5	5	0.0123	0.0016	-0.0052
10	5	0.0119	0.0016	-0.0050
15	5	0.0110	0.0016	-0.0047
20	5	0.0100	0.0016	-0.0043
0	10	0.0248	0.0032	-0.0103
5	10	0.0238	0.0033	-0.0100
10	10	0.0226	0.0033	-0.0095
15	10	0.0218	0.0032	-0.0092
20	10	0.0198	0.0031	-0.0084

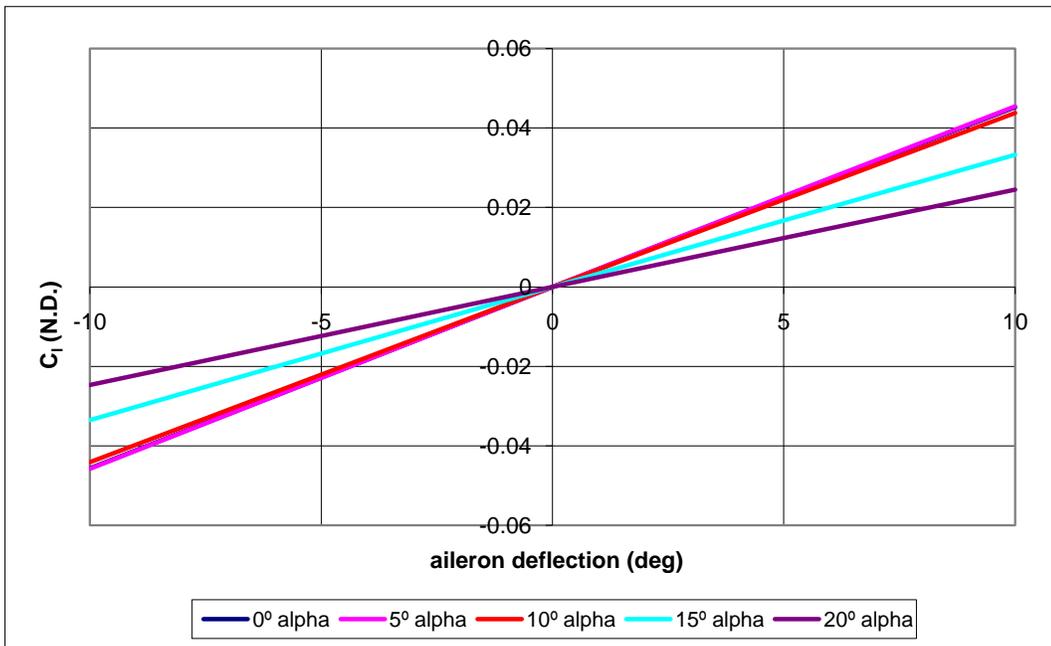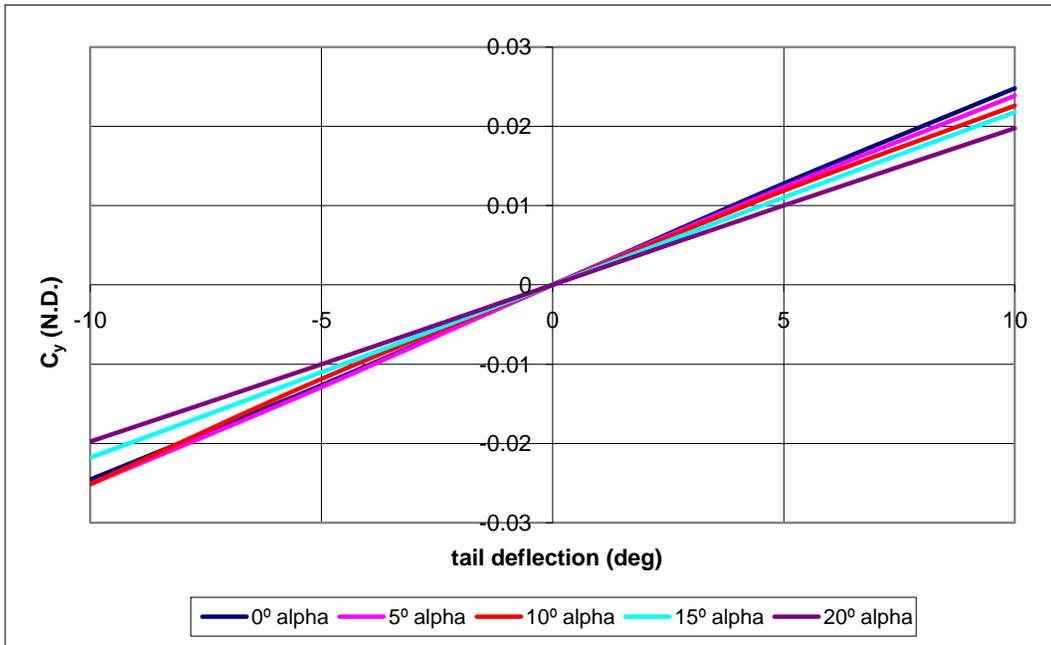**Figure 82: Meridian VORSTAB Model 4 Sideforce Coefficient due to Rudder Input**
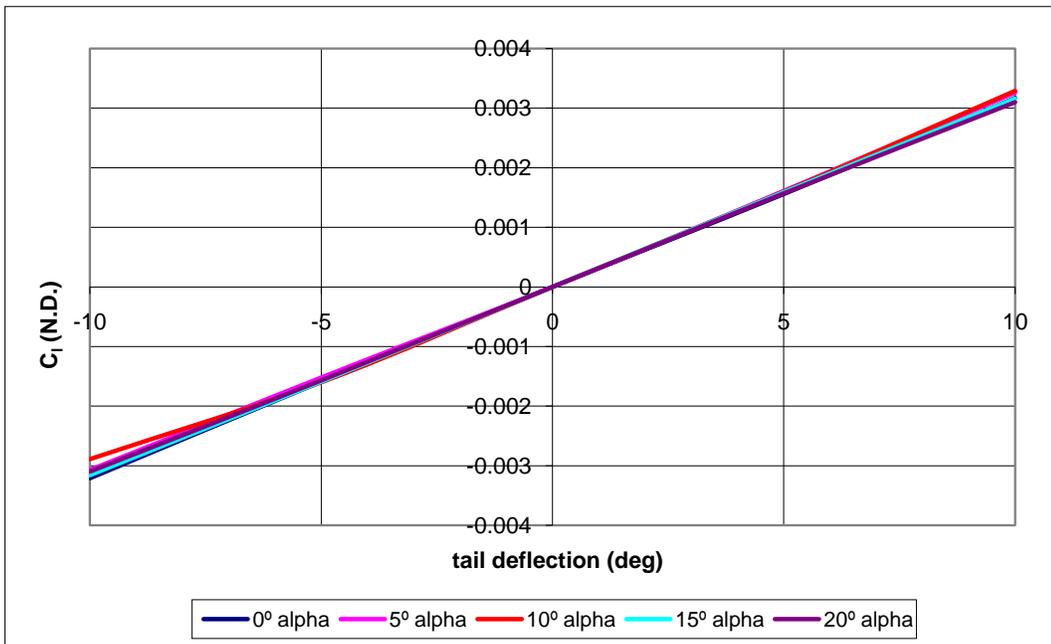
Figure 83: Meridian VORSTAB Model 4 Rolling Moment Coefficient due to Rudder Input
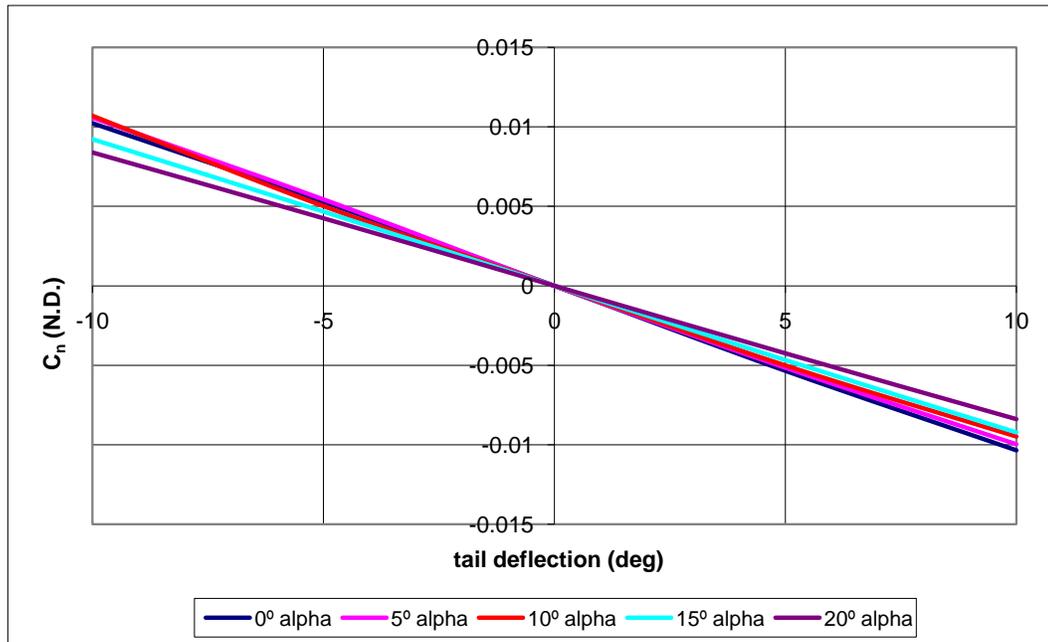
Figure 84: Meridian VORSTAB Model 4 Yawing Moment Coefficient due to Rudder Input

Again, these derivatives will be greatly influenced by having a fuselage presents in the model.

9.2.5   Meridian VORSTAB Conclusions

The results from VORSTAB varied greatly from model to model. These variations make it very difficult to draw any conclusions from VORSTAB. Since the first model is the only one that has the exact configuration it would be expected that it is the most accurate, but this was not the case. The forth model's results with the closest to the AAA results. Table 48 shows the results compared to Dr. Roskam's typical ranges, Ref [5]. These ranges are for conventional aircraft, and the ranges are a function of Mach number. The only results that are not shown in this table are the

first model. Model 1's results were not valid at all, so they were completely ignored.

The first model was used as a stepping stone to create the other models.

Table 48: Meridian VORSTAB Stability and Control Derivatives Dr. Roskam's Typical Ranges

Stability and Control Derivatives							
Derivative (1/rad)	Model 2	Model 3	Model 4	Typical Ranges	Within Range (Yes/No)		
				Dr. Roskam	Model 2	Model 3	Model 4
$C_{L\alpha}$	7.2337	7.1675	5.3308	1.0 to 8.0	Yes	Yes	Yes
$C_{D\alpha}$	15.580	-6.1068	0.1020	0.0 to 2.0	No	No	Yes
$C_{m\alpha}$	-0.8522	-0.4038	-0.1609	-4.0 to 1.0	No	No	Yes
C_{Lq}	7.1682	7.1767	3.7241	0.0 to 30.0	Yes	Yes	Yes
C_{mq}	-8.5662	-8.5688	-3.7942	-90.0 to 0.0	Yes	Yes	Yes
$C_{l\beta}$	-0.1083	-0.1031	-0.1060	0.1 to -4.0	Yes	Yes	Yes
C_{lp}	-0.2913	-0.292	-0.2960	-0.1 to -0.8	Yes	Yes	Yes
C_{lr}	-0.2263	-0.2316	-0.2320	0.0 to 0.6	No	No	No
$C_{y\beta}$	0.7695	0.8228	0.6383	-0.1 to -2.0	No	No	No
C_{yp}	-0.1010	-0.1065	-0.1229	-0.3 to 0.8	Yes	Yes	Yes
C_{yr}	0.2091	0.1261	0.1291	0.0 to 1.2	No	No	No
$C_{n\beta}$	0.0991	0.0773	0.0940	0.0 to 4.0	Yes	Yes	Yes
C_{np}	-0.0312	-0.0242	0.0226	-0.5 to 0.1	Yes	Yes	Yes
C_{nr}	-0.0748	-0.046	-0.0666	0.0 to -1.0	Yes	Yes	Yes
$C_{L\delta e}$	0.0974	0.0922	0.0858	0.0 to 0.6	Yes	Yes	Yes
$C_{D\delta e}$	-0.9313	1.3450	0.0040	Negligible	No	No	No
$C_{m\delta e}$	-0.3867	-0.3600	-0.3304	0.0 to -4.0	Yes	Yes	Yes
$C_{l\delta a}$	0.2628	0.2625	0.2606	0.0 to 0.4	Yes	Yes	Yes
$C_{l\delta r}$	0.0117	0.0123	0.0178	-0.04 to 0.04	Yes	Yes	Yes
$C_{y\delta a}$	0.0565	0.0567	0.0583	Negligible	No	No	No
$C_{y\delta r}$	0.1303	0.1248	0.1463	0.0 to 0.5	Yes	Yes	Yes
$C_{n\delta a}$	0.0692	0.0688	0.0670	-0.08 to 0.08	Yes	Yes	Yes
$C_{n\delta r}$	-0.0559	-0.0479	-0.0612	-0.15 to 0.0	Yes	Yes	Yes

There are multiple derivatives that do not fall into the typical ranges. All of the models have a high drag coefficient except the forth. The forth model also has the

most derivatives that fall into the typical ranges described. Table 49 shows a comparison of the second, third, and fourth model next to AAA. The forth model predicted several of the derivatives the best.

Table 49: Meridian AAA and VORSTAB Comparison

Stability and Control Derivatives							
Derivative (1/rad)	Model 2	Model 3	Model 4	AAA	% Diff. Model 2	% Diff. Model 3	% Diff. Model 4
$C_{L\alpha}$	7.2337	7.1675	5.3308	5.1648	40.06	38.78	3.21
$C_{D\alpha}$	15.58	-6.1068	0.102	0.1409	10957.49	-4434.14	-27.61
$C_{m\alpha}$	-0.8522	-0.4038	-0.1609	-0.6207	37.30	-34.94	-74.08
C_{Lq}	7.1682	7.1767	3.7241	4.6179	55.23	55.41	-19.36
C_{mq}	-8.5662	-8.5688	-3.7942	-13.973	-38.69	-38.68	-72.85
$C_{l\beta}$	-0.1083	-0.1031	-0.106	-0.0776	39.56	32.86	36.60
C_{lp}	-0.2913	-0.292	-0.296	-0.5546	-47.48	-47.35	-46.63
C_{lr}	-0.2263	-0.2316	-0.232	0.1099	-305.91	-310.74	-311.10
$C_{y\beta}$	0.7695	0.8228	0.6383	-0.4789	-260.68	-271.81	-233.28
C_{yp}	-0.101	-0.1065	-0.1229	-0.1465	-31.06	-27.30	-16.11
C_{yr}	0.2091	0.1261	0.1291	0.3217	-35.00	-60.80	-59.87
$C_{n\beta}$	0.0991	0.0773	0.094	0.1386	-28.50	-44.23	-32.18
C_{np}	-0.0312	-0.0242	0.0226	-0.0351	-11.11	-31.05	-164.39
C_{nr}	-0.0748	-0.046	-0.0666	-0.1338	-44.10	-65.62	-50.22
$C_{L\delta e}$	0.0974	0.0922	0.0858	0.4149	-76.52	-77.78	-79.32
$C_{D\delta e}$	-0.9313	1.345	0.004	0.0117	-8059.83	11395.73	-65.81
$C_{m\delta e}$	-0.3867	-0.36	-0.3304	-1.6709	-76.86	-78.45	-80.23
$C_{l\delta a}$	0.2628	0.2625	0.2606	0.2316	13.47	13.34	12.52
$C_{l\delta r}$	0.0117	0.0123	0.0178	-0.0253	-146.25	-148.62	-170.36
$C_{y\delta a}$	0.0565	0.0567	0.0583	0	-----	-----	-----
$C_{y\delta r}$	0.1303	0.1248	0.1463	-0.3681	-135.40	-133.90	-139.74
$C_{n\delta a}$	0.0692	0.0688	0.067	-0.0134	-616.42	-613.43	-600.00
$C_{n\delta r}$	-0.0559	-0.0479	-0.0612	0.1481	-137.74	-132.34	-141.32

The fourth model best predicted the Meridian stability and control derivatives when compared to AAA. There are several derivatives that are extremely far off, but the fuselage will have an impact on most of these. After modeling these three different aircraft it can be concluded that VORSTAB works best with traditional style aircraft, such as the YAK-54. The Meridian is not a typical style of aircraft and the VORSTAB results were not what were expected. These results should not be completely ignored, because they brought up possible issues that the Meridian might have. For example, the downward swoop of the fuselage could result in downwash and flow separation. This downwash and flow separation possible could render the tails ineffective and the aircraft unresponsive to tail inputs. It is recommended that several more wing and tail models be created to determine if it predicts the stability and control derivatives well as seen from the Meridian results.

9.3   Linearized Model of the Meridian

For the information and data on the state space model of the Meridian please refer to Appendix B.

9.4   FLUENT Modeling of the Meridian

As learned from the VORSTAB model of the Meridian, the main concern is the downwash created over the fuselage that could blank out the v-tails. The first flight tests also resulted in very high drag. These two problems, downwash and drag, drove the need for a FLUENT model to be created. A 3-D model was desired, but due to time constraints this was not done. Therefore, a 2-D side profile of the fuselage was

created to see the downwash that was produced from the high camber. A complete 3-D model of the Meridian should eventually be created.

9.4.1   GAMBIT Mesh Generation

A large farfield was created around the axial-crosscut of the fuselage. The farfield was broken into six individual sections; forward (above and below) of the fuselage, aft (above and below) of the fuselage, above the fuselage, and below the fuselage. Above and below the fuselage had a height of 20 maximum thicknesses of the fuselage, and forward and aft had a length of 20 lengths of the fuselage. This created a large enough area where the flow could be appropriately modeled. The size of the farfields depends on the flow being modeled and the shape of the object. A very fine mesh is desirable everywhere, but this would take a large amount of computer memory and time to run. Different farfields allow the designer to create finer meshes in the more critical sections of the flow. For the 2-D Meridian fuselage the critical flow section was the boundary layer of the Meridian walls. This is where the flow can separate. The flow at a large distance from the fuselage is not as critical as the flow near the walls. The following are the steps taken to create the six farfields and their meshes:

Step 1: Import the axial cross-section of the fuselage (points created as a text file). The tip of the nose will be on the (0, 0, 0) point. Figure 85 shows the Meridian cross-section.
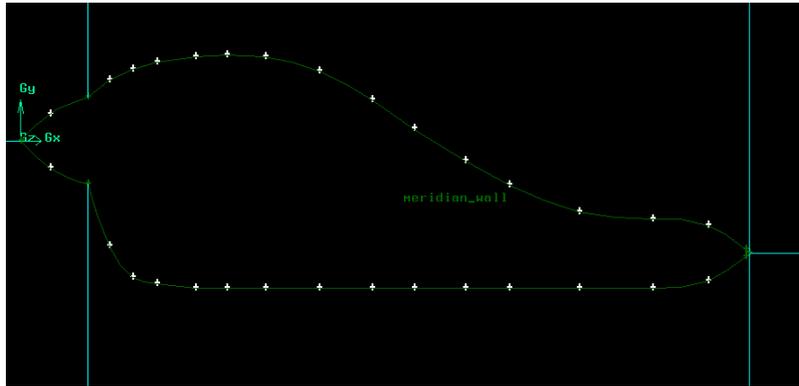
Figure 85: Meridian Fuselage Axial Cross-Section for FLUENT

Step 2: Create a line that extend from the tip of the nose (labeled point M) to 20 times the length of the fuselage forward, labeled point A.

Step 3: Repeat step 2, but extend from the tip of the tail (labeled point N) to aft of the fuselage, labeled point B.

Step 4: Copy the point, on the upper surface, where the nose cone meets the fuselage cowling (labeled point K) up to 20 times the maximum thickness minus the current height of the point, called point C.

Step 5: Repeat step 4, but use the point on the lower surface where the nose cone meets the lower fuselage cowling (labeled point L) called point D.

Step 6: Copy the point N up the same height as the point created in step 4, and then copy the same point to the height created in step 5, labeled points E and F respectively.

Step 7: Copy the points A and B to the heights created in step 4 and step 5 labeled points G, H, I and J respectively. There should be 3 points forward of the fuselage, 3

points aft, 2 points above and below the nose cone, and 2 points above and below the tip of the tail.

Step 8: Use the NUMS tool to create a curved line on the upper surface of the nose cone. Repeat on the lower surface of the nose cone, upper surface of the fuselage, and lower surface of the fuselage. This creates four individual lines.

Step 9: Next use the line tool to create a line from point M to point A.

Step 10: Use the line tool to create 3 lines from point N to points B, E and F.

Step 11: Use the line tool to create a line from point K to point C. Then repeat with point L to point D.

Step 12: Create lines A-G, A-H, G-C, H-D, C-E, D-F, E-I, F-J, B-I, and B-J. Figure 86 shows the Meridian axial cross-section and the newly created lines to create the farfields. The Meridian cross-section is the small white shape in the middle.
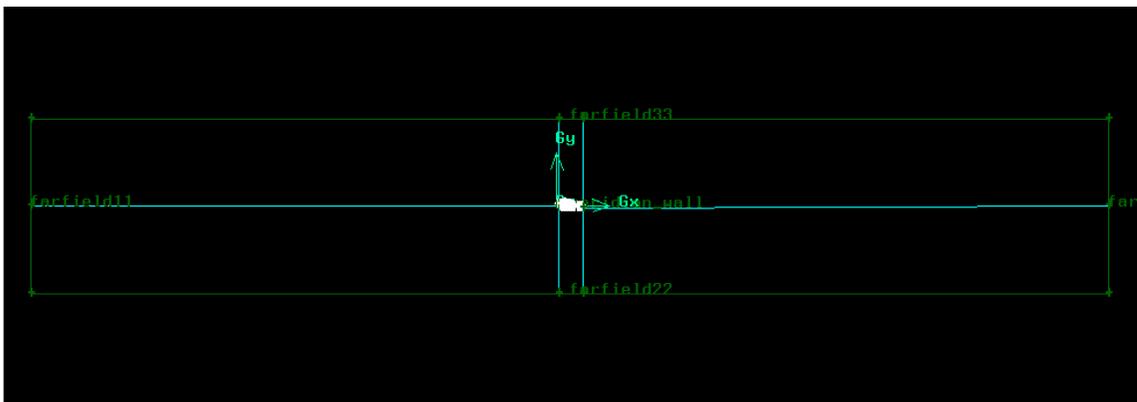
Figure 86: Meridian Fuselage with Farfield Divisions

Step 13: Create the six different farfield and the Meridian body face. Table 50 shows the corresponding lines to each face.

Table 50: Meridian Farfield Edges

Face Name	Edges
Farfield 1	AG, GC, CK, KM, AM
Farfield 2	AH, HD, DL, LM, AM
Farfield 3	CE, EN, NK, CK
Farfield 4	LN, NF, DF, DL
Farfield 5	EI, IB, NB, EN
Farfield 6	FJ, JB, NB, FN
Meridian	MK, KN, ML, LN

Step 14: Create 'Edge Meshes' using Table 51. The small intervals should be closer to the Meridian wall, on all lines that have first lengths.

Table 51: Meridian Edge Meshes

Edge	Interval Count	Properties
AG, AH, CK, DL, EN, FN, BI, BJ	100	First Length = 0.25
CG, DH, EI, FJ, NB	100	First Length = 0.25
CE, DF, KN, LN	70	Successive Ratio = 1
KM, LM	8	Successive Ratio = 1
MA	92	First Length = 0.20

Step 15: Create 'face meshes' in the six farfields. The meshes is denser towards the Meridian body. Figure 87 shows the meshes concentrated towards the fuselage body. The lower image is a zoomed in image of the upper picture.
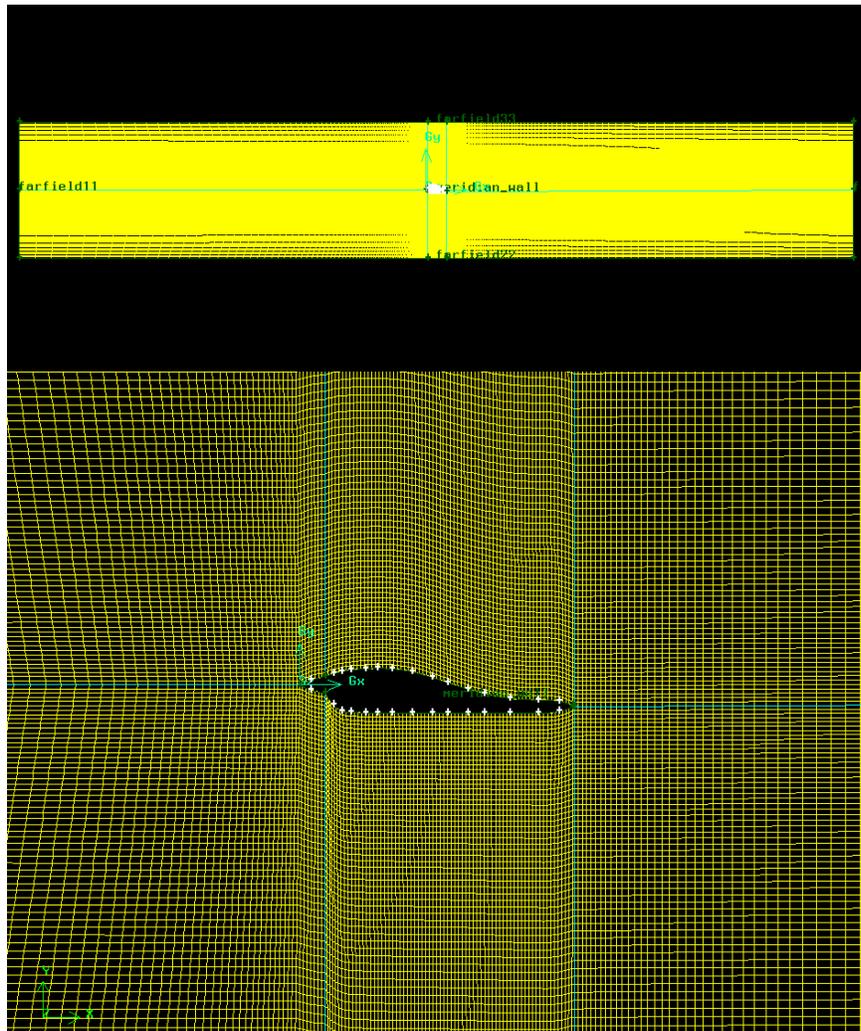
Figure 87: Meridian Farfield Meshes

Step 16: Create five groups of edges. Group 1 as edge AG and AH, Group 2 as CG, CE and EI, Group 3 as DH, DF and FJ, Group 4 as BI and BJ, and Group 5 as MK, KN, ML and LN. With the groups created, their corresponding boundary conditions were set. Groups 1, 2 and 3 were velocity inlets, Group 4 was a pressure outlet, and Group 5 was a wall.

These boundary conditions work because the farfields are so big that the flow can be considered unaffected by the fuselage body or totally recovered from the flow

disturbances. The boundary conditions can be modified in FLUENT if they are not what were desired. With the GAMBIT model fully created export the 2-D mesh and import it into FLUENT.

9.5   FLUENT Model Generation

The FLUENT model can be run in many different methods depending on what the goals the designer is trying to achieve. For the Meridian, the goal was to observe the boundary layer on the fuselage, and observe the flow separation and/or downwash that were produced from the high convergence and downward camber. Several different turbulent methods were tested to verify which one was the most accurate. For the Meridian, the results did not very greatly from one method to the next. Therefore, the method chosen was the one that has the most accurate results in aerodynamics. The following are the setup criteria for the FLUENT model.

- Solver – Segregated, because of limited memory

- Viscous – Turbulent, Spalart-Allmaras; set the turbulence factors to 0.1 for an initial guess.

- No Energy Equation because the flow is not compressible

- Materials – Set the density and viscosity to the values that the Meridian will fly in. At 1,000 m the approximate values are 1.112 kg/m^3 and 1.758x10^{-5} kg/m-s respectively.

- Operating Conditions – Set this to zero to work in terms of absolute pressure. If left at the default setting the pressures reported would be in terms of gauge pressure.

- Boundary Conditions – The types of boundary conditions chosen in GAMBIT were the desired ones for this model, but the values had to set.

  o Velocity Inlets – 61.7 m/s in the x-direction and 0.0 m/s in the y-direction. For angles of attack the velocity components could be changed. The model did not converge doing this, so a new mesh was created for each angle of attack chosen. To create the new mesh the same method as before was used, but the imported Meridian cross-section was imported at the correct angle of attack.

  o Pressure Outlet – 0 Pascals for the gauge pressure

  o Wall – Set the wall roughness height to $3x10^{-5}$ m and roughness constant to 0.5. These were the values used by AAA when designing the aircraft.

- Solution – SIMPLE for the pressure-velocity coupling, PRESTO! for the pressure discretization, and Second-Order Upwind for the other discretizations. These were determined using the online FLUENT help, Ref [19].

- Residuals – $1x10^{-6}$

- Monitor – Lift and drag

- Iterate until converged

The mesh generation and FLUENT runs were repeated for several different angles of attack. Multiple angles of attack allow the designer to see the changes in the flow as the aircraft body changes orientation.

9.5.1   Meridian FLUENT Results

The angles of attack checked for the Meridian fuselage were -4˚, 0˚, 2˚, 5˚, and 10˚. A large amount of lift was produced by the large camber in the fuselage. The down camber on the tail lowered the total pressure on the upper surface and also results in extra lift. The large boundary layer that built up from this negative camber increases the drag. The lift and drag were determined in terms of wing area, 3.35 m^2. Using the wing area as a reference, allows the designer to compare this lift and drag to the lift and drag with the rest of the aircraft. Table 52 shows the lift and drag found at all angles of attack.

Table 52: Meridian Fuselage Cross-Section FLUENT Lift and Drag

α (deg)	C_{l_f}	C_{d_f}	L/D
-4	0.1080	0.0651	1.658
0	0.4030	0.0286	14.10
2	0.5479	0.0414	13.22
5	0.6456	0.0917	7.039
10	0.8458	0.2573	3.287

As seen from the lift to drag results, the Meridian fuselage will generate a large amount of lift. At low angles of attack, the lift to drag ratio is close to what the design of the overall aircraft was. Typically, the lift produced by the fuselage can be neglected due the small value, but the Meridian's lift is too large to neglect. The overall magnitude of the fuselage lift is not extremely high, but when compared to the amount of drag the fuselage produces it is considered high. The highly cambered wings will produce much more lift. Also, the 3-D effects on the fuselage will change these numbers some. Most likely the actual numbers will be less than this.

The FLUENT results can best be shown in the form of pictures. The downwash, flow separation, and boundary layer can all easy be seen in the velocity magnitude, velocity angle, total pressure, stream function, vorticity profiles. Figure 88 shows the velocity magnitude of the air around the Meridian. From left to right, top to bottom the figures are in an order of 0˚, 2˚, 5˚, 10˚, and -4˚.
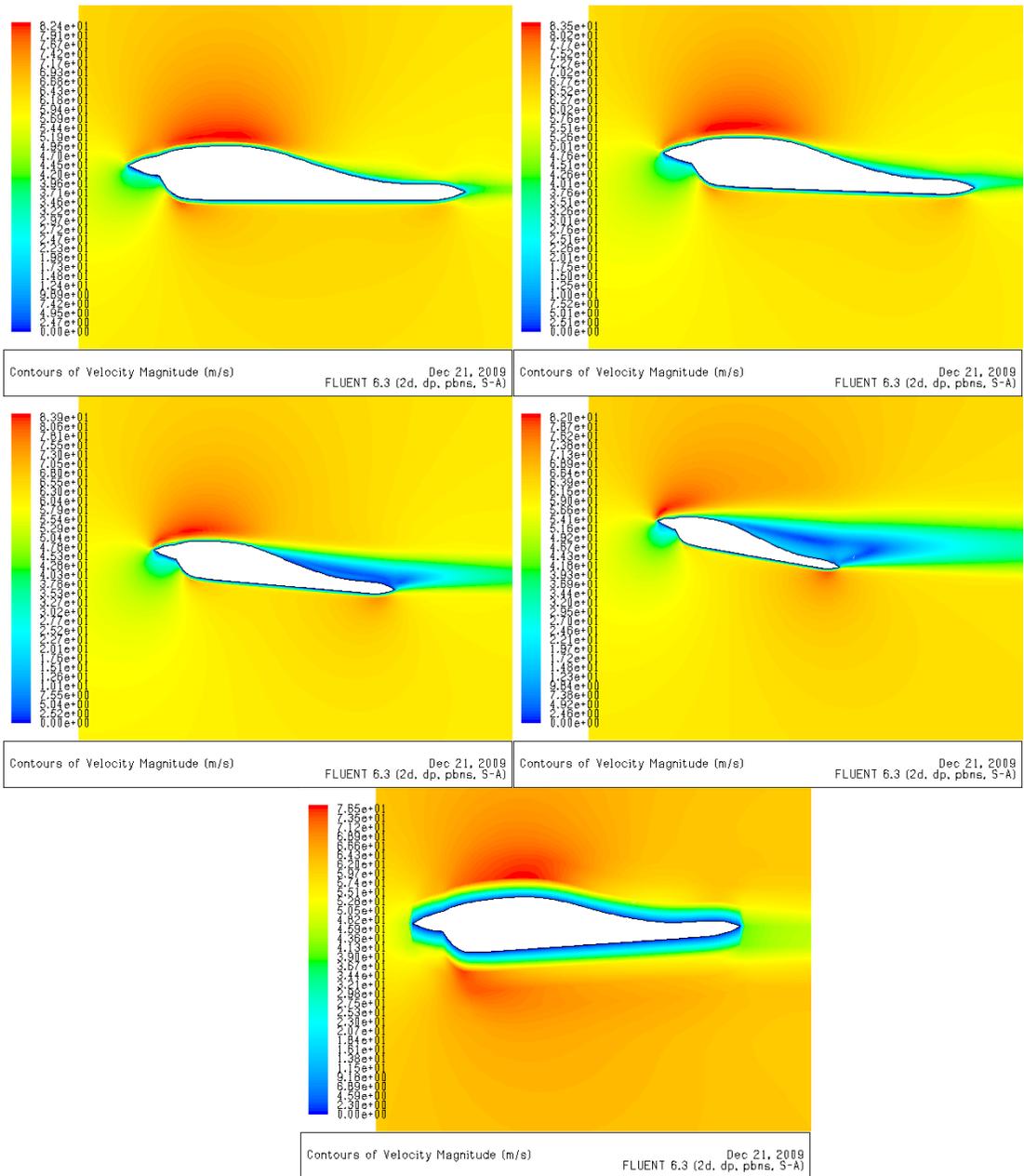
Figure 88: Meridian FLUENT Velocity Magnitude Profile for All Angle of Attacks

It can be seen, as the angle of attack increase the boundary layer increases also. Basically, the boundary layer is the thickness of air that is not traveling at free-stream velocity. The average thickness is directly related to the Reynolds Number of

the flow and the length of the surface. A Cartesian coordinate system is used for the boundary layer definitions. The x-coordinate is parallel with the surface at each point, and the y-coordinate is normal to the surface. Eq [28] shows an estimate for the average thickness of the boundary layer, and Eq [29] show the definition of Reynolds Number, Ref [20].

- $\bar{\delta} = \sqrt{vL/U_\infty}$ Eq [28]

- $Re = U_\infty L/v$ Eq [29]

There are three common measurements of the boundary layer thickness, δ. One method is defined as the distance from the wall where the velocity reaches 99 percent of the free stream velocity, u = 0.99U. This method is somewhat arbitrary since any percentage could have been picked. The reason 100 percent of the free stream velocity was not chosen is that it is difficult to pinpoint the exact location where this happens. It is appropriate to assume 99 percent is close enough for accuracy. The second method is the displacement thickness, δ^*, and there is no arbitrariness in this method. Displacement thickness is the theoretical distance that the wall would have to move outward, in a frictionless flow, to maintain the same mass flux as the authentic flow. Eq [30] shows the displacement thickness, Ref [20]. The upper boundary goes to infinity, because u/U goes to 0 exponentially fast in the y direction, as y goes to infinity.

- $\delta^* = \int_0^\infty (1 - u/U)dy$ Eq [30]

  o "u" is a function of the variable "y".

The third method is the momentum thickness, θ, and is defined as the amount of momentum, $\rho U^2 \theta$, loss due to the boundary layer. This momentum thickness can be determined using Eq [31], Ref [20]. Again in this equation "u" is a function of the variable "y".

- $$\theta = \int_0^\infty u/U(1 - u/U)dy$$
  Eq [31]

The type of definition does not matter when it comes to boundary layer. Each method has its benefits and downfalls. For example, the second and third methods are difficult to develop an equation for the velocity, u. As stated earlier the first method chooses an arbitrary number, but this is the easiest to use with experimental data. FLUENT depicts the velocity magnitude by varying the color. This is depicted by the blue area around the fuselage. The boundary layer flow stays attached to the fuselage and follows the contour of it. Boundary layers will build up in the y-direction as the flow travels over the body. The size of the boundary layer is extremely thick at high angles of attack. For a typical aircraft wing the boundary layer thickness is on the order of one centimeter. At higher angles of attack, 5° and 10°, and large fuselage curvatures the flow separates completely from the fuselage. This is seen as the blue area that does not follow the fuselage contour, but instead starts flowing turbulently. The direction of the flow can be shown by viewing the velocity angle in Figure 89. The orientation of the angles is 0° to the right and 90° straight up.
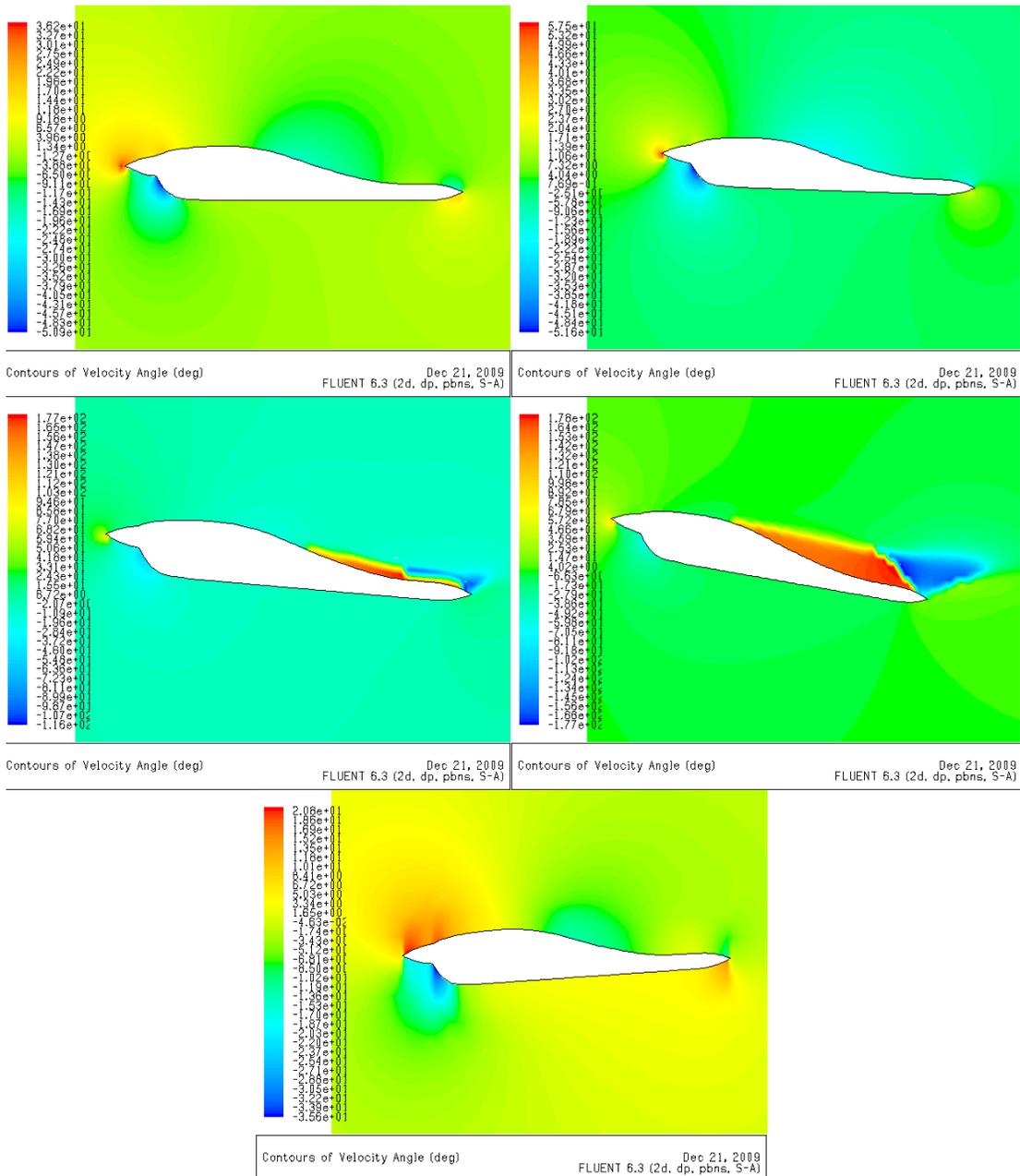
Figure 89: Meridian FLUENT Velocity Angle Profile for All Angles of Attack

A change in direction is expected around the fuselage. If the contour of the fuselage has smooth transitions and small curvatures the flow should follow the fuselage shape. The changes in flow direction that are not expected are the ones at

angles of attack 5˚ and 10˚. Separation occurs at these angles of attack near the empennage. Similar to the velocity magnitude, the velocity angle depicts its changes with changes in color. A smooth change is depicted with a slow transition in color, and a sudden change with a dramatic change in color. This separation bubble is where the flow can travel in many directions and possible have complete flow reversal. The direction of the velocity for angles of attack -4˚, 0˚, and 2˚ follows the contour of the fuselage pretty well. There are a few sudden changes, but this is expected when the flow encounters a disturbance in the path. For example, the flow changes direction abruptly at the nose cone of the aircraft. The flow stops at this point and begins to travel around that spot.

At higher angles of attack, 5˚ and 10˚, there are unexpected turns in the flow. The pressure gradient along the surface determines how the flow travels over a surface. A favorable pressure gradient will be upstream of the highest point, and this will cause the streamlines of the flow to converge and a decrease in pressure. An adverse pressure gradient is the opposite of the favorable pressure gradient. Downstream of the highest point the streamlines diverge and result in an increase in pressure. These pressure gradients not only affect the pressure, but also the velocity. A favorable pressure gradient will increase the free stream velocity, and an adverse pressure gradient will decrease the free stream velocity. Figure 90 depicts the velocity profiles along a curved surface, Ref [20].

$$\mu \left(\frac{\partial^2 u}{\partial y^2} \right)_{wall} = \frac{\partial p}{\partial x}.$$
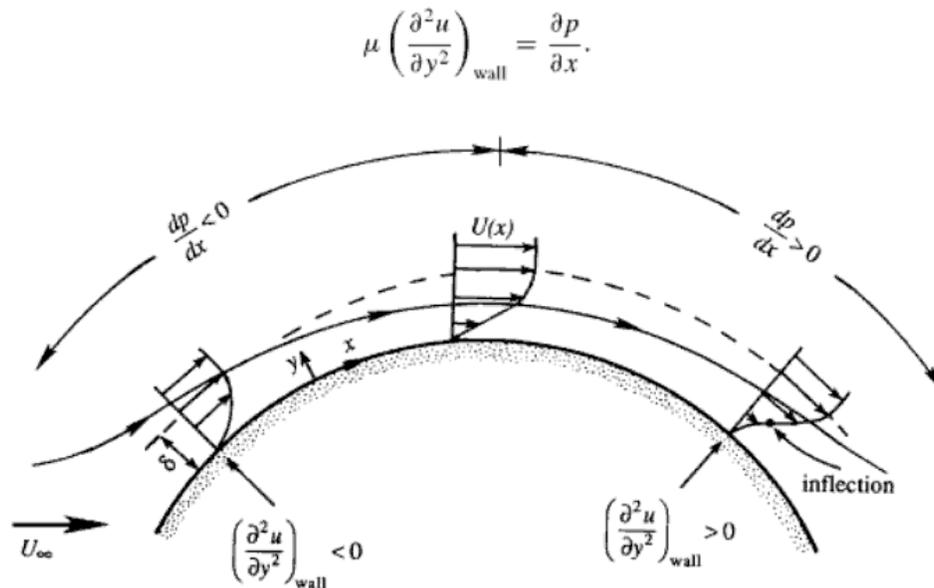
Figure 90: Velocity Profile in Boundary Layer with Favorable and Adverse Pressure Gradient (From Ref [20])

The inflection point is where the $\partial^2 u/\partial y^2 = 0$, or in other words where the curvature of the velocity profile changes signs. A strong enough adverse pressure gradient can cause the flow to separate from the wall. If the flow continues with an adverse pressure gradient the flow will reverse directions. The backward flow will meet the forward flow at some point and begins to flow forward again. Where these two flows, backwards and forwards, meet is where the stress vanishes. Figure 91 shows a representation of the flow separating from an adverse pressure gradient and then flow reversal happening, Ref [20]. At low Reynolds numbers, a large steady vortex will form behind this separation point. This is where the flow swirls in an area, but it does not shed off the body. This is seen at both the higher angles of attack. Separation is a function of the flow geometry and whether the boundary layer

is laminar or turbulent. A blunt body or sudden change in shape can lead to a steep

pressure gradient, and therefore leads to separation happening quickly.
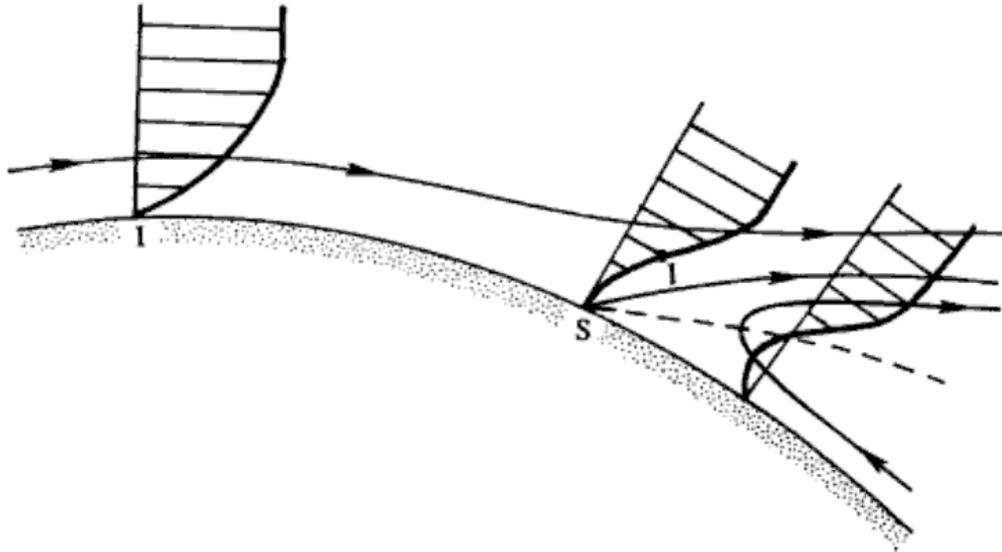
Figure 91: Velocity Profile with Flow Separation at Point S (dashed line u = 0, From Ref. [20])

The flow separation is very apparent at the high angles of attack with the

velocity angles flow turning red. The dark red and dark blue are flow reversal points.

To avoid separation and higher drag a structure should have a gradual change in size

and shape. At the higher angles of attack the geometry changes more suddenly and

this causes separation to happen more quickly. Figure 92 shows the total pressure in

the flow.
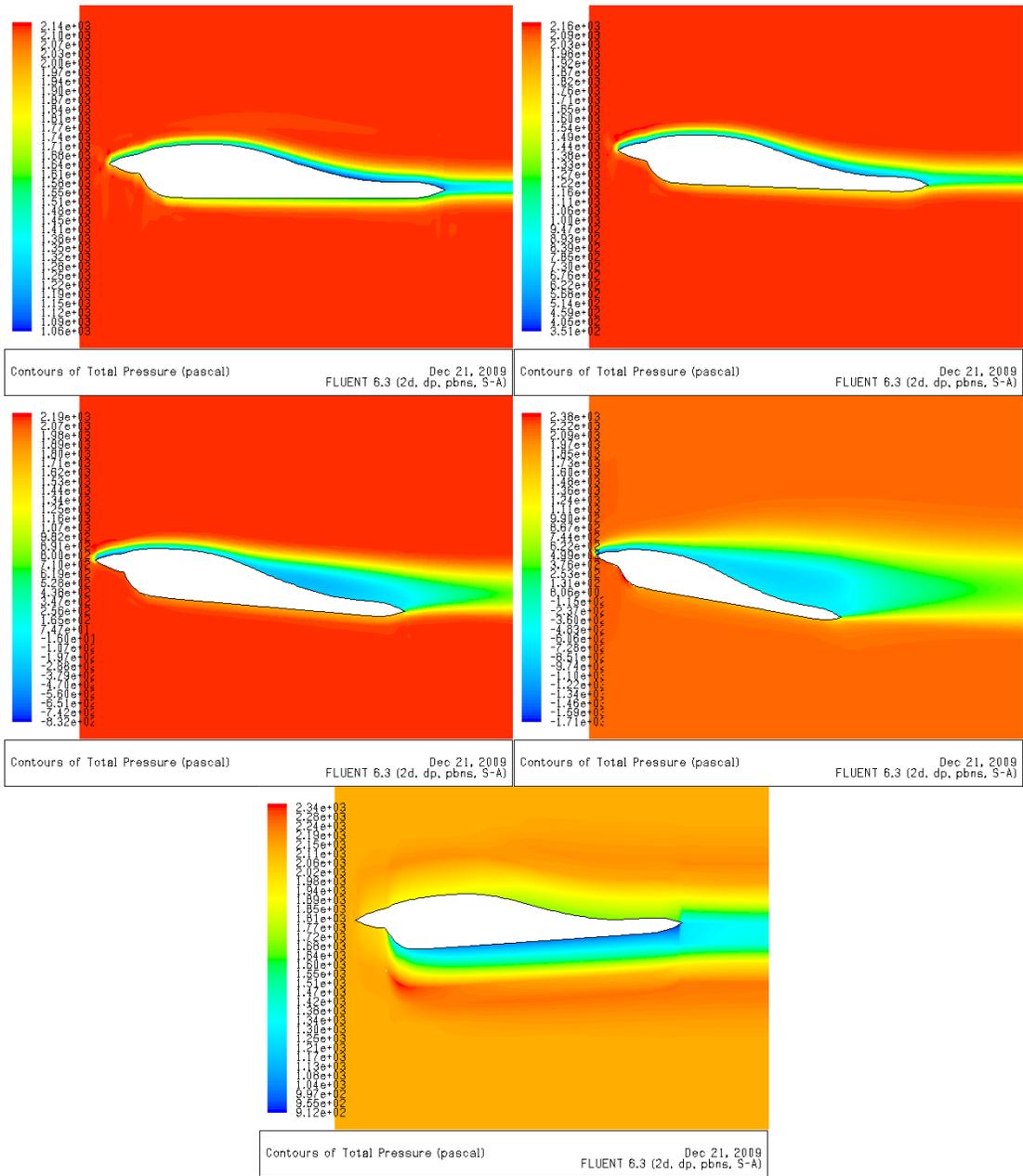
Figure 92: Meridian FLUENT Total Pressure Profile for All Angles of Attack

The total pressure is directly related to the flow velocity and the aircraft shape and angle of attack. Certain angles of attack will affect the flow field pressure much more than others. This is seen at angles of attack of 10˚ and -4˚. The colors move

away from the red color to a yellow or orange color. These changes in color are a reduction in the total pressure due to the fuselage contour and flow velocity. This is one of the reasons for the very low lift to drag ratio at these two angles of attack. The total pressure is lower where the boundary layer is located and the where the flow separates from the body due to the small velocity. Total pressure is a function of the velocity squared, Eq [32].

- $$p_T = \frac{1}{2}\rho V^2 + p_s$$ Eq [32]

At the -4˚ angle of attack the boundary layer on the lower surface is very thick. This is due to the sudden change in shape on the cowling. It is similar to the flow encountering a step, and this causes the flow to separate very quickly. The flow path can be seen in Figure 93 showing the stream functions. Stream functions have a constant value along a streamline. These stream functions can be used to analytically determine the velocity and its direction.
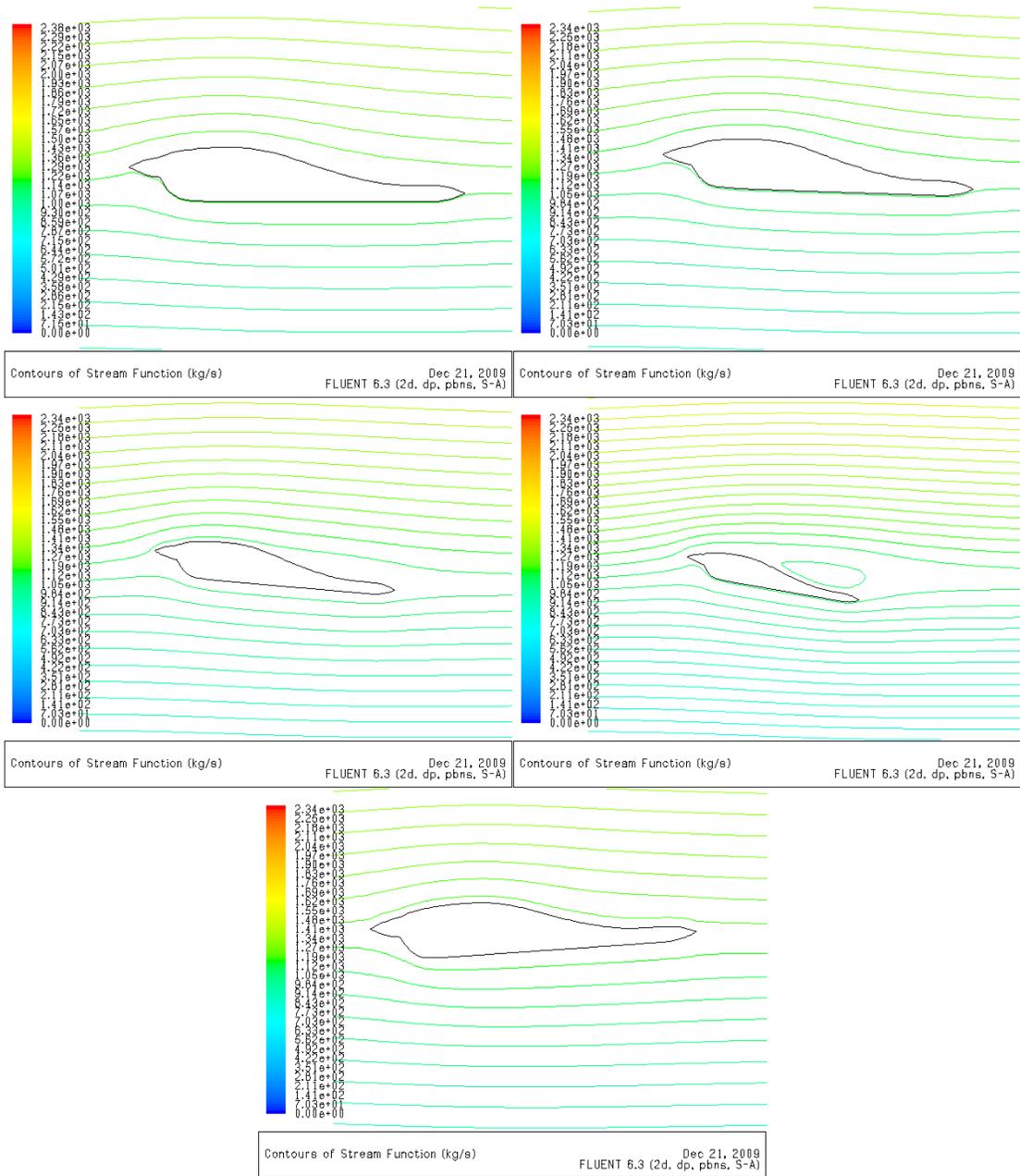
Figure 93: Meridian FLUENT Stream Function Profile at All Angles of Attack

Stream functions are defined to be constant along a stream line, and the $\Delta\psi$ between two streamlines is the volume of the flow between those streamlines. This can be thought of as the volume flowing through a streamtube bounded by those two

streamlines. The units for stream function are kg/s. A stream function normally has units of kg/s-m, but this model is 2-D and has no depth. There is also a unitless form of stream function and is defined by Eq [33] (without the bar), Ref [21]. To determine the velocity components from the stream function Eq [34] and Eq [35] should be used, Ref [21].

- $\Psi = \bar{\Psi}/\rho$ Eq [33]

- $u = \partial\Psi/\partial y$ Eq [34]

- $v = -\partial\Psi/\partial x$ Eq [35]

At the high angle of attack, 10˚, it is seen that the stream function travels in a complete closed path around the empennage. This is due to the flow separating from the fuselage and traveling in this closed path. The rest of the flow travels over the top of this circulation.

Vorticity is defined as twice the angular velocity, Ref [20]. This is found by calculating the average rotation rate of two perpendicular lines and then multiplying it by two. Irrotational flow will have a magnitude of zero vorticity. This is why the dark blue area is very close to zero in Figure 94. There is high vorticity around the abrupt curved spots on the fuselage. The boundary layer also is a lighter shade of blue, because the flow in this area has rotation.

Using Stokes' theorem circulation can be written as Eq [36], Ref [20]. As seen from this equation circulation is related to the rotation of the flow. Higher angular velocity will produce more circulation around a finite area. Circulation can be thought of as the strength of vorticity or vortex. Lift is related to circulation using

Eq [37], Ref [6]. This is known as the Kutta-Joukowski theorem. On most computational fluid dynamics programs circulation is used as a step to calculate the forces on a body. When a body is generating lift the circulation is finite. This means that the lift is directly related to the boundary layer vorticity.

- $\Gamma = \int_A \omega \cdot dA$

  Eq [36]

- $L = \rho V \Gamma$

  Eq [37]
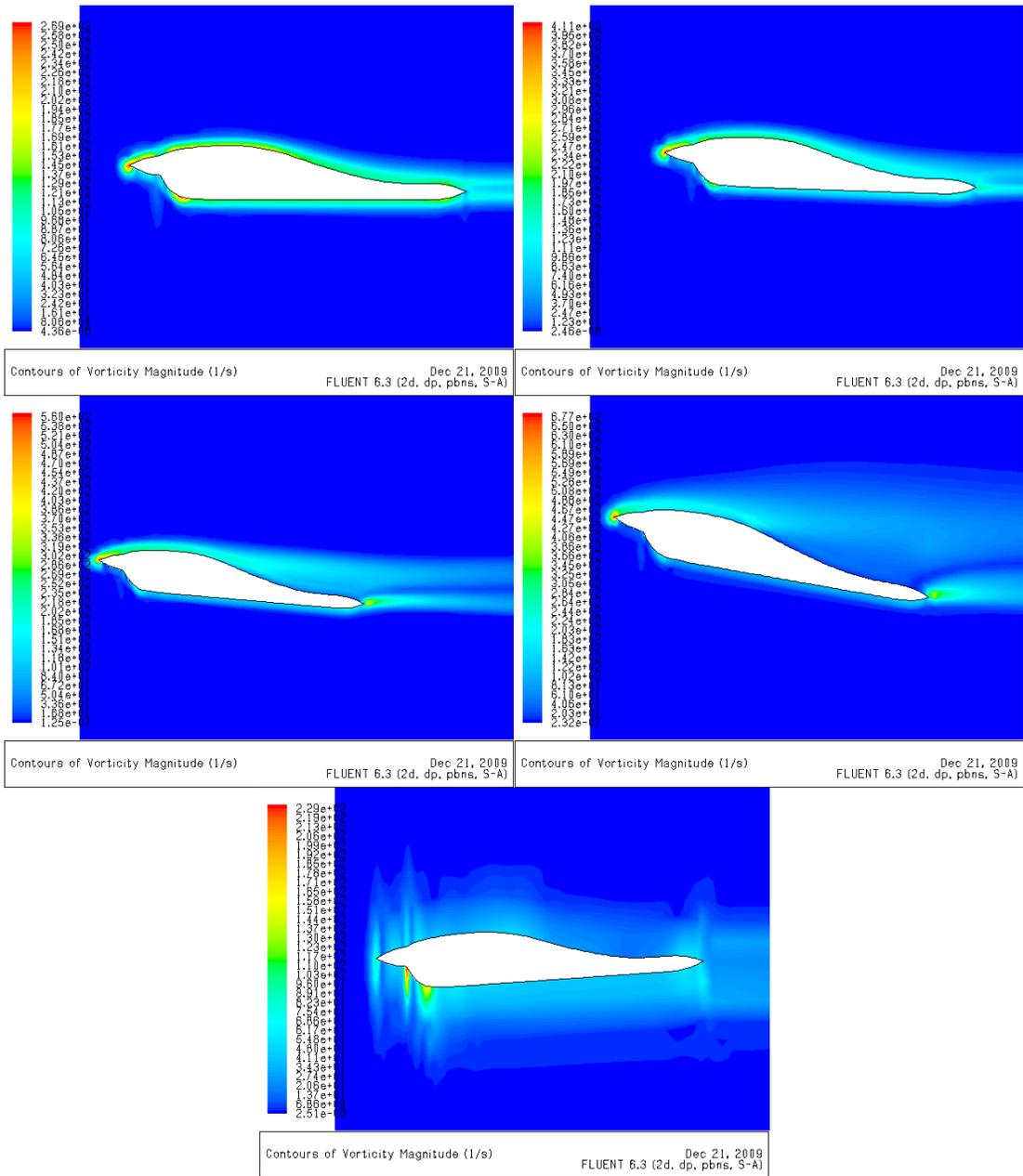
Figure 94: Meridian FLUENT Vorticity Magnitude Profile at All Angles of Attack

Kutta-Joukowski Theorem is used to estimate the lift produced by an airfoil or wing. The lift produced by a wing is a slightly manipulated form of Eq [37], because it is in terms of per unit of span. Therefore, that equation is multiplied by the amount

of span that generates lift. This theorem explains why the fuselage generates lift. For example, for an airfoil to generate lift the lower surface must have higher pressure than the upper surface. In order for this to happen in a uniform flow the upper surface velocity must increase and the lower surface velocity must decrease. This difference in pressures or velocities over a length will produce the lift. If a line of circulation, l', is used to define an area of integration then circulation can be determined for this airfoil or wing section. This is depicted in Figure 95, Ref [6] to help explain how circulation will produce lift.
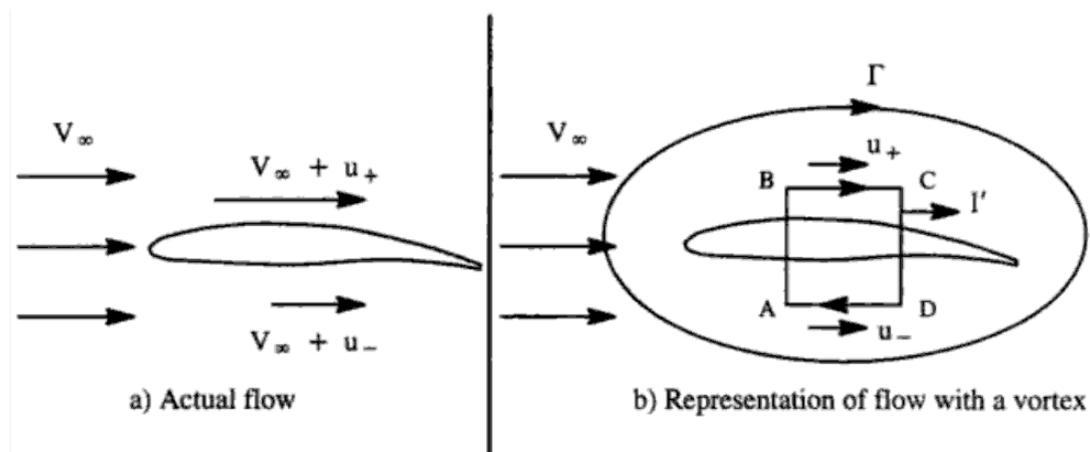
Figure 95: Circulation around an Airfoil Producing Lift (From Ref [6])

9.6   Method Comparison Meridian

Since time and resources did not allow for a 3-D FLUENT model to be created the stability and control derivatives from FLUENT were not able to be determined. Lift and drag that was produced by the fuselage, in a 2-D since, was found. Digging into the VORSTAB output files the theoretical fuselage lift and drag can be found. AAA does not calculate the lift of the fuselage, but rather the

158

contribution of the wing and fuselage combination. Since AAA uses this combination the individual wing lift was subtracted from the wing-fuselage lift to determine the individual fuselage lift. This resulted in an extremely small lift, and was negligible when compared to the VORSTAB and FLUENT results. The comparisons lift and drag values for the Meridian fuselage are shown in Table 53. The VORSTAB results shown in this table are for Models 2 and 3, because they are the only results that VORSTAB will generate fuselage data. Model 1 calculated downwash so high that the pressure on the fuselage was too high to continue calculating the fuselage data. The forth model did not have a fuselage present for calculations.

Table 53: Meridian Fuselage Lift and Drag Method Comparison

Method	$\alpha = 0°$			$\alpha = 5°$			$\alpha = -5°$ and $-4°$ (FLUENT)		
	C_l	C_d	L/D	C_l	C_d	L/D	C_l	C_d	L/D
FLUENT	0.403	0.029	14.09	0.548	0.092	5.975	0.108	0.065	1.659
VORSTAB									
Model 2	0.010	1.460	0.007	0.019	2.827	0.007	0.003	0.486	0.005
Model 3	0.001	0.598	0.001	0.009	0.072	0.119	-0.006	1.606	-0.004

As seen from these results the FLUENT fuselage seems to produce much more lift and less drag than the other two methods. The 3-D effects will reduce the lift, but also they will also help the flow to stay attached to the fuselage and avoid separation. This would reduce the drag. Therefore, the lift to drag ratio for FLUENT might be correct, but the individual values might be off. Model 2 and Model 3 for the VORSTAB drag results are very high. This is due to the high downwash produced in

159

by VORSTAB. Fuselages do not typically produce much lift. These VORSTAB lift to drag ratios are nowhere near the expected value.

Similar to the YAK-54 and MantaHawk the stability and control derivatives from both methods, VORSTAB and AAA, can be compared to one another. Table 54 shows the comparison for the Meridian stability and control derivatives.

Table 54: Meridian AAA and VORSTAB Comparison

Longitudinal Coefficients and Stability Derivatives					
Derivative (1/deg)	AAA	VORSTAB			
		Model 1	Model 2	Model 3	Model 4
$C_{L\alpha}$	5.1648	-0.0929	7.2337	7.1675	5.3308
$C_{D\alpha}$	0.1409	0.0000	15.5804	-6.1068	0.1020
$C_{m\alpha}$	-0.6207	-0.2268	-0.8522	-0.4038	-0.1609
C_{Lq}	4.6179	34.603	7.1682	7.1767	3.7241
C_{mq}	-13.973	-17.109	-8.5662	-8.5688	-3.7942
$C_{l\beta}$	-0.0776	2.2804	-0.1083	-0.1031	-0.1060
C_{lp}	-0.5546	1.1605	-0.2913	-0.2920	-0.2960
C_{lr}	0.1099	-0.6586	-0.2263	-0.2316	-0.2320
$C_{y\beta}$	-0.4789	-1.2031	0.7695	0.8228	0.6383
C_{yp}	-0.1465	-0.2153	-0.101	-0.1065	-0.1229
C_{yr}	0.3217	-4.5412	0.2091	0.1261	0.1291
$C_{n\beta}$	0.1386	2.4115	0.0991	0.0773	0.0940
C_{np}	-0.0351	1.1294	-0.0312	-0.0242	0.0226
C_{nr}	-0.1338	2.0948	-0.0748	-0.0460	-0.0666
$C_{L\delta e}$	0.4149	------	0.0974	0.0922	0.0858
$C_{D\delta e}$	0.0117	------	-0.9313	1.3450	0.0040
$C_{m\delta e}$	-1.6709	------	-0.3867	-0.3600	-0.3304
$C_{l\delta a}$	0.2316	------	0.2628	0.2625	0.2606
$C_{l\delta r}$	-0.0253	------	0.0117	0.0123	0.0178
$C_{y\delta a}$	0.0000	------	0.0565	0.0567	0.0583
$C_{y\delta r}$	-0.3681	------	0.1303	0.1248	0.1463
$C_{n\delta a}$	-0.0134	------	0.0692	0.0688	0.0670
$C_{n\delta r}$	0.1481	------	-0.0559	-0.0479	-0.0612

Model 1 produced such a high amount of downwash that the program could not calculate all the derivatives, and the ones it could were done with inaccurate downwash. Model 4 does not contain the fuselage so the results only show what the

wings and v-tail produce in terms of stability and control derivatives. The VORSTAB results are unstable in many different modes as discussed earlier and the AAA results are stable in every mode.

The same typical ranges that applied to the YAK-54 and MantaHawk apply to the Meridian as well. These ranges again were developed by Dr. Roskam, Ref [5] for what a conventional aircraft can expect the control derivatives to be approximately. These ranges are a function of Mach number. Table 55 shows the VORSTAB and AAA Meridian results compared to typical ranges from Dr. Roskam, Ref [5].

Table 55: Meridian VORSTAB and AAA Stability and Control Derivatives Typical Ranges

						Within Range (Yes/No)			
Stability and Control Derivatives									
	Model 2	Model 3	Model 4	AAA	Typical Ranges Dr. Roskam	Model 2	Model 3	Model 4	AAA
$C_{L\alpha}$	7.234	7.168	5.331	5.165	1.0 to 8.0	Yes	Yes	Yes	Yes
$C_{D\alpha}$	15.58	-6.107	0.102	0.141	0.0 to 2.0	No	No	Yes	Yes
$C_{m\alpha}$	-0.852	-0.404	-0.161	-0.621	-4.0 to 1.0	No	No	Yes	Yes
C_{Lq}	7.168	7.177	3.724	4.618	0.0 to 30.0	Yes	Yes	Yes	Yes
C_{mq}	-8.566	-8.569	-3.794	-13.97	-90.0 to 0	Yes	Yes	Yes	Yes
$C_{l\beta}$	-0.108	-0.103	-0.106	-0.078	0.1 to -4.0	Yes	Yes	Yes	Yes
C_{lp}	-0.291	-0.292	-0.296	-0.555	-0.1 to -0.8	Yes	Yes	Yes	Yes
C_{lr}	-0.226	-0.232	-0.232	0.110	0.0 to 0.6	No	No	No	Yes
$C_{y\beta}$	0.770	0.823	0.638	-0.479	-0.1 to -2.0	No	No	No	Yes
C_{yp}	-0.101	-0.107	-0.123	-0.147	-0.3 to 0.8	Yes	Yes	Yes	Yes
C_{yr}	0.209	0.126	0.129	0.322	0.0 to 1.2	No	No	No	No
$C_{n\beta}$	0.099	0.077	0.094	0.139	0.0 to 4.0	Yes	Yes	Yes	Yes
C_{np}	-0.031	-0.024	0.023	-0.035	-0.5 to 0.1	Yes	Yes	Yes	Yes
C_{nr}	-0.075	-0.046	-0.067	-0.134	0.0 to -1.0	Yes	Yes	Yes	No
$C_{L\delta e}$	0.097	0.092	0.086	0.415	0.0 to 0.6	Yes	Yes	Yes	Yes
$C_{D\delta e}$	-0.931	1.345	0.004	0.012	Negligible	No	No	No	No
$C_{m\delta e}$	-0.387	-0.360	-0.330	-1.671	0.0 to -4.0	Yes	Yes	Yes	Yes
$C_{l\delta a}$	0.263	0.263	0.261	0.232	0.0 to 0.4	Yes	Yes	Yes	Yes
$C_{l\delta r}$	0.012	0.012	0.018	-0.025	-0.04 to 0.04	Yes	Yes	Yes	Yes
$C_{y\delta a}$	0.057	0.057	0.058	0.000	Negligible	No	No	No	Yes
$C_{y\delta r}$	0.130	0.125	0.146	-0.368	0.0 to 0.5	Yes	Yes	Yes	No
$C_{n\delta a}$	0.069	0.069	0.067	-0.013	-0.08 to 0.08	Yes	Yes	Yes	Yes
$C_{n\delta r}$	-0.056	-0.048	-0.061	0.148	-0.15 to 0	Yes	Yes	Yes	No

As seen from the table not all of the control derivatives fall within the typical ranges. This does not necessarily mean that the aircraft is unstable. The rudder input is a symmetrical deflection of the v-tail and unsymmetrical deflection is an elevator input. In some cases the AAA results do not fall into the expected range, but the VORSTAB results do. This does not mean that VORSTAB was correct in that case and that AAA was incorrect. The Meridian might just have higher values in some derivatives than a typical aircraft has.

From these results it can be determined that VORSTAB is most affective with less complex aircraft. The Meridian was very difficult to model and achieve accurate results. This does not mean that VORSTAB is not a high fidelity tool or inaccurate, but rather should be used on aircraft that have a simpler design. The fuselage model was changed many times until results that were closer to the desired results were achieved. Basically it was very similar to guessing and checking. This is not necessarily bad, because many times the meshes of a FLUENT model have to be remade until the results are what was desired or expected. It is very difficult to determine if these programs are producing the correct results without comparing their results with actual fight tests. After that comparison one can draw a better conclusion about the validity of the results.

10 Conclusions and Recommendations

After analyzing the three aircraft with AAA and VORSTAB conclusions about both software programs were drawn. AAA is a valid method for quickly estimating the stability and control derivatives, even at a low Reynolds number. It is a rather affordable software program and easy to use. A downfall to the program is that a low fidelity method is used to derive the derivatives. A downfall of VORSTAB is that it is very difficult to make a VORSTAB model and requires someone with experience or guidance. The VORSTAB model also takes a considerable longer amount of time to create than AAA. VORSTAB uses a high fidelity method to derive the stability and control derivatives. For low Reynolds number, AAA overestimates estimates the drag and this was one of the main reason that a VORSTAB model was created for all of the vehicles. These are the obvious downfalls and benefits to both programs.

For the YAK-54, VORSTAB showed that the drag, C_{Do}, was lower than AAA predicted, as expected. This is a major advantage of VORSTAB is that the drag estimation is closer to the actual drag. From the flight test data, VORSTAB estimated many derivatives better than the AAA program did. Some of the derivatives from VORSTAB are obvious that they are wrong and these should be ignored. For example, the yawing moment due to aileron deflection has results that are not symmetric, but opposite, for positive and negative aileron deflections. It is known that a positive and negative aileron deflection should result in the same magnitude for this derivative. These improvements from VORSTAB can be significant in creating a

valid YAK-54 model. From these results, both software programs are a valid engineering tool and both should be used for deriving the derivatives.

Similar to the YAK-54, VORSTAB predicted a lower drag than AAA for the MantaHawk. Without flight test it cannot be determined if VORSTAB or AAA predicted the drag best. The MantaHawk wrecked early into the first flight test and hardly any data was collected. From the small amount of data and explanation from the flight test team the vehicle wrecked from a pitching moment error. AAA did not predict this problem and said the vehicle should be stable in all modes. Most of AAA's data is based on conventional aircraft and not a flying wing. VORSTAB predicted that the MantaHawk was stable in every mode but the pitching moment stability. It also estimated all of the derivatives to be much lower than AAA results. This can have a significant effect on the control of the aircraft. Even if VORSTAB was incorrect about the instability it would give the designers an idea of something that should be investigated. Therefore, a recommendation for VORSTAB would be to create a model for preliminary design and use it to determine if there is a possible instability issue. Then the flight test team can use precaution when design the flight tests and flying the aircraft. The instability mode can be tested in the flight tests, and having the pilot aware of possible instability will dramatically improve the safety.

From the Meridian results, VORSTAB was found to be completely invalid. The complex shape of the fuselage, v-tail configuration, and highly cambered wings were difficult for VORSTAB to handle. Since VORSTAB worked for both of the other aircraft, it was determined that this software should only be used on aircraft that

have an extremely conventional configuration and a smaller amount of camber. The MantaHawk did not have a conventional shape, but there was not a large camber. From the VORSTAB output file, the highly cambered fuselage, a large amount of downwash was produced. This was the source of most of VORSTAB's problems. A wing and tail model should be created to model the drag if there is a complex fuselage body. Once the flight tests have been repeated several times and the stability and control derivatives have been determined a VORSTAB model should be created. Then modifications can be made to this VORSTAB model until the expected results are achieved. This would give the designer a general idea for ways to improve the models in the future.

FLUENT was used to determine if there was a possible downwash problem over the fuselage and if the fuselage was producing a large amount of drag. At high angle of attack the flow separated from the fuselage and even began to have complete flow reversal at 10˚ angle of attack. Since this was a 2-D model the 3-D effects will help prevent the flow from separating. Tufting should be added to the empennage and flight tested to determine if there is flow separation and turbulent flow. After this investigation, a trip strip could possible be added to the empennage in order to reenergize the flow and prevent separation. These trip strips can later be removed if it is found that the separation is not a problem. The drag was determined to be much lower than VORSTAB was estimating and the flight tests were showing. The high drag was a result on having an unpainted surface, cowling with large gaps, no fairing, and more. With improvements made to the aircraft the drag has reduced

dramatically. It is recommended that a complete 3-D FLUENT model be created of the Meridian. This model will be difficult to create, so it should be created in steps. The wings and tails will not be that difficult to create and should be done first. Then the fuselage should be created. It is a very complex geometry so the CAD model should be used to import the fuselage. If Tgrid is available it should be used to import the complete model and create the mesh. All of these recommendations will help with future and current design projects.

11 <u>References</u>

[1] Roskam, J., "Airplane Flight Dynamics and Automatic Flight Controls," DARcorporation, Lawrence, KS, 2003.

[2] Lan, E., and Roskam, J., "Airplane Aerodynamics and Performance," DARcorporation, Lawrence, KS, 2003.

[3] Roskam, J., "Airplane Design Part VI: Preliminary Calculation of Aerodynamic, Thrust and Power Characteristics," DARcorporation, Lawrence, KS, 2004.

[4] "Advanced Aircraft Analysis," *DARcorporation Website,* [http://www.darcorp.com/Software/AAA/ , Retrieved 6 January, 2010].

[5] Anderson, J. D., "Modern Compressible Flow," *Linearized Subsonic Flow*, 3rd ed., New York, New York,   2003, pp. 324-333.

[6] Lan, E. C., "VORSTAB-A Computer Program for Calculating Lateral-Directional Stability Derivatives with Vortex Flow Effect," NASA CR-172501, January 1985.

[7] Lan, E. C., "User's Manual for VORSTAB Code (Version 3.2)," Department of Aerospace Engineering at the University of Kansas, Revised 2006.

[8] Jager, R., "Test and Evaluation of the Piccolo II Autopilot System on a One-Third Scale Yak-54," Department of Aerospace Engineering at the University of Kansas, April 2008.

[9] Keshmiri, S., Leong, E., Jager, R., and Hale, R., "Modeling and Simulation of the Yak-54 Scaled Unmanned Aerial Vehicle Using Parameter and System Identification," AIAA-2008-6900, August 2008.

[10] Leong, E., "A and B Matrix Construction Using Roskam Method," *MatLab Code*, September 2007.

[11] Arnold, E., Burns, R., and Grorud, D., "AE 721: Interim Final Review of a Small Scale UAV," The University of Kansas Aerospace Engineering Department, December 2009.

[12] Sweeten, B., "The Meridian UAV Flight Performance Analysis Using Analytical and Experimental Data," AIAA-2009-1899.

[13] Donovan, W., "The Meridian Critical Design Review," June 25, 2007, Technical Report CReSIS TR 123.

[14] Leong, H. and Jager, R., "Development of a Pilot Training Platform for UAVs Using a 6DOF Nonlinear Model with Flight Test Validation," AIAA-2008-6368.

[15] Royer, D., Keshmiri, S., Sweeten, B., "Modeling and Sensitivity Analysis of the Meridian Unmanned Aerial Vehicle," AIAA Conference Submitted.

[16] Keshmiri, S., Royer, D., Tom, J., "The Meridian System Identification Flight Tests in Dugway, UT," Fall 2009.

[17] "Spatial Discretization," *Fluent Inc.*, September 2006, [http://my.fit.edu/itresources/manuals/fluent6.3/help/html/ug/node992.htm].

[18] Kundu, P. K., and Cohen, I. M., "Fluid Mechanics," 4rd ed., Burlington, Massachusetts, 2008.

[19] Anderson, J. D., "Fundamentals of Aerodynamics," 4rd ed., New York, New York, 2007, pp. 404-437.

[20] Mixon, B., D. and Chudoba, B., "The Lockheed SR-71 *Blackbird* – A Senior Capstone Re-Engineering Experience," AIAA-2007-698.

[21] Malmuth, N., D., " Theoretical Aerodynamics in Today's Real World, Opportunities and Challenges," AIAA-2005-5059.

[22] Alford, L. and Altman, A., "Wavelike Characteristics of Low Reynolds Number Aerodynamics," AIAA-2004-4973.

[23] Chudoba, B. and Smith, H., "A Generic Stability and Control Methodology For Novel Aircraft Conceptual Design," AIAA-2003-5388.

Appendix A

The following files are posted with my thesis on the KU website.

- For the input file of the YAK-54 go to YAK_input and for the output file go to YAK_output.
- For the input file of the MantaHawk go to MantaHawk_input and for the output file go to MantaHawk_output.
- For the input file of the Meridian Model 1 go to Meridian1_input and for the output file go to Meridian1_output.
- For the input file of the Meridian Model 2 go to Meridian2_input and for the output file go to Meridian2_output.
- For the input file of the Meridian Model 3 go to Meridian3_input and for the output file go to Meridian3_output.
- For the input file of the Meridian Model 4 go to Meridian4_input and for the output file go to Meridian4_output.

Appendix B

YAK 54:

The linear state space model is developed using the Roskam method and a program written by Edmond Leong, Ref [22]. It is developed in the form of **x˙=Ax+Bu**. The program uses the control derivatives found from VORSTAB. The following A and B matrices were determined from this method for both longitudinal and lateral-directional modes.

$$A\_long = \begin{bmatrix} -0.4156 & 29.3521 & 0 & 6.9963 \\ -0.0042 & -0.2024 & 0.9979 & -0.2657 \\ 0.0020 & -2.3397 & -0.2101 & 0.0208 \\ 0 & 0 & 1.0000 & 0 \end{bmatrix}$$

$$B\_long = \begin{bmatrix} 0 \\ -0.0002 \\ -0.0338 \\ 0 \end{bmatrix}$$

$$A\_lat = \begin{bmatrix} -0.1664 & 0 & -0.6102 & 0.0218 \\ 1.0000 & 0 & 0 & 0 \\ -0.0000 & -0.0592 & -0.0151 & -0.9995 \\ -0.0090 & 0 & 1.7468 & -0.0621 \end{bmatrix}$$

$$B\_lat = \begin{bmatrix} 3.1788 & 0.3604 \\ 0 & 0 \\ -0.0011 & 0.0104 \\ 0.5780 & -1.4499 \end{bmatrix}$$

The longitudinal dynamics should have two complex conjugate roots. These two modes are Phugoid and Short Period. Table 56 shows the longitudinal mode analysis summary and also compares it to the results that AAA control derivatives produce, Ref [13]. Table 57 shows the lateral-directional mode analysis summary and also compares it to the results that AAA control derivatives produce, Ref [13].

Table 56: YAK-54 Longitudinal Modes

Eigenvalues	Damping	Frequency (rad/sec)	Mode
VORSTAB			
0.281	-1.0	0.281	?
-0.426	1.0	0.426	?
-0.342+1.60i	0.209	1.63	?
-0.342-1.60i	0.209	1.63	?
AAA			
-0.205+0.133i	0.839	0.24	Phugoid
-0.205-0.133i	0.839	0.24	Phugoid
-9.87+1.73i	0.985	10	Short Period
-9.87-1.73i	0.985	10	Short Period

Table 57: YAK-54 Lateral-Directional Modes

Eigenvalues	Damping	Frequency (rad/sec)	Mode
VORSTAB			
-2.12e-5	1.0	2.12e-5	Spiral
-0.149	1.0	0.149	Roll
-0.0473+1.323i	0.0358	1.32	Dutch Roll
-0.0473-1.323i	0.0358	1.32	Dutch Roll
AAA			
0.0105	1	0.0105	Spiral
-16.7	1	0.0599	Roll
-1.22+65.3i	0.18	6.65	Dutch Roll
-1.22-65.3i	0.18	6.65	Dutch Roll

It is obvious from the results that VORSTAB is not correct. This is most likely due to the fact that the state space model was created with a mixture of the VORSTAB derivatives and the AAA derivatives. VORSTAB does not give every derivative necessary to make the model and this is why some of the AAA derivatives were used. The coupling of the two programs does not work.

Several flight tests were conducted to perform system identification on the YAK-54. The only two modes tested were the Dutch Roll mode and Phugoid mode. These tests resulted in a damping ratio for the Phugoid mode of 0.575 and 0.303 for the Dutch Roll, Ref [13].

MantaHawk:

The linear state space model is developed using the Roskam method and a program written by Edmond Leong, Ref [22]. It is developed in the form of $\mathbf{\dot{x}=Ax+Bu}$. The program uses the control derivatives found from VORSTAB. The following A and B matrices were determined from this method for both longitudinal and lateral-directional modes.

$$A\_long = \begin{bmatrix} -0.1495 & 43.6531 & 0 & -32.1740 \\ -0.0063 & -0.0926 & 0.9997 & 0 \\ -0.0137 & -0.1245 & -0.0425 & 0 \\ 0 & 0 & 1.0000 & 0 \end{bmatrix}$$

$$B\_long = \begin{bmatrix} -0.0521 \\ -0.0176 \\ -1.2486 \\ 0 \end{bmatrix}$$

$$A\_lat = \begin{bmatrix} -0.1728 & 0 & -0.6085 & 0.0120 \\ 1.0000 & 0 & 0 & 0 \\ -0.0001 & 0.2723 & -0.0031 & -0.9999 \\ -0.0001 & 0 & 0.1791 & -0.0035 \end{bmatrix}$$

$$B\_lat = \begin{bmatrix} 2.2078 & 2.2078 \\ 0 & 0 \\ 0.0010 & 0.0010 \\ -0.0875 & -0.0875 \end{bmatrix}$$

The longitudinal dynamics has only one complex conjugate root and two different real roots. There are typically two roots that are defined as Phugoid and Short Period modes. When the center of gravity is ahead of the neutral point it will cause Phugoid and Short Period roots to approach real roots (x-axis), but it still does not explain the two different real roots, Ref [&^%]. Table 58 shows the longitudinal mode analysis summary. Table 59 shows the lateral-directional mode analysis summary.

Table 58: MantaHawk Longitudinal Modes

Eigenvalues	Damping	Frequency (rad/sec)	Mode
VORSTAB			
0.0714	-1.0	0.0714	?
-0.449	1.0	0.449	?
0.0467+0.699i	-0.0666	0.701	?
0.0467-0.699i	-0.0666	0.701	?

Table 59: MantaHawk Lateral-Directional Modes

Eigenvalues	Damping	Frequency (rad/sec)	Mode
VORSTAB			
4.27e-5	-1.0	4.27e-5	Spiral
-0.533	1.0	0.533	Roll
0.177+0.581i	-0.291	0.607	Dutch Roll
0.177-0.581i	-0.291	0.607	Dutch Roll

Again, these results are not accurate since a mixture of both AAA and VORSTAB derivatives were used to create the state space model. The vehicle did not go under enough flight tests to verify any of the results.

Meridian:

The linear state space model is developed using the Roskam method and a program written by Edmond Leong, Ref [22]. It is developed in the form of **x˙=Ax+Bu**. The program uses the control derivatives found from VORSTAB. The following A and B matrices were determined from this method for both longitudinal and lateral-directional modes of the Meridian model with the large empennage, Model 2.

$$
A\_long = \begin{bmatrix}
0.0232 & 6.7443 & 0 & -32.1740 \\
-0.0016 & -0.0673 & 0.9996 & 0 \\
-0.0014 & -0.5584 & -0.0383 & 0 \\
0 & 0 & 1.0000 & 0
\end{bmatrix}
$$

$$
B\_long = \begin{bmatrix}
1.4761 \\
-0.0008 \\
-0.1899 \\
0
\end{bmatrix}
$$

$$A\_lat = \begin{bmatrix} -0.0545 & 0 & -0.3085 & -0.0423 \\ 1.0000 & 0 & 0 & 0 \\ -0.0001 & 0.1589 & 0.0060 & -0.9999 \\ -0.0039 & 0 & 0.1876 & -0.0094 \end{bmatrix}$$

$$B\_lat = \begin{bmatrix} 0.7485 & 0.0333 \\ 0 & 0 \\ 0.0004 & -0.0010 \\ 0.1320 & -0.1066 \end{bmatrix}$$

The longitudinal dynamics has only two complex conjugate roots. Also, one of the roots is unstable, since its eigenvalue is positive. Table 60 shows the longitudinal mode analysis summary and also compares it to the results that AAA control derivatives produce, Ref [18]. Table 61 shows the lateral-directional mode analysis summary and also compares it to the results that AAA control derivatives produce, Ref [18].

Table 60: Meridian Model 2 Longitudinal Modes

Eigenvalues	Damping	Frequency (rad/sec)	Mode
VORSTAB			
0.0518+0.208i	-0.241	0.215	
0.0518-0.208i	-0.241	0.215	
-0.093+0.73i	0.126	0.736	
-0.093-0.73i	0.126	0.736	
AAA			
	0.116	0.255	Phugoid
	0.116	0.255	Phugoid
	0.435	7.58	Short Period
	0.435	7.58	Short Period

Table 61: Meridian Model 2 Lateral-Directional Modes

Eigenvalues	Damping	Frequency (rad/sec)	Mode
VORSTAB			
-0.0316	1.0	0.0316	
-0.232	1.0	0.232	
0.103+0.473i	-0.213	0.484	Dutch Roll
0.103+0.473i	-0.213	0.484	Dutch Roll
AAA			
	1	-109 sec	Spiral
	1	0.154 sec	Roll
	0.144	4.14	Dutch Roll
	0.144	414	Dutch Roll

Removing the camber, Model 3, resulted in the following matrix A and B from the VORSTAB results.

$$
A\_long = \begin{bmatrix}
0.0232 & 41.1159 & 0 & -32.1740 \\
-0.0016 & -0.0668 & 0.9996 & 0 \\
-0.0014 & -0.3381 & -0.0383 & 0 \\
0 & 0 & 1.0000 & 0
\end{bmatrix}
$$

$$
B\_long = \begin{bmatrix}
-2.1317 \\
-0.0007 \\
-0.1769 \\
0
\end{bmatrix}
$$

$$
A\_lat = \begin{bmatrix}
-0.0546 & 0 & -0.2938 & -0.0433 \\
1.0000 & 0 & 0 & 0 \\
-0.0001 & 0.1589 & 0.0002 & -0.9999 \\
-0.0030 & 0 & 0.1461 & -0.0058
\end{bmatrix}
$$

$$
B\_lat = \begin{bmatrix}
0.7478 & 0.0349 \\
0 & 0 \\
0.0004 & 0.0010 \\
0.1311 & -0.0913
\end{bmatrix}
$$

The longitudinal dynamics has two complex conjugate roots. These two roots are Phugoid mode and Short Period mode. The lateral-directional mode has 3 stable roots, when the spiral mode is usually unstable. Table 62 shows the longitudinal mode analysis summary and also compares it to the results that AAA control derivatives produce, Ref [18]. Table 63 shows the lateral-directional mode analysis summary and also compares it to the results that AAA control derivatives produce, Ref [18].

Table 62: Meridian Model 3 Longitudinal Modes

Eigenvalues	Damping	Natural Frequency	Mode
VORSTAB			
-5.64e-3+0.196i	0.0287	0.196	
-5.64e-3-0.196i	0.0287	0.196	
-0.0353+0.601i	0.0586	0.602	
-0.0353-0.601i	0.0586	0.602	
AAA			
	0.116	0.255	Phugoid
	0.116	0.255	Phugoid
	0.435	7.58	Short Period
	0.435	7.58	Short Period

Table 63: Meridian Model 3 Lateral-Directional Modes

Eigenvalues	Damping	Frequency (rad/sec)	Mode
VORSTAB			
-0.0245	1.0	0.0245	
-0.257	1.0	0.257	
0.111+0.436i	-0.246	0.45	
0.111-0.436i	-0.246	0.45	
AAA			
	1	-109 sec	Spiral
	1	0.154 sec	Roll
	0.144	4.14	Dutch Roll
	0.144	4.14	Dutch Roll

For the same reason as the other two aircrafts this state space models are not accurate. Flight tests were performed in Dugway, UT. During these flight tests the Dutch Roll and Short Period modes were initiated, so system identification could be performed. From the flight tests and analysis of that data from the flight test team the Dutch Roll damping ratio of 0.2163 and natural frequency of 3.5341 rad/sec. AAA was closer to the flight test data than the VORSTAB results. Also, as expected the results from the model without camber had results closer to the flight test data. The Short Period had a damping ratio of 0.5973 and a natural frequency of 3.6723 rad/sec. All of the flight test results and analysis were taken from Ref [23]. Similar to the Dutch Roll the model without the camber had better results. For complex geometry it would be wise to use both AAA and VORSTAB as a means to determine the stability and control derivatives. Aircraft that have noncomplex or standard geometry, like the YAK-54, VORSTAB's results should be more accurate.